MIDDLE BLACK SEA JOURNAL OF HEALTH SCIENCE

AUGUST 2025 VOLUME 11 ISSUE 3

ISSN 2149-7796

MIDDLE BLACK SEA JOURNAL OF HEALTH SCIENCE (MBSJHS)

Middle Black Sea Journal of Health Science

The Middle Black Sea Journal of Health Science, which is international journal, is published by Ordu University Institute of Health Sciences on behalf of the Middle Black Sea Universities Collaboration Platform

e-ISSN 2149-7796

Middle Black Sea Journal of Health Science

Editorial Office

Ordu University

Institute of Health Sciences

Cumhuriyet Campus

52200, Ordu, TÜRKİYE

Tel: +90 (452) 234 5010-6105

Fax: +90 (452) 226 52 28

E-mail: ukaraman@odu.edu.tr

Correspondence Address: Ulku KARAMAN, PhD, Assoc. Prof. Dr.
Institute of Health Sciences,
Ordu University,
Cumhuriyet Campus,
52200 Center/ Ordu TÜRKİYE

Phone: +90 452 234 50 10
Fax: +90 452 226 52 55
Email: ukaraman@odu.edu.tr
ulkukaraman44@hotmail.com

Web site: https://dergipark.org.tr/en/pub/mbsjohs

Sort of Publication: Periodically

Publication Date and Place: 30 /08/ 2025, ORDU, TÜRKİYE

Publishing Kind: Online

Indexing: *Türkiye Citation Index, SOBIAD, Rootindexing, Academic Resource ındex, Fatcat index, Researcgate, EuroPub, Gooogle Scholar, Turk Medline, Index Copernicus*

The Middle Black Sea Journal of Health Science, which is international journal, is published by Ordu University Institute of Health Sciences on behalf of the Middle Black Sea Universities Collaboration Platform

Aims and Scope

Middle Black Sea Journal of Health Science is an international journal that publishes original clinical and scientific research. Middle Black Sea Journal of Health Science, published by Ordu University, publishes basic innovations in health education, case reports, reviews, letters to the editor, case reports and research articles.

The aim of the journal is to contribute to the international literature with clinical and experimental research articles, case reports, reviews and letters to the editor in the field of health sciences.

The target audience of the journal is all scientists working in the field of health, graduate students and researchers in this field.

Middle Black Sea Journal of Health Science is an open access, independent and impartial, international journal based on double-blind peer-reviewed principles.

The publication language of the journal is English. The journal is published every three months, in February, May, August and November, and four volumes are completed.

Middle Black Sea Journal of Health Science - adheres to the standards of publication ethics in health science research, Higher Education Council's Scientific Research and Publication Ethics Directive, Committee on Publication Ethics (COPE), Directory of Open Access Journals (DOAJ), Open Access Scholarly Publishers It also adopts the ethical publishing principles published by the Association (OASPA) and the World Association of Medical Editors (WAME).

No fee is charged from the authors for the evaluation and publication of the article.

Publication Ethics Statement

Middle Black Sea Journal of Health Science - adheres to the standards of publication ethics in health science researches, Higher Education Council's Scientific Research and Publication Ethics Directive, Committee on Publication Ethics (COPE), Directory of Open Access Journals (DOAJ), Open Access Scholarly Publishers It also adopts the ethical publishing principles published by the Association (OASPA) and the World Association of Medical Editors (WAME); The address for the principles expressed under the Principles of Transparency and Best Practice in Scholarly Publishing is given below.

https://publicationethics.org/resources/guidelines-new/principles-transparency-and-best-practice-scholarly-publishing

Submitted research is original, has not been published before and should not be in the evaluation process of another journal. Each article is double blinded by one of the editors and at least two referees. Plagiarism, duplication, fraudulent authorship / denied authorship, research / data fabrication, article slicing, slicing publishing, copyright infringement and concealing conflict of interest are considered unethical behavior.

All articles that do not comply with ethical standards are removed from publication even if they are accepted. This situation is valid for articles containing possible irregularities and inconveniences detected after publication.

Research Ethics

• The authors are responsible for the compliance of the articles with the ethical rules.

• Ethical standards of the Declaration of Helsinki must be followed in human studies.

• Attention should be paid to ethical principles in designing, reviewing and conducting the research.

• The research team and the participants should be fully informed about the purpose of the research, the participation rules and, if any, the risks involved.

• Confidentiality of the information and answers given by the research participants should be ensured. Research should be designed in a way that preserves the autonomy and dignity of its participants.

• Participants in the research should take part in the research voluntarily and should not be under any coercion.

• The research should be planned in a way that does not put the participants at risk.

• Be clear about research independence; If there is a conflict of interest, it should be indicated.

• In experimental studies, written informed consent must be obtained from the participants who decide to participate in the research. The legal guardian's consent must be obtained for children, those under guardianship and those with confirmed mental illness.

• If the study is to be carried out in an institution or organization, the necessary approval should be obtained from this institution or organization.

• In studies with a human element, it should be stated in the "method" section that "informed consent" was obtained from the participants and the ethics committee approval was obtained from the institution where the study was conducted.

Authors' Responsibility

The authors are responsible for the compliance of the articles with scientific and ethical rules. The author should provide assurance that the article is original, has not been published elsewhere, and is not being reviewed for publication elsewhere, in another language. Copyright laws and treaties in

practice must be observed. Corresponding materials (eg tables, figures or large quotations) should be used with necessary permissions and acknowledgments. Work or sources of other authors, contributors should be appropriately used and cited in references.

All authors should have a direct contribution in academic and scientific terms in the submitted article, accordingly, the "author" is someone who contributes to the conceptualization and design of a published research, obtaining, analyzing or interpreting data, writing the article or reviewing it critically in terms of content. Other conditions for being an author are planning or executing and / or revising the work in the article.

Funding, data collection, or general supervision of the research group alone does not provide authorship rights. All individuals designated as authors must meet all the criteria listed, and any individual who meets the above criteria can be shown as an author. The name order of the authors should be a joint decision. All authors must indicate the author order signed on the

Copyright Agreement Form.

All individuals who do not meet the sufficient criteria for authorship but contributed to the study should be listed in the "thank you" section. Examples of these are people who only provide technical support, help with writing or just provide general support, financial and material support.

All authors must declare financial relationships, conflicts of interest and competition of interest that have the potential to affect the results of the research or scientific evaluation. If writer detects a significant error or inaccuracy in his published manuscript, he / she bears the responsibility to immediately contact and cooperate with the editor for correction or retraction of these inaccuracies.

Editor and Referee Responsibilities

The editor-in-chief evaluates the articles regardless of the authors' ethnicity, gender, sexual orientation, nationality, religious belief, and political philosophy. It ensures that the articles submitted for publication go through a fair double-blind peer review. It guarantees that all information about the submitted articles will remain confidential until the article is published. The editor-in-chief is responsible for the overall quality of the content and publication. It should publish an error page or make a correction when necessary.

Editor in Chief; It does not allow any conflict of interest between authors, editors and referees. It has full authority to appoint a referee and is responsible for making the final decision on the articles to be published in the journal.

Reviewers should not have conflicts of interest with the authors and / or financial supporters of the research. They should reach an impartial judgment as a result of their evaluation. They must ensure that all information regarding submitted articles is kept confidential and report to the editor if they

notice any copyright infringement or plagiarism on the part of the author. In cases where the subject of the article is not his area of expertise or cannot return on time, the referee should inform the editor of this situation and state that he cannot be a referee.

Referees and editorial board members cannot discuss articles with other people. Care should be taken to keep the identity of the referees anonymous. In some cases, with the decision of the editor, the relevant referees' comments on the article may be sent to other referees who interpret the same article.

Publication Policy

Authors undertake that their publications are created in accordance with all universal ethical rules and research is accepted accordingly.

Authors are responsible for all statements in their work. Submitted studies should be prepared in line with the journal's writing rules. Studies that do not comply with the spelling rules are rejected or sent back to the authors for correction.

The journal has the right to make corrections in the accepted works without changing the content and meaning.

The journal accepts the research provided that it has not been published in another journal or publication.

All authors should indicate their relationships with individuals or organizations that may have conflicts of interest. Support received for the study, if any, should be stated in detail. Conflicts of interest should also be indicated on the title page.

In the management and publication processes of the journal, attention is paid to the publishing principles of "International Committee of Medical Journal Editors (ICMJE)" and "Committee on Publication Ethics (COPE)".

Evaluation process

-Only articles uploaded to the journal's system are evaluated. Studies sent via e-mail are not considered.

- All submitted studies go through pre-evaluation, language editor, statistical editor and referee evaluation processes. The evaluation process is carried out by the editor of the journal.

Pre-Evaluation Process

After the article is uploaded to the journal, the pre-evaluation process begins. At this stage, the editor examines the article in terms of content, form, purpose and scope of the journal. As a result of this thinning

• Decides that the work is not suitable for the journal and declines the work.

• Resend the work to the responsible author for corrections.

• The study sends to the language editor and can request a correction.

• The study is evaluated by sending it to a statistics advisor. After this evaluation, the author may ask for a correction.

• Can direct the article to the referees and initiate the referee evaluation process.

Referee Evaluation Process

All articles in the journal are double-blind peer-reviewed. In order to ensure the impartial evaluation process, each article is evaluated by at least two independent referees who are experts in their fields. If there is no consensus among the referees, the article is evaluated by the third referee. The editor in chief makes the final decision in the decision-making process of all articles.

Revision

Authors should mark the changes they made in the main text in color while submitting the article revision files. The responses to the referees should be specified in a separate Word file. Revised articles should be submitted to the journal within one month following the decision letter. If the revised version of the article is not uploaded within the specified time, the revision option can be canceled. If the authors need additional time for revision, they must submit their publication requests to the journal before the end of one month.

Articles accepted for publication are checked again for grammar, punctuation and format.

Accepted articles are edited in accordance with the journal's publication format and the final version is sent to the responsible author in pdf format before publication, and approval is obtained for publication. Authors should review the article and approve for publication. If the article requires any correction other than the publication format, the request for correction is notified to the editor at ulkukaraman44@hotmail.com. Requests for correction are evaluated by the editor and notified to the responsible author. Articles that are not approved by the corresponding author are not published.

Plagiarism

The similarity rate of the articles should be made over iThenticate and should be at most 20%, excluding the "References" section.

The journal is published online only.

The journal is free and does not require any publication fee from researchers.

GENERAL RULES

Middle Black Sea Journal of Health Science publishes experimental and observational research articles, clinical reviews, case reports and review articles on health science. Manuscripts must be submitted online at https://dergipark.org.tr/en/login

All submissions must be accompanied by a signed statement of scientific contributions and responsibilities of all authors and a statement declaring the absence of conflict of interests.

Any institution, organization, pharmaceutical or medical company providing any financial or material support, in whole or in part, must be disclosed in a footnote. Manuscripts must be prepared in accordance with ICMJE-Recommendations for the Conduct, Reporting, Editing and Publication of Scholarly Work in Medical Journals (updated in December 2013 - http://www.icmje.org/icmje-recommendations.pdf).

An approval of research protocols by an ethical committee in accordance with international agreements (Helsinki Declaration of 1975, revised 2002 - available at http://www.vma.net/e/policy/b3.htm, "Guide for the care and use of laboratory animals - www.nap.edu/catalog/5140.html/) is required for experimental, clinical and drug studies. A form stating that the patients have been informed about the study and consents have been obtained from the patients is also required for experimental, clinical and drug studies. All submissions must be accompanied by a letter that states that all authors have approved the publication of the paper in the Middle Black Sea Journal of Health Science.

Submission of the studies requiring ethical committee decision must be accompanied by a copy of the submission to the ethical committee.

SUBMISSION POLICY

Submission of a paper to Middle Black Sea Journal of Health Science is understood to imply that it deals with original material not previously published and is not being considered for publication elsewhere. Manuscripts submitted under multiple authorships are reviewed on the assumption that all listed Authors concur with the submission and that a copy of the final manuscript has been approved by all Authors. After acceptation of an article, it should not be published elsewhere in the same form, in either the same or another language, without the written consent of the Editors and Publisher.

If excerpts from other copyrighted works are included, the Author(s) must obtain written permission from the copyright owners and credit the source(s) in the article.

The layout and style should adhere strictly to the instructions. No revisions or updates will be incorporated after the article has been accepted and sent to the Publisher (unless approved by the Editors).

SUBMISSION PROCEDURE

The Middle Black Sea Journal of Health Science welcomes submitted manuscripts online at http://dergipark.gov.tr/login Manuscripts submitted online are received on the day of submission and quickly assigned to reviewers. Through individual Author Centers on this website, authors can view the status of their manuscripts as they progress through the review process. Notification of the disposition of each manuscript will be sent by e-mail to the corresponding author on the day of decision.

To establish your account for online submission, go to http://dergipark.gov.tr/register/ Authors are encouraged to check for an existing account. If you are submitting for the first time, and you do not have an existing account, then you must create a new account. If you are unsure about whether or not you have an account, or have forgotten your password, enter your e-mail address into the Password Help section on the log-in page. If you do not have

an account, click on the Create Account link on the top right of the log-in page. You then will be able to submit and monitor the progress of your manuscripts. Once you have logged in, you will be presented with the Main Menu and a link to your Author Centre. Submit your manuscript from the Author Centre. At the end of a successful submission and you will

receive an e-mail confirming that the manuscript has been received by the journal. If this does not happen, please send an e-mail to ulkukaraman44@hotmail.com

To submit your manuscript online, please prepare the text and illustrations according to the instructions listed below. You may enter and exit the manuscript submission process at the completion of each step. After submission of the manuscript, however, you will not be able to edit it.

Web submission is required- instructions are available for downloading on the website https://dergipark.org.tr/en/pub/mbsjohs/writing-rules

COPYRIGHT TRANSFER AGREEMENT

A signed COPYRIGHT RELEASE FORM by all authors of the manuscript should be sent during manuscript submission. http://mbsjohs.odu.edu.tr/files/copyright_transfer_form_1.pdf

Middle Black Sea Journal of Health Science

Editorial Office

Ordu University, Institute of Health Sciences

Cumhuriyet Campus
52200, Ordu, TÜRKİYE
Tel: +90 (452) 226 52 14-5234
Fax: +90 (452) 226 52 28
E-mail: ulkukaraman44@hotmail.com
Authors should write their information exactly (Full address, telephone and fax numbers, e-mail address).

PREPARING ELECTRONIC MANUSCRIPTS

In the writing of words for the studies, "Oxford English Dictionary (https://www.oed.com)" should be taken as a reference. The symbols of the units used in the text should be given according to the http://www.bipm.org/en/si/

Author should submit manuscript in both ways as explain in below:

1- The text must be single-spaced, 12-point font (except with URL addresses); and all illustrations, figures, and tables must be placed within the text at the appropriate points, rather than at the end.

2- Files you need to add:

Title Page,
Full Text,
Tables,
Figures,
Images,
Copyright Form,
Similarity Report (Similarity should be at most 20%.).
Cover Letter
Ethics Committee Approval.

3- Please insert all attachments that are tables, figures and graphics into the text file in appropriate place.

When mentioning parasites, bacteria, virus and fungi in the main text and references, the genus and species names must be italicized, and the genus name must be written with an initial capital letter.

Abbreviations should be expanded at first mention and used consistently thereafter.

Graphic files: Each figure should be a separate file.

All figure files must be submitted in sufficiently high resolution.

Electronic submission of articles via the Web

http://dergipark.gov.tr/mbsjohs

Full instructions for uploading data and files etc. are given on the website when submitting a manuscript. It is the responsibility of the Authors to create the proper files as instructed above for the electronically submitted manuscript. The editorial office cannot make conversions beyond the supported file types.

ORGANIZATION OF THE ARTICLE

Manuscripts should be prepared electronically using "Time News Roman" font, formatted according to A4 page size, single-spaced from beginning to end, 2.5 cm margins on all sides and 12-point font. Words should not be hyphenated to fit on a line. Pages should be numbered.

Title page: A separate title page should be submitted with all submissions and this page should include:

The title page should include full and short title English.

Meeting and congress presentations of the manuscript must be stated, if any.

Name(s), affiliations, highest academic degree(s) and ORCID ID's of the author(s),

Example: Ulku Karaman[1], Yeliz Kasko Arici[2], Cemil Colak[3]

[1]Institution of the first author, e -mail, orcid no

[2]Second Author's Institution, e -mail, orcid no

[3]Third Author's Institution, e -mail, orcid no

Name, address, telephone (including the mobile phone number) and fax numbers, and email address of the corresponding author,

Ethics Committee Approval: Ethics committee approval was received for this study from ……. Clinical Research Ethics Committee of …… University (No……..).

Author Contributions: Concept: …….., Design: …….., Literature search:……..... Data Collection and Processing: ……..., Analysis and Interpretation:……, Writing - ……

Acknowledgements:

Conflict of Interest:

Financial Disclosure:

Note: Kongress participation……..

In the article sent, the sections that should be below are listed.

1. Abstract, 2. Keywords, 3. Introduction, 4. Methods, 5. Results, 6. Discussion, 7. Conclusion, 8. References, Tables and Figures sections.

1. Abstract Page: The first page should include abstracts written English, and key words. The abstract of Original Articles should be structured with subheadings (Objective, Methods, Results, and Conclusion) (average 200-400 word).

2. Keywords: Provide at least 3-6 keywords and avoiding general and plural terms and multiple concepts. These keywords will be used for indexing purposes. Key words in should follow the abstract. Please select keywords in Turkish Science Terms (http://www.bilimterimleri.com).

3. Introduction: The objectives of the research should be clearly stated in this section. Relevant background information and recent published studies should be described concisely and be cited appropriately.

4. Methods: This section should contain all the details necessary to reproduce the experiments. Avoid re-describing methods already published; only relevant modifications should be included in the text. Experimental subjects when human subjects are used, manuscripts must be accompanied by a statement that the experiments were undertaken with the understanding and written consent of each subject.

When experimental animals are used, the methods section must clearly indicate that adequate measures were taken to minimize pain or discomfort.

5 Results: These sections should present the results and interpret them in a clear and concise manner. Results should usually be presented descriptively and be supplemented by figures.

6. Discussion: Extensive citations and discussion of published literature should be being used.

7. Conclusion: In this section, the results obtained from the article should be written.

8. Literature references:

Care should be taken to cite Türkiye-based studies and journal of national during the granting of resources (www.atifdizini.com).

References should be listed according to the order of appearance in the text, and "in parentheses" should be indicated in the relevant places. References should be written according to the "Vancouver" system of the American National Library of Medicine (U.S. National Library of Medicine; http://www.nlm.nih.gov/).

Examples: Hypotension is one of the most common and critical problems in hemodialysis patients (1,2).

References

While citing publications, preference should be given to the latest, most up-to-date publications.

If an ahead-of-print publication is cited, the DOI number should be provided.

The accuracy of references is the responsibility of the author. The references should include only articles that are published or in press.

Unpublished data, submitted manuscripts, or personal communications should be cited within the text only. Personal communications should be documented by a letter of permission.

All items in the list of references should be cited in the text and, conversely, all references cited in the text must be presented in the list.

The abbreviations of journal titles should conform to those adopted by the List of Serial Title Word Abbreviations, CIEPS/ISDS, Paris, 1985 (ISBN 2-904938-02-8).

Journal titles should be abbreviated in accordance with the journal abbreviations in Index Medicus/ MEDLINE/PubMed.

For citation of references with one to six authors, the names of all authors should be included, and for the articles with more than six authors, “et al.” should be written after typing the six names. The surnames of authors should be written exactly, and the initials of their names should be indicated with capital letter without any punctuation mark.

Please use the following style for references:

Examples

Journal: Stephane A. Management of Congenital Cholesteatoma with Otoendoscopic Surgery: Case Report. J Med Sci 2010;30(2): 803-7.

Levine WC, Pope V, Bhoomkar A, Tambe P, Lewis JS, Zaidi AA, et al. Increase in endocervical CD4 lymphocytes among women with nonulcerative sexually transmitted diseases. J Infect Dis. 1998;177(1):167–174.

Chapter in Edited Book: Hornbeck P. Assay for antibody production. In: Colign JE. Kruisbeek AM, Marguiles DH, editors. Current Protocols in Immunology. New York: Greene Publishing Associates; 1991. p. 105-32.

Book with a Single Author: Fleiss JL. Statistical Methods for Rates and Proportions. Second Edition. New York: John Wiley and Sons; 1981. p. 105-32.

Editor(s) as Author: Balows A. Mousier WJ, Herramaflfl KL, editors. Manual of Clinical Microbiology. Fifth Edition. Washington DC: IRL Press. 1990. p. 105-32.

Conference Paper: Entrala E, Mascaro C. New structural findings in Cryptosporidium parvum oocysts. Eighth International Congress of Parasitology (ICOPA VIII); October 10-14; Izmir-Türkiye: 1994. p. 1250-75

Thesis: Erakinci G. Searching for antibodies against parasites in donors. Izmir: Ege University Health Sciences Institute. 1997.

Article in Electronic Format: Morse SS. Factors in the emergence of infectious diseases. Emerg Infect Dis (serial online) l995 Jan-Mar (cited 1996 June 5): 1(1): (24 screens). Available from: URL: http:/ www.cdc.gov/ncidodlElD/cid.htm.

ILLUSTRATIONS AND TABLES

Illustrations:

The illustrations should be numbered in Arabic numerals according to the sequence of appearance in the text, where they are referred to as Figure. 1, Figure. 2, etc.

If illustrations (or other small parts) of articles or books already published elsewhere are used in papers submitted to MBSJHS, the written permission of the authors and publisher concerned must be included with the manuscript. The original source must be indicated in the legend of the illustration in these cases.

Like the rest of the submission, the figures too should be blind. Any information within the images that may indicate an individual or institution should be blinded. To prevent delays in the evaluation process, all submitted figures should be clear in resolution and large in size (minimum dimensions: 100 × 100 mm).

Tables: Tables should be so constructed together with their captions and legends.

Tables should be included in the main document, presented after the reference list, and they should be numbered consecutively in the order they are referred to within the main text. Tables of numerical data should each be typed (with one-spacing) and numbered in sequence in Arabic numerals (Table 1, 2, etc.). They are referred to in the text as Table 1, Table 2, etc. The title of each table should appear above it. A detailed description of its contents and footnotes should be given below the body of the table.

Revisions: Authors should mark the changes they made on the main text in color while submitting their article revision files. The responses to the referees should be specified in a separate Word file. Revised articles should be sent to the journal within one month following the decision letter. If the revised version of the article is not uploaded within the specified time, the revision option may be canceled. If the authors need additional time for revision, they are required to submit their extension requests to the journal before the end of one month.

PROOFS, OFFPRINTS, MISCELLANEOUS

Proofs

Proofs will be sent by e-mail, as a pdf. Only printer's errors may be corrected; no change in, or additions to, the edited manuscript will be allowed at this stage. It should be kept in mind that proofreading is solely the authors' responsibility. A form with queries from the copyeditor may accompany the proofs. Please answer all queries and make any corrections or additions required. Corrections to the proofs must be returned by e-mail within 48 hours after receipt. If the publisher receives no response from the authors after 3 days, it will be assumed that there are no errors to correct and the article will be published.

Page charges

The journal is free and does not require any publication fee from the authors.

The journal is only published online.

The similarity rate of the articles should be done through iThenticate and should be at most 20% excluding the "References" part.

The editorial board has the authority to make necessary revisions in the format of the manuscript (without making any revision in the context) that does not comply with the above-mentioned requirements.

TYPES OF ARTICLES

The studies submitted to the Journal are accepted in Original research, Short papers, Case report, Review articles,

a) Original research: Prospective, retrospective and all kinds of experimental studies

Structure

Title

Abstract should be structured with subheadings (Objective, Methods, Results, and Conclusion) (average 200-400 word)

Key words

Introduction

Methods

Results

Discussion

Conclusion

Acknowledgements

References (most 40)

Whole text should not exceed 4500 words except for resources and English summary.

b) Short papers: Prospective, retrospective and all kinds of experimental studies

Structure

Title

Abstract should be structured with subheadings (Objective, Methods, Results, and Conclusion) (average 200-400 word)

Key Words

Introduction

Methods

Results

Discussion

Conclusion

Acknowledgements

References (most 20)

Whole text should not exceed 2700 words except for resources and English summary.

c) Case Report: They are rarely seen articles which differs in diagnosis and treatment. They should be supported by enough photographs and diagrams.

Structure

Title

Abstract (average 100-300 word)

Key words

Introduction

Case report

Discussion

Conclusion

Acknowledgements

References (most 20)

Whole text should not exceed 2200 words except for resources and English summary.

d) Review articles

Structure

Title

Abstract (average 200-400 word)

Key words

Introduction

The compilation text also including appropriate sub-headings,

Conclusion

Acknowledgements

References (most 50)

Whole text should not exceed 6550 words except for resources and English summary.

Middle Black Sea Journal of Health Science

AUGUST 2025 **VOLUME 11** **ISSUE 3**

CONTENTS

EDITORIAL

Dear Readers

We are pleased to meet with the readers a second time with this third issue of our journal where several health disciplines come together in this house. Since the initiation of its journey, our journal has focused on delivering knowledge to general physicians, specialists, and researchers via an inter-disciplinary approach.

Contents of the current issue range broadly from neurology and family medicine to pediatrics and anesthesiology, medical biology and pharmacology, microbiology and obstetrics and gynecology and other clinical directions. The necessity of a universal language has been further emphasized in the motion of health sciences knowledge and encounter in today world. In addition to representing the collective expertise and distinct foci of each discipline, we work to create an interdisciplinary space on the pages of our journal.

We would like to thank with all our heart our great authors for their important papers, and the diligent reviewers for making every issue a great one, as well as our faithful readers for their ever-interest! Along with this issue, may your scientific discovery & professional pursuit be enriched with another great volume and wish you healthy days.

Sincerely,

Prof. Dr. Ülkü KARAMAN

Editor

Middle Black Sea Journal of Health Science / Mid Blac Sea J Health Sci

August 2025; 11(3): 151-159

ORGINAL ARTICLE

DOI: 10.19127/mbsjohs.1603923

Investigation of Antibiotic Susceptibility Profiles of *Escherichia coli* Strains Grown in Urine Cultures

Hacer Özlem Kalaycı[1](ID), Mustafa Kerem Çalgın[1](ID), Yunus Emre İbik[1](ID)

[1]Ordu University, Faculty of Medicine, Deparment of Medical Microbiology, Ordu, Türkiye

Received: 18 December 2024, Accepted: 01 May 2025, Published online: 30 August 2025

Abstract

Objective: *Escherichia coli (E. coli)* is the most commonly isolated agent in urinary tract infections, and since antibiogram test results take a long time, empirical antibiotics are usually chosen when starting treatment. Since antibiotic susceptibilities show geographical differences, regional susceptibility results should be known. The aim of this study was to retrospectively determine the antibiotic susceptibilities of *E. coli* strains isolated from urine cultures between April 2021 and April 2024 in the Microbiology laboratory of Ordu University Medical Faculty Hospital.

Method: Urine samples were processed in the laboratory according to routine microbiological standards and examined with the BD Phoenix M50 automated bacterial identification and antibiotic susceptibility testing systems.

Results: During the study period, 38151 urine samples were sent to the laboratory and *E. coli* growth was detected in 4241 (31.7%) of them. The most sensitive antibiotics in *E. coli* were nitrofurantoin (2.8%), fosfomycin (4.3%), imipenem (4.4%) and amikacin (4.5%), while the most resistant antibiotics were ampicillin (60.4%), ceftazidime (36. 2%), levofloxacin (36.1%), trimethoprim/sulfamethoxazole (TMP-SXT) (35.1%), ciprofloxacin (32.1%) and amoxicillin-clavulanic acid (AMC) (31.5%). In addition, resistance rates have changed over the years.

Conclusion: As a result of increasing antibiotic resistance, treatment of urinary tract infections becomes more difficult. For this reason, determining regional antibiotic resistance profiles will help to ensure success in treatment by selecting appropriate antibiotics and to prevent unnecessary use of antibiotics.

Keyword: Antibiotic resistance, *E. coli*, urinary tract infection, fosfomycin.

Suggested Citation Kalayci HÖ, Calgin MK, Ibik YE. Investigation of Antibiotic Susceptibility Profiles of *Escherichia coli* Strains Grown in Urine Cultures. Mid Blac Sea Journal of Health Sci, 2025;11(3):151-159.

Address for correspondence/reprints:

E-mail: ozlemtekeli55@hotmail.com

Hacer Özlem Kalaycı

Telephone number: +90 (506) 284 19 59

INTRODUCTION

Urinary tract infection (UTI) is defined as the presence of bacteriuria and/or pyuria with clinical findings including dysuria, pollakuria, fever, costovertebral angle tenderness and urinary incontinence. It is the second most common among all infectious diseases and peaks in sexually active women aged 15-24 years and postmenopausal women (1). It has been reported that an average of 5 million cases is diagnosed with UTI every year in our country (2,3). In UTI, mostly a single bacterium is the causative agent and the most frequently isolated agent is *Escherichia coli* (*E. coli*). Complicated UTI should be treated rapidly in patients with underlying diseases such as urinary tract stones, diabetes mellitus and prostatic hyperplasia. Since the antibiogram test takes a long time to result, antibiotics are usually started empirically in the treatment of UTI. Due to antibiotic resistance, the antibiotic used after the correct diagnosis affects the success of the treatment. For this reason, the resistance profile of the hospital should be monitored at certain intervals in order to make appropriate antibiotic selection in treatment (4).

Antibiotic resistance rates against urinary pathogens may vary geographically and even different resistance patterns may be observed in different hospitals in the same region. There are also changes in resistance rates in the same center over time. Therefore, resistance rates especially against urinary pathogens should be determined at certain times and empirical antibiotic treatment should be planned in line with these data (5).

This study aimed to guide empirical antibiotic selection by determining the resistance rates of *E. coli* strains grown in urine cultures against antibiotics.

METHODS

In this study, *E. coli* strains isolated from urine cultures obtained between April 2021 and April 2024 in Ordu University Medical Faculty Hospital Microbiology laboratory were retrospectively analyzed. Morning urine samples or urine that had been in the bladder for 4 hours or more were collected by midstream urine collection method. Pediatric bags were used in children who could not provide urine specimens and Foley catheter specimens were used in patients with catheters. Urine samples collected in sterile urine containers were inoculated on sheep blood and EMB agar by quantitative inoculation (colony counting) method with a 0.001 ml standard extract without waiting. The samples were incubated at 37°C for 24 hours. A growth of one species of bacteria at 104 or more colony-forming units (cfu)/mL in urine was considered suggestive of bacteriuria, or a growth of two species of bacteria at 105 cfu/mL was considered suggestive of UTI. Bacterial species identification, antibiotic resistance patterns and extended spectrum beta-lactamase (ESBL) production were determined using the BD

Phoenix™ M50 automated bacterial identification and antibiotic susceptibility testing system. European Committee on Antimicrobial Susceptibility Testing (EUCAST) recommendations were used for bacterial identification and antibiotic susceptibility determination. The limitation of our study is that ESBL confirmation tests were not performed, and resistance results were reported according to the results obtained from the automated diagnosis system. Numbers and percentages were used for categorical variables in the statistical description of the data.

Information such as age, gender, growth agent and antibiotic resistance status of the patients were obtained and recorded on the laboratory information management system.

RESULTS

38151 urine culture specimens received by our laboratory were retrospectively analyzed. The causative microorganism growth was detected in 13368 of the urine culture samples, and *E. coli* was detected in 4241 (31.7%) of them. Of the samples with *E. coli* growth, 3260 were female, 981 were male and 33% of the patients were over 65 years of age. Of the samples with E. coli, 7.8% were from clinics, 3.4% from intensive care unit and the rest from outpatients.

Table 1. Antibacterial resistance rates of *E. coli* isolates by years

	2021-2022 (n=1404)		***2022-2023*** (n=1377)		***2023-2024*** (n=1460)		
	%	**n**	**%**	**n**	**%**	**n**	**%**
Nitrofurantoin	3.7	51	2.9	39	1.9	28	2.8
Fosfomycin	5.1	71	4.3	58	3.5	51	4.3
Imipenem	4.2	59	4.3	60	4.5	65	4.4
Amikacin	1.5	21	5.8	80	6.3	91	4.5
Meropenem	7.5	105	5.2	71	2.4	35	4.9
Piperacillin tazobactam	8.1	114	11.2	154	11.6	169	10.3
Gentamicin	19.7	277	12.2	168	12.5	182	14.8
GSBL	25.3	355	25.9	358	30.5	446	27.3
Ceftriaxone	31.8	447	30.3	416	31.8	461	31.4
Amoxicillin clavulanate	29.7	324	31	346	33.9	406	31.5
Ciprofloxacin	40.1	564	44.5	614	45.2	661	32.1
TMP-SXT	33.8	475	35.7	489	35.7	518	35.1
Levofloxacin	33.8	475	36.1	497	38.3	560	36.1
Ceftazidime	35.6	501	35	480	37.6	544	36.2
Ampicillin	57.1	801	61.5	846	62.5	912	60.4

TMP-SXT: Trimetoprim/sulfametoksazol. GSBL: Genişlemiş Spektrumlu Beta-laktamaz

Table 2: Distribution of *E.coli* strains according to clinics

Outpatient	*n*	*%*
Pediatrics	1382	32.6
Urology	911	21.5
Gynegology and obstetrics	427	10.1
Other clinics	1044	24.6
Inpatient		
Intensive Care Units	145	3.4
Wards	332	7.8
Total	4241	100

The most sensitive antibiotics in *E. coli* were nitrofurantoin (2.8%), fosfomycin (4.3%), imipenem (4.4%) and amikacin (4.5%), while the most resistant antibiotics were ampicillin (60.4%), ceftazidime (36. 2%), levofloxacin (36.1%), trimethoprim/sulfamethoxazole

(TMP-SXT) (35.1%), ciprofloxacin (32.1%) and amoxicillin-clavulanic acid (AMC) (31.5%). 1159 (27.3%) *E. coli* strains were positive for ESBL enzyme. The antibiotic resistance rates of *E. coli* according to years are given in Table 1. The distribution of urine samples with *E. coli* growth according to clinics is shown in Table 2.

DISCUSSION

UTI treatment should be initiated by evaluating guideline recommendations and local epidemiologic data (6). The gold standard diagnostic test in the diagnosis of UTI is urine culture. However, the process of determination of the causative pathogen in urine culture and antibiogram takes two days and therefore empirical treatment is initiated in most clinics. In this context, the antibiotic to be selected in empirical treatment should be chosen correctly. For this, the most common causative agents of the region or health center and the antibiotic resistance of the causative agents should be monitored and analyzed well (7,8). In order to start empirical antibiotic treatment in patients diagnosed with urinary tract infection, the resistance rate against the drug to be given should be below 20% (9).

The most common causative agent of urinary tract infections in our country and in the world is E. coli. Due to increasing resistance rates, the current antibiotic susceptibility profile should be taken into consideration for empirical treatment to be effective (10). Keskin et al. found the frequency of *E. coli* in urinary tract infections to be 73% (11). Similar to our study, Çakır and Acar found a prevalence of *E. coli* in urinary tract infections of 39.1% (12). In our study, *E. coli* was the most common causative agent (31.7%). According to our data, nitrofurantoin, fosfomycin, imipenem, amikacin, meropenem, piperacillin-tazobactam and gentamicin have low resistance rates.

Oral antibiotics are frequently preferred as the first choice in empirical treatment. In studies, the rate of resistance to ampicillin in *E. coli* strains was found to be more than 60% (13–16). In our country, AMC resistance is observed between 38.5-46% in *E. coli* strains (14,17,18). Due to high resistance rates, ampicillin and AMC are not recommended in the treatment of urinary infections in our country. In our study, a resistance rate of 60.4% to ampicillin and 31.5% to AMC was found. When we analyzed our data according to years, we observed an increase in resistance rates for both ampicillin and AMC. This is thought to be due to the fact that these antibiotics are still frequently preferred in our hospital.

The resistance rate of piperacillin/tazobactam, the other beta lactam/beta lactamase combination in our study, was found to be low (10.3%) as in other studies conducted in Türkiye (3,14,19). Especially in urinary tract infections caused by ESBL positive E. coli, piperacillin/tazobactam can be used effectively in treatment to prevent carbapenem resistance

(20). In our study, an increase in the resistance rate of piperacillin/tazobactam was found over the years.

Fluoroquinolones and TMP-SXT are among the most commonly used antimicrobial agents in empirical treatment due to their ease of oral administration. In the IDSA guidelines, TMP-SXT is recommended as the first choice, and quinolones are recommended as an alternative in regions with over 20% resistance to this antimicrobial agent. However, resistance to these antibiotics has increased in recent years (1,6,21). Avcıoğlu and Behçet found ciprofloxacin resistance in 41% and TMP-SXT resistance in 40% of *E. coli* strains isolated from urine (17). Duran et al. determined ciprofloxacin resistance as 42.9% and TMP-SXT resistance as 42.6% (14). Yüksek et al. found ciprofloxacin resistance to be 31.8% and resistance to TMP-SXT to be 38.9% (22). Çakır and Acar found 20.3% resistance to ciprofloxacin and 31.3% resistance to TMP-SXT (12). In our study, ciprofloxacin resistance rate was 32.1% and TMP-SXT resistance rate was 35.1%, which is lower than the resistance rates in Türkiye. However, due to the resistance rates detected, both fluoroquinolones and TMP-SXT are not an appropriate approach in the empirical treatment of urinary tract infections in our region. In our study, an increase in resistance to both ciprofloxacin and TMP-SXT was observed over the years.

In the Infectious Diseases Society of America (IDSA) guidelines, nitrofurantoin and fosfomycin with low resistance rates are recommended in the treatment of uncomplicated urinary tract infections due to their ease of oral use (23,24). In our country, resistance rates to these two agents are generally below 10% (3,14,17,18). In our study, resistance rates to fosfomycin and nitrofurantoin were 4.3% and 2.8%, respectively, and when we analyzed our data according to years, we observed a decrease in resistance rates. Our findings support that these two antibiotics may be appropriate empirical treatment options in our region.

Due to the widespread use of cephalosporins, especially third generation cephalosporins in urinary tract infections, resistance rates have increased in our country (25). In the study of Tuna et al., resistance to ceftriaxone was found to be 14.3% (8). In our study, ceftriaxone resistance rate was 31.4%. When we analyzed the resistance of *E. coli* to ceftriaxone over the years, no change was observed.

ESBL positivity in *E. coli* is increasing day by day and makes treatment difficult. In studies conducted in our country, ESBL positivity rate in *E. coli* strains isolated from urine samples varies between 8-42% (6,19,26). In our study, the rate of ESBL positive *E. coli* strains was 27.3%.

Aminoglycosides are successfully used in urinary infections because they can eradicate

bacteria in the urinary system at a high rate and reach high concentrations in urine. Although their use is limited especially in patients with renal failure due to their nephrotoxicity, they are preferred in the treatment of resistant infections due to their low resistance profiles (3,18,19,27). In our study, the low resistance rate to amikacin (4.5%) indicates that this agent is an important alternative for our region. However, when we look at the resistance profile of amikacin over the years, a significant increase is observed. Amikacin should be used more carefully due to this increase. Gentamicin, on the other hand, has shown a decrease in resistance over the years.

Carbapenems are frequently preferred in parenteral treatment of UTIs caused by resistant microorganisms. In many studies, the lowest resistance rates were reported against carbapenems in urinary tract infections caused by *E. coli* (19,27). Çaycı et al. found imipenem resistance to be 0.12% for *E. coli* and 0.15% for meropenem (13). Kömürlüoğlu et al. found imipenem resistance in *E. coli* isolates as 1.5% and meropenem resistance as 1.3% (27). In our study, imipenem resistance was 4.4% and meropenem resistance was 4.9%. When we analyzed the resistance rates of *E. coli* according to the years, imipenem resistance did not change, while meropenem resistance decreased. We think that this is due to the addition of amikacin to the treatment protocol instead of meropenem in inpatients.

In other studies, *E. coli* was isolated in 60.4%-72.8% of outpatients and 39-46% of ward patients (28–30). In our study, *E. coli* was isolated in 88.8% of the samples obtained from outpatients, while it was isolated in 11.2% of the ward patients.

CONCLUSION

In conclusion, our study shows that nitrofurantoin may be a good treatment alternative with a low resistance rate in the treatment of urinary tract infections caused by *E. coli*. Our data will guide clinicians in choosing the appropriate antibiotic and preventing unnecessary antibiotic use. Therefore, it is also important for each center to create its own data and follow it regularly.

Ethics Committee Approval: Approval for this study was obtained from the Ordu University Non-Interventional Research Ethics Committee (Date: 11/10/2024 Number: 146).

We state that the parents have given their written informed consent to be involved in the study, in accordance with the Declaration of Helsinki.

Peer-review: Externally peer-reviewed

Author Contributions: Concept: HKO, MKÇ, YEİ, Design: HKO, MKÇ, YEİ, Data Collection and Processing: HKO, MKÇ, YEİ,

Analysis and Interpretation: HKO, MKÇ, YEİ, Writing: HKO, MKÇ, YEİ

Conflict of Interest: The authors declared no conflict of interest.

Financial Disclosure: The authors declared that this study has not received no financial support.

REFERENCES

1. Kaye KS, Gupta V, Mulgirigama A, Joshi AV, Scangarella-Oman NE, Yu K, et al. Antimicrobial resistance trends in urine Escherichia coli isolates from adult and adolescent females in the United States from 2011 to 2019: rising ESBL strains and impact on patient management. Clin Infect Dis. 2021;73(11):1992-9.
2. Forbes BA, Sahm DF, Weissfeld AS. Diagnostic microbiology. s.288-302, St Louis: Mosby (2007).
3. Budak S, Utku S, Aksoy EE, Karakeçe E, Aydemir H, Budak GG, et al. Investigating the distribution of the bacteria that lead to urinary tract infections and antibiotic susceptibility of E. coli. New J Urol. 2015;10(1):21-4.
4. Sierra-Díaz E, Hernández-Ríos CJ, Bravo-Cuellar A. Antibiotic resistance: Microbiological profile of urinary tract infections in Mexico. Cir Cir. 2019;87(2):176-82.
5. Temoçin F, Köse H. Evaluation of Extended Spectrum Beta-lactamase Production Rates and Antibiotic Susceptibilities of Escherichia coli and Klebsiella pneumoniae Strains Isolated from Urine Cultures of Outpatients. ANKEM Derg. 2018;32(3):79-86.
6. McLellan LK, Hunstad DA. Urinary tract infection: pathogenesis and outlook. Trends Mol Med. 2016;22(11):946-57.
7. Çalgın MK, Çetinkol Y, Erdil A. Antibiotic resistance rates and bacteria isolated from urine samples of pediatric patients in Ordu. Bozok Med J. 2017;7(1):64-9.
8. Tuna A, Arslan F, Akkuş I, Böke E, Şahin O, Kaçmaz B, et al. Investigation of resistance rates of Escherichia coli strains isolated from urine cultures to antibiotics frequently used in clinics. Kırıkkale University Med J. 2024;26(1):1-4.
9. Sucu N, Aktoz-Boz G, Bayraktar O, Çaylan R, Aydın K, Köksal İ. The change of antibiotic susceptibilities of uropathogen Escherichia coli strains in years. Klimik Journal. 2004;17(2):128-31.
10. Jadoon SA, Ahmed A, Irshad R. Spectrum of bacterial culture and drug sensitivity vs resistance in uncomplicated urinary tract infection. J Ayub Med Coll Abbottabad. 2018;30(3):432-8.
11. Keskin BH, Çalışkan E, Kaya S, Köse E, Şahin I. Bacteria that cause urinary system

infections and antibiotic resistance rates. Journal of Turkish Society of Microbiology. 2021;51(3):254-62.

12. Çakır A, Acar H. Comparison of empiricular antibiotic and culture antibiogram sensitivity for urinary tract infection in emergency department. Turk J Clin Lab. 2023;14(2):285-93.

13. Çaycı YT, Karacan G, Yoosefi M, Bilgin K, Vural DG, Birinci A. Retrospective evaluation of gram-negative bacteria and their antibiotic susceptibility isolated from urine cultures in children. Ahi Evran Med J. 2021;6(2):168-73.

14. Duran H, Çeken N, Atik TK. Antibiotic resistance rates of Escherichia coli and Klebsiella pneumoniae strains isolated from urine culture: A four-year analysis. ANKEM Derg. 2020; 34(2):41-7.

15. Kengne M, Dounia AT, Nwobegahay JM. Bacteriological profile and antimicrobial susceptibility patterns of urine culture isolates from patients in Ndjamena, Chad. Pan Afr Med J. 2017;28(1).

16. Samancı Aktar G, Ayaydın Z, Rahmanalı Onur A, Gür Vural D, Temiz H. Resistance rates against various antimicrobials in Escherichia coli strains isolated from urine samples. Kocaeli Med J. 2018;7(1):8-13.

17. Avcıoğlu F, Behçet M. Evaluation of resistance rates of Escherichia coli isolates of urinary tract infection to various antibiotics. Journal of Turkish Society of Microbiology. 2020;50(3):172-7.

18. Gündüz A, Mansur A. Antimicrobial resistance rates in Escherichia coli strains isolated in urine cultures of outpatients: five years analysis. Turk Bull of Hyg and Exp Bio. 2023;80(1):23-32.

19. Teker B, Sever N, Garashova D. The effect of age and gender on antibiotic resistance of Escherichia coli isolates of urinary tract infection. Online Turk J Health Sci. 2021;6(2):300-9.

20. Aydemir O, Terzi HA, Köroğlu M, Altındiş M. Piperacillin / tazobactam in-vitro activity in Escherichia coli and Klebsiella pneumoniae strains with extended spectrum beta-lactamase production. Online Turk J Health Sci. 2019;4(2):118-27.

21. Mancuso G, Midiri A, Gerace E, Marra M, Zummo S, Biondo C. Urinary tract infections: the current scenario and future prospects. Pathogens. 2023;12(4):623.

22. Yüksek G, Memiş N, Öksüz S. Antibiotic susceptibility of Escherichia coli strains isolated from urine samples. J DU Health Sci Inst. 2021;11(2):137-42.

23. Gupta K. Acute simple cystitis in females. UpToDate Post TW Ed UpToDate Waltham MA. 2023.

24. Gupta K, Hooton TM, Naber KG, Wullt B, Colgan R, Miller LG, et al. International

clinical practice guidelines for the treatment of acute uncomplicated cystitis and pyelonephritis in women: a 2010 update by the Infectious Diseases Society of America and the European Society for Microbiology and Infectious Diseases. Clin Infect Dis. 2011;52(5):e103-20.

25. Mert D, Çeken S, Ertek M. The isolated bacteria from culture and antibiotic susceptibilities in urinary tract infections. Turk Bull of Hyg and Exp Bio. 2020;77(1):25-32.

26. Aşgın N, Çakmaklıoğulları EK. In-vitro antibiotic resistance profile of *E. coli* strains isolated from community-acquired paediatric urinary tract infections in Karabük province. J Contemp Med. 2017;7(3):241-5.

27. Kömürlüoğlu A, Aykaç K, Özsürekçi Y, Başaranoğlu ST, Bıçakçıgil A, Liste Ü, et al. Antibiotic resistance distribution of gram-negative urinary tract infectious agents: single center experience. Turkish J Pediatr Dis. 2018;12(1).

28. Avcıküçük H, Altın N. Evaluation of the distribution and antibiotic resistance profile of strains isolated from urine specimens. Klimik Journal. 2022;35(2):95-102.

29. Çilburunoğlu M, Kirişci O, Yerlikaya H, Uğurlu H, Aral M, Muratdağı G. The evaluation of the distribution and antimicrobial susceptibility profile of strains isolated from urine specimens at a university hospital. Sakarya Med J. 2020;10(4):677-83.

30. Kalyoncu BN, Koçoğlu E, Özekinci T, Biçer RT, Aydın G, Önder N, et al. Evaluation of urinary system pathogens and their antibiotic resistance profiles isolated in a city hospital in Istanbul. ANKEM Derg. 2023;37(1):18-27.

Middle Black Sea Journal of Health Science / Mid Blac Sea J Health Sci
August 2025; 11(3): 160-178

ORGINAL ARTICLE **DOI:** 10.19127/mbsjohs.1632988

The Impact of Vitamin D on Follicular Development and Inflammatory Markers in Experimental Polycystic Ovary Syndrome

Seçil Tan[1(ID)], Gülçin Abban Mete[2(ID)], Semih Tan[3(ID)], Nazlı Çil[2(ID)], Mücahit Seçme[4(ID)], Yavuz Dodurga[5(ID)], Ergun Mete[6(ID)]

[1]Pamukkale University, Institute of Health Sciences, Department of Cancer Molecular Biology, Denizli, Türkiye
[2]Pamukkale University, Faculty of Medicine, Department of Histology and Embryology, Denizli, Türkiye
[3]Ordu University, Faculty of Medicine, Department of Histology and Embryology, Ordu, Türkiye
[4]Ordu University, Faculty of Medicine, Department of Medical Biology, Ordu, Türkiye
[5]Pamukkale University, Faculty of Medicine, Department of Medical Biology, Denizli, Türkiye
[6]Pamukkale University, Faculty of Medicine, Department of Medical Microbiology, Denizli, Türkiye

Received: 4 February 2025, Accepted: 29 June 2025, Published online: 30 August 2025

Abstract

Objective: Polycystic ovary syndrome (PCOS) is a prevalent endocrine disorder among women of reproductive age, characterized by chronic anovulation, infertility, hyperandrogenism, and hirsutism. Additionally, PCOS is associated with metabolic disturbances such as insulin resistance, obesity, endothelial dysfunction, and metabolic syndrome. Recent research suggests that chronic inflammation and vitamin D deficiency may play a role in these comorbidities. However, studies investigating the relationship between vitamin D and PCOS have yielded conflicting results. Moreover, the immunohistochemical mechanisms by which inflammatory cytokines, including IL-1β, IL-6, and TNF-α, affect ovarian tissue in PCOS remain unclear.

Method: This study aimed to evaluate the short-term and mid-term effects of vitamin D on IL-1β, IL-6, and TNF-α expression in the ovaries of a dehydroepiandrosterone (DHEA)-induced PCOS rat model. Two different vitamin D administration strategies were investigated: pre-treatment (daily administration starting two hours before PCOS induction) and post-treatment (daily administration starting on day 20 of DHEA injection and continuing throughout the experimental period). The effects of vitamin D on ovarian inflammation and follicular morphology were analyzed.

Results: According to hematoxylin-eosin staining results, the number of cystic follicles was significantly increased in the PCOS group (Group 2: 7.17±0.87) compared to the control group (Group 1: 2.17±0.40, p=0.002), whereas early vitamin D treatment significantly reduced this number (Group 3: 4.00±0.51, p=0.009). However, in the long-term PCOS group (Group 4: 8.33±1.74), the number of cystic follicles was the highest among all groups, showing no significant difference compared to Group 2 (p=0.747). In the short term, vitamin D did not significantly alter IL-1β, IL-6, or TNF-α expression in ovarian tissue but effectively reduced the number of cystic follicles. However, in the prolonged exposure group, an increase in IL-1β, IL-6, and TNF-α expression was observed. Although RT-PCR analysis revealed increased expression levels of IL-

.

1β, IL-6, and TNF-α genes in all groups compared to the control group, a statistically significant elevation was observed only in the long-term PCOS group for IL-6 (p=0.016) and IL-1β (p=0.036).
Conclusion: While vitamin D has demonstrated anti-inflammatory properties, it also plays a crucial role in follicular development, oocyte maturation, ovulation, and menstrual cycle regulation. The observed increase in inflammatory cytokines in vitamin D-treated groups might suggest a transient physiological response potentially associated with efforts to restore disrupted reproductive processes. In the short term, vitamin D significantly reduced cystic follicle formation but did not markedly impact ovarian inflammation markers. Long-term studies are required to determine the sustained effects of vitamin D at the molecular and tissue levels and to elucidate the precise stage at which it begins to mitigate the metabolic consequences of PCOS

Keywords: Vitamin D, Polycystic Ovary Syndrome (PCOS), Folliculogenesis, Inflammatory Cytokines, Ovarian Morphology

Suggested Citation Tan Secil, Abban Mete G, Tan S, Çil N, Secme M, Dodurga Y, Mete E. The Impact of Vitamin D on Follicular Development and Inflammatory Markers in Experimental PCOS. Mid Blac Sea Journal of Health Sci, 2025;11(3):160-178.

Address for correspondence/reprints:

Seçil Tan

Telephone number: +90 (553) 613 68 53

E-mail: secilytan@gmail.com

INTRODUCTION

Polycystic ovary syndrome (PCOS), first described in 1935, is a complex of symptoms characterized by hyperandrogenism, hirsutism, and polycystic ovarian morphology. PCOS is one of the most common endocrine disorders in women of reproductive age and is associated with long-term metabolic and cardiovascular complications (1,2). Clinical studies have linked PCOS with impaired glucose tolerance, cardiovascular diseases, type II diabetes, follicular maturation arrest, abnormal androgen production in theca cells, obesity, endometrial hyperplasia, and increased risks of endometrial and ovarian cancers (3,4). Although its etiology remains unclear, genetic and environmental factors are considered key contributors to PCOS pathogenesis. While the diagnostic criteria for PCOS remain under debate, the molecular pathways connecting PCOS to its metabolic complications also remain contentious. Recent studies suggest that chronic low-grade inflammation plays a significant role in PCOS pathogenesis and the development of associated metabolic complications (5). A study reported increased macrophage counts and elevated expression of TNF-α, IL-1, and IL-6 in the theca layer and stroma of polycystic ovaries (6). Similarly, elevated levels of TNF-α, IL-1, and IL-6 were found in serum and follicular fluid in another study (7), though some studies reported no changes in their expression (8).

Metformin and clomiphene citrate are the most commonly used medications for PCOS treatment, particularly to improve ovulation. However, long-term use of these drugs may lead to adverse effects such as multiple follicle development, ovarian hyperstimulation, multiple and ectopic pregnancies, and neural tube defects (9). This highlights the need for alternative therapies. Current research explores the efficacy of antioxidants and agents such as vitamin D in PCOS treatment. Beyond its role in calcium metabolism and bone mineralization, vitamin D is also crucial for reproductive function. Studies suggest that vitamin D deficiency is associated with infertility, adequate vitamin D intake improves outcomes in vitro fertilization, and it may also help treat primary dysmenorrhea (9,10).

In PCOS patients, vitamin D has been shown to regulate body mass index, insulin resistance, hyperandrogenism, and menstrual cycles (11). However, despite numerous studies investigating the relationship between PCOS and vitamin D, the results remain inconclusive. This study aims to examine the effects of vitamin D on inflammation, particularly on the proinflammatory cytokines IL-1, IL-6, and TNF-α, in the ovaries of rats with experimentally induced PCOS.

METHODS

This study was approved by the Pamukkale University Animal Experiments Ethics Committee under the protocol number PAUHDEK-2015/03. A total of 34 prepubertal Wistar albino female rats, 21 days old, were obtained from the Pamukkale University Experimental Research Unit for the study. Optimal environmental conditions recommended for all subjects were maintained by the same facility. The rats were housed in cages within a room providing a 12-hour light/dark cycle, 60-70% relative humidity, and a controlled temperature of 20-24°C. They were fed ad libitum with pellet feed containing 21% crude protein (Purina) and provided with fresh drinking water daily

Separation of Experimental Groups and Induction of Experimental PCOS

This study was designed as a completely randomized controlled experimental animal model study. Rats were selected using non-probability sampling method, aged 21 days and weighing 45-50 g. After weighing the rats they were randomly divided into five groups and marked. Trans-dehydroandrosterone (Sigma, St. Louis, MO, USA) was used to induce experimental PCOS a previously designed (12,13). For rats weighing approximately 50 g, 3 mg of DHEA was dissolved in 0.01 ml of 95% ethanol and then mixed with 0.09 ml sesame oil. This mixture was administered daily via subcutaneous injection for 20 days. The rats were weighed every three days, and the dose was adjusted accordingly if weight changes occurred. In Groups I, II, III, and V, injections were terminated on the 21st day, while in Group

IV, injections were terminated on the 41st day, after which the ovaries were collected, and the animals were sacrificed.

Group I (N=6): Served as the control group, receiving only sesame oil (0.2 ml/100 g) via subcutaneous injection daily for 20 days.

Group II (N=6): Administered DHEA (6 mg/100 g in 0.2 ml sesame oil) via subcutaneous injection daily for 20 days to induce PCOS.

Group III (N=6): Administered vitamin D (120 ng/100 g) daily, followed 2 hours later by DHEA (6 mg/100 g in 0.2 ml sesame oil), both via subcutaneous injection for 20 days.

Group IV (N=6): Administered DHEA (6 mg/100 g in 0.2 ml sesame oil) via subcutaneous injection daily for 20 days. From the 20th day onward, DHEA administration continued with the addition of vitamin D (120 ng/100 g), given 2 hours prior to DHEA, for an additional 20 days.

Group V (N=10): Administered vitamin D (120 ng/100 g) via subcutaneous injection daily for 20 days.

Collection of Vaginal Smear Samples and Determination of Menstrual Cycle Stages

Vaginal smear samples were collected from all groups starting from the 10th day of the experiment until the 21st day. Additionally, in Group IV, smear samples were collected from the 30th to the 40th day. The stages of the menstrual cycle were determined, and rats that did not exhibit the estrus phase were considered to have developed PCOS.

Preparation of Tissues and Sectioning

The rats were sacrificed under general anesthesia induced by intraperitoneal injection of a combination of 30 mg/kg ketamine hydrochloride and 6 mg/kg 2% xylazine hydrochloride, followed by decapitation. The left ovaries were placed in Eppendorf tubes containing 500 µl of TRIzol and stored at -80°C for PCR analysis. The right ovaries were placed in tissue preservation cassettes and fixed in 10% formaldehyde (Tekkim Formaldehyde, Lot: 070312510). Using the light microscopy follow-up method, the tissues were embedded in paraffin blocks, and 3-micrometer-thick sections were prepared using a Leica RM-2125 Rotary Microtome. These sections were mounted on lysine-coated slides (Marienfeld Laboratory Glassware Histobond (+), Lot: 23573). Immunohistochemical staining was then performed on the sections to determine TNF-α, IL-6, and IL-1β activation. The slides were subsequently examined double blind under an Olympus BX-51 light microscope equipped with an Olympus DP72 digital camera.

Immunohistochemical Staining Method

Following deparaffinization, tissue sections were rehydrated by passing them through a descending ethanol series, spending 2 minutes

in each step. The sections were then rinsed with tap water and placed in phosphate-buffered saline (PBS; Thermo Fisher, Gibco Lot: 70011044) for 10 minutes. To block endogenous peroxidase activity, a solution of 30% H_2O_2 in methanol (1:9 ratio) was applied. The slides were washed three times with PBS, after which a serum blocking solution was applied and incubated for 10 minutes at room temperature. Once the blocking solution (Histostain-Plus kit, 1018708A, İnvitrogen) was removed, the primary antibody was carefully applied dropwise to the moistened slides.

The slides were incubated overnight with the following primary antibodies: IL-1β (F2212, Santa Cruz Biotechnology), TNF-α (NB600-587, Novus Biotechnology) and IL-6 (NB600-1131) diluted 1:100. Antibodies were prepared in PBS. After incubation, the sections were rinsed three times with PBS for 2 minutes per wash. A broad-spectrum secondary antibody was then applied for 20 minutes, followed by another round of three PBS washes for 2 minutes each. The sections were then treated with horseradish peroxidase-conjugated streptavidin (HRP-SA; Reagent C) for 10 minutes. After three additional PBS washes, the sections were treated with the DAB-Plus Substrate Kit (1018723A, Invitrogen) for 3–10 minutes to visualize the staining. Subsequently, the sections were counterstained with Harris hematoxylin (Merck), rinsed with tap water, and dehydrated through an ascending ethanol series (70%, 80%, 90%, and 100%) for 2 minutes at each concentration. Finally, the slides were mounted with coverslips using Entellan.

The intensity of staining was evaluated using the following scale:

- (+++): Strong staining
- (++): Moderate staining
- (+): Weak staining
- (+/-): Very weak staining
- (-): No staining
- (/): Structure not observed

RNA Isolation Using TRIzol

Tissue samples were homogenized in TRIzol reagent (500 µL per sample) to ensure complete lysis. After homogenization, 200 µL of chloroform was added to each sample, followed by vigorous shaking for 15 seconds. The samples were then incubated at room temperature for 2–3 minutes and centrifuged at 12,000 xg for 15 minutes at 4°C to separate the phases. The upper aqueous phase, containing RNA, was carefully transferred to a new tube. An equal volume of isopropanol was added, and the mixture was gently inverted several times to precipitate the RNA. The samples were incubated at room temperature for 10 minutes and centrifuged at 12,000 xg for 10 minutes at 4°C. The resulting RNA pellet was washed with 75% ethanol, vortexed briefly, and centrifuged

again at 10,000 xg for 5 minutes at 4°C. The ethanol was removed, and the RNA pellet was air-dried for a few minutes before being dissolved in an appropriate volume of RNase-free water. The concentration and purity of the isolated RNA were determined using Nanodrop (Thermo, USA) by measuring absorbance at 260 nm and 280 nm. The RNA samples were then stored at -80°C until further analysis.

cDNA Synthesis

cDNA synthesis was performed from the isolated RNA using the ‘‘High-Capacity cDNA Reverse Transcription Kit’’ (Lot No: 00325690; AB Applied Biosystems, Lithuania) following the manufacturer’s protocol. Following the preparation of the reaction mixture, the samples were incubated sequentially at 25°C for 10 minutes, 37°C for 120 minutes, and 85°C for 5 minutes to complete the cDNA synthesis. The synthesized cDNA was stored at -20°C until use for RT-PCR analysis.

Real-Time Polymerase Chain Reaction (RT-PCR)

TNF-α, IL-1β, IL-6 gene expression was performed on RT-PCR according to the SYBR Green qPCR Master Mix (Applied Biosystems, USA) protocol. The forward and reverse sequences of these genes are summarized in Table 1. GAPDH was used as the reference housekeeping gene. All reactions were performed using the StepOnePlus Real-Time PCR system (Applied Biosystems, USA).

.

Table 1. Forward and reverse primer sequences of the genes used in the study

Gene Name	Primer sequence
GAPDH	Fw: TCATCTCCGCCCCTTCCGCT Rw: GAGCAATGCCAGCCCCAGCA
IL-6	Fw: TCCTACCCCAACTTCCAATGCTC Rw: TTGGATGGTCTTGGTCCTTAGCC
IL-1β	Fw: CACCTCTCAAGCAGAGCACAG Rw: GGGTTCCATGGTGAAGTCAAC
TNF-α	Fw: AAATGGGCTCCCTCTCATCAGTTC Rw: TCTGCTTGGTGGTTTGCTACGAC

Statistical Analysis of Data

The ovarian sections of all subjects were examined for the counts of corpus luteum, primordial, primary, secondary, tertiary, and cystic follicles. All values are presented as mean ± standard error. In non-parametric data, differences between groups were evaluated with the Kruskal-Wallis test, and differences between two groups were evaluated with the Mann-Whitney U test. The conformity of the data to normal distribution was evaluated with the Shapiro-Wilk test. Statistical analyses were performed using the SPSS V.21 (DEMO, IBM Corp., Armonk, NY, USA) software package

and a p-value of <0.05 was considered statistically significant.

The web-based "RT² Profiler™ PCR Array Data Analysis" program was used for gene expression analysis. The method relies on comparing two expression results within ±3 standard deviations (SD), enabling the relative quantification of gene expression levels between the control and dose groups. Group comparisons were statistically analyzed using the "Student's t-test" function within the same program.

RESULTS

Evaluation of Ovarian Morphology and Follicle Counts with Hematoxylin-Eosin Staining

Ovarian morphology and follicle counts were assessed using hematoxylin-eosin staining. The statistical comparisons of follicle counts among groups are presented in Table 2. The table includes comparative analyses and significance levels for different follicle types (primordial, primary, secondary, tertiary, and cystic) and the corpus luteum.

Table 2. The statistical comparisons of follicle counts among groups

Compared Groups	Primordial Follicle	Primary Follicle	Secondary Follicle	Tertiary Follicle	Cystic Follicle	Corpus Luteum
1-2	0.009**	0.041*	0.002**	0.002**	0.002**	1.000
1-3	0.043*	0.108	0.013*	0.083	0.002**	0.567
1-4	0.006**	0.006**	0.016*	0.718	0.002**	0.402
1-5	0.286	0.014*	0.008**	0.042*	1.000	0.067
2-3	0.111	0.179	0.003**	0.003**	0.009**	0.565
2-4	0.598	0.410	0.071	0.131	0.747	0.402
2-5	0.038*	0.871	0.003**	0.006**	0.002**	0.067
3-4	0.070	0.003**	0.004**	0.127	0.020*	0.204
3-5	0.805	0.003**	0.613	0.094	0.002**	0.138
4-5	0.019*	0.096	0.004**	0.002**	0.002**	0.934

In Group 1, follicles at all stages of development were observed in the ovarian tissue. The granulosa layers of secondary and tertiary follicles appeared thick and normal, while the ovarian stroma exhibited a normal appearance (Figure 1A-B).

In Group 2, the number of cystic follicles (7.17±0.87) was significantly higher compared to the control group (Group 1: 2.17±0.40, p=0.002). In these follicles, thinning of the granulosa cell layers, degeneration of the cells, and separation between cells were observed. Additionally, the ovarian stroma showed areas of cellular depletion, forming gaps in certain regions (Figure 1C-D).

In Group 3, cystic follicles persisted but were significantly reduced in number (4.00±0.51) compared to Group 2 (p=0.009). Although

cellular depletion in the ovarian stroma was still observed, it was less pronounced than in Group 2 (Figure 1. E-F).

In Group 4 (long-term), the number of cystic follicles (8.33±1.74) was the highest among all groups and showed no significant difference compared to Group 2 (p=0.747). Extensive cellular loss in the ovarian stroma, similar to Group 2, was observed, with gaps evident in the tissue (Figure 1G-H).

In Group 5, which received only vitamin D, no cystic follicles were observed. While minimal cellular loss was noted in certain areas of the ovarian stroma, these changes were sparse. Follicles at all developmental stages appeared normal, and no degeneration was detected in granulosa cells (Figure 1I-J).

PCOS significantly reduced the number of primordial follicles in Group 2 compared to the control group (Group 1: 5.50±0.88; Group 2: 1.67±0.47, p=0.009), indicating that PCOS adversely affects early follicular development. Similar effects were observed in the long-term PCOS group (Group 4: 1.50±0.50, p=0.006). Secondary follicles were also significantly affected, as evident from the difference between Group 1 (2.67±0.42) and Group 2 (0.17±0.16, p=0.002). However, early administration of vitamin D appeared to mitigate these effects, as demonstrated by the significantly increased number of secondary follicles in Group 3 (4.67±0.42). In Group 4, the number of secondary follicles was 1.00±0.36, slightly higher than in Group 2 but significantly lower than in the control group (p=0.008). A similar pattern was observed in tertiary follicles. The number of tertiary follicles in Group 2 (0.50±0.22) was significantly lower than in the control group (Group 1: 2.17±0.16, p=0.003). In Group 3, the number of tertiary follicles (2.83±0.30) was significantly higher than in Group 2 (p=0.003) and comparable to the control group (Group 1: 2.17±0.16). In Group 4, the number of tertiary follicles (1.67±0.55) was slightly higher than in Group 2 but significantly lower than in the control group (p=0.042).

Immunohistochemical Analysis: Expression of Inflammatory Markers in Ovarian Tissue

The results of immunohistochemical staining among the groups are shown in Figures 2, 3, and 4, and the scoring of staining results is summarized in Table 3. IL-1β expression was not observed in Groups 1, 2, 3, and 5, while moderate expression was detected in the corpus luteum of Group 4 (Figure 2).

IL-6 expression was moderate in oocytes of Groups 1 and 3, while strong positive expression was observed in Groups 4 and 5 (Figure 3). No IL-6 expression was observed in granulosa cells or theca layers in any group. Moderate IL-6 expressions were observed in the corpus luteum of Group 3, while strong positive expression was detected in Group 4. Weak positive IL-6 expression was noted in ovarian stromal cells of Groups 3 and 4,

whereas moderate expression was observed in Group 5. In terms of ovarian connective tissue, strong IL-6 expression was detected in Groups 3 and 4, while moderate expression was noted in Group 5.

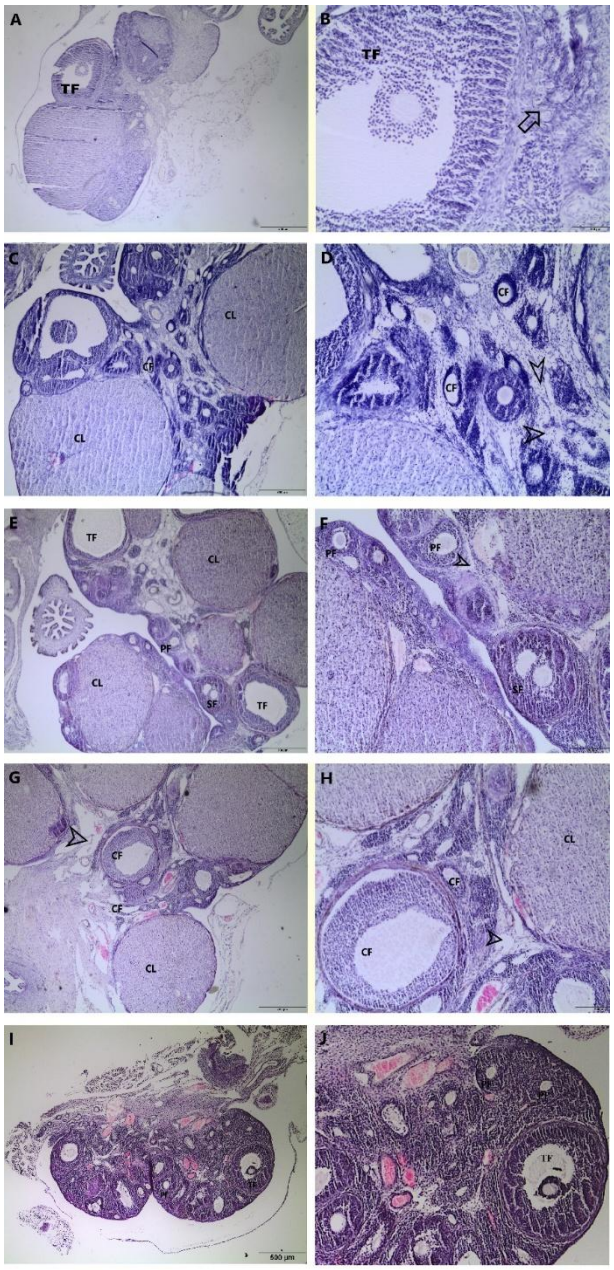

Figure 1. General view of ovarian tissue. Group 1 (A, B), Group 2 (C, D), Group 3 (E, F), Group 4 (G, H), Group 5 (I, J). Primordial follicle: (arrow), primary follicle: (PF), secondary follicle: (SF), tertiary follicle: (TF), corpus luteum: (CL), cystic follicle: (CF), stromal cellular loss and openings (arrowhead). Hematoxylin–eosin staining.

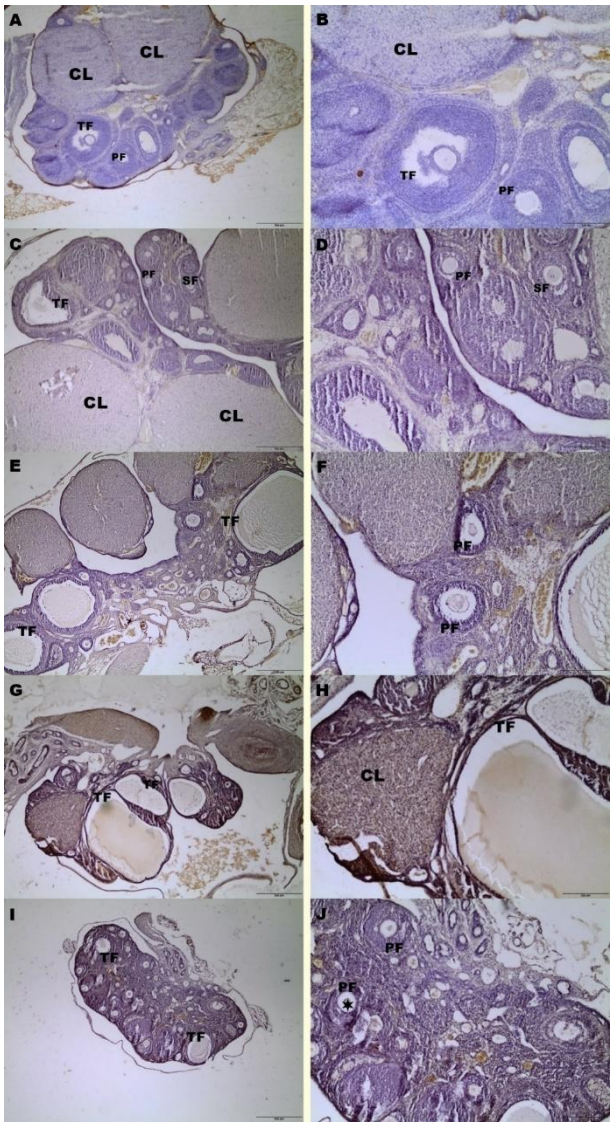

Figure 2. Expression of IL-1β in ovarian tissue. Group 1 (A, B), Group 2 (C, D), Group 3 (E, F), Group 4 (G, H), Group 5 (I, J). IL-1β primary antibody dilution ratio: 1:100. DAB, counterstained with hematoxylin.
Primary follicle: (PF), secondary follicle: (SF), tertiary follicle: (TF), corpus luteum: (CL), cystic follicle: (CF), oocyte: (asterisk).

TNF-α expression was negative in oocytes of Group 1, moderate in Groups 2 and 3, and strong in Groups 4 and 5 (Figure 4). No TNF-α expression was observed in granulosa cells or theca layers in any group. Moderate positive TNF-α expression was detected in the corpus luteum of Groups 3 and 4, while no expression

was observed in Groups 1, 2, and 5. In ovarian stromal cells, weak TNF-α expression was noted in Groups 3 and 4, whereas moderate expression was observed in Group 5. Regarding ovarian connective tissue, strong positive TNF-α expression was found in Groups 4 and 5, while it was negative in the other groups.

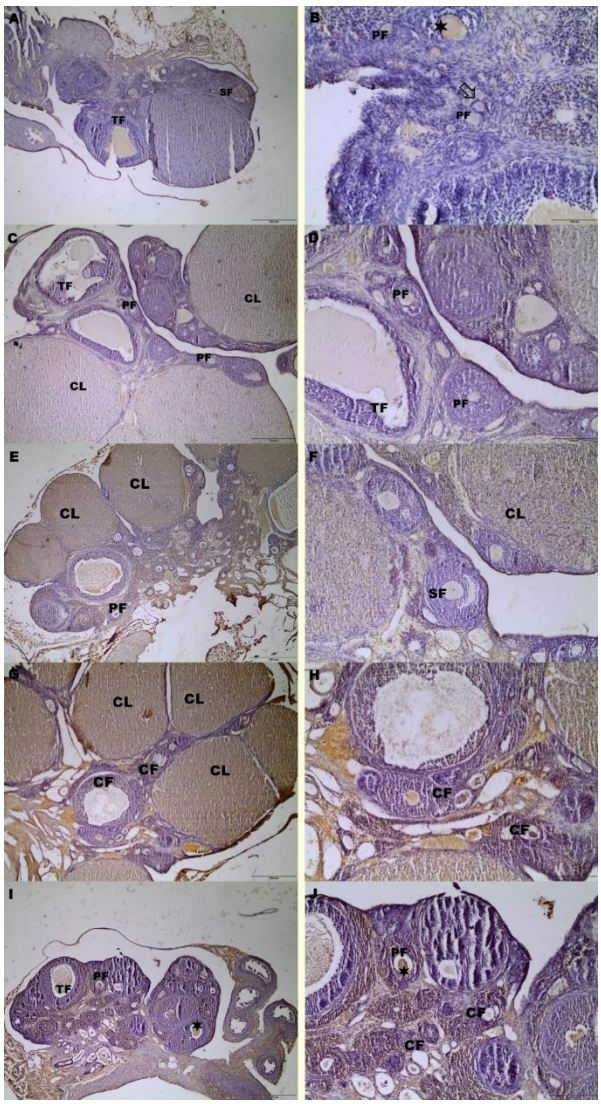

Figure 3. Expression of IL-6 in ovarian tissue. Group 1 (A, B), Group 2 (C, D), Group 3 (E, F), Group 4 (G, H), Group 5 (I, J). IL-6 primary antibody dilution ratio: 1:100. DAB, counterstained with hematoxylin.
Primordial follicle: (arrow), primary follicle: (PF), secondary follicle: (SF), tertiary follicle: (TF), corpus luteum: (CL), cystic follicle: (CF), oocyte: (asterisk).

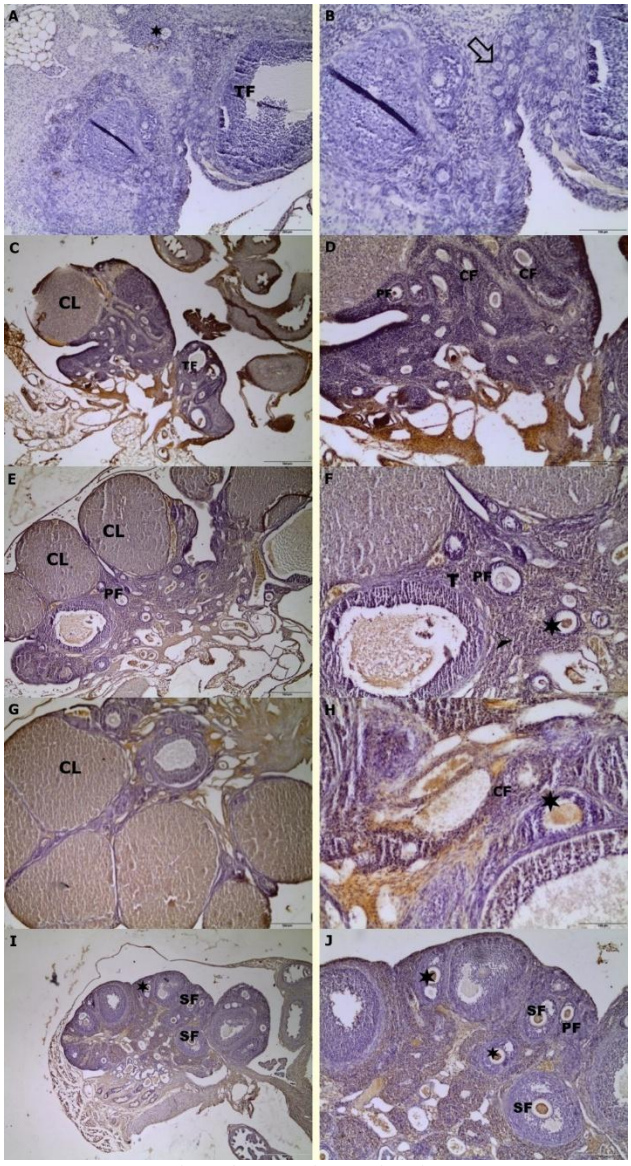

Figure 4. Expression of TNF-α in ovarian tissue. Group 1 (A, B), Group 2 (C, D), Group 3 (E, F), Group 4 (G, H), Group 5 (I, J). TNF-α primary antibody dilution ratio: 1:100. DAB, counterstained with hematoxylin.Primordial follicle: (arrow), primary follicle: (PF), secondary follicle: (SF), tertiary follicle: (TF), corpus luteum: (CL), cystic follicle: (CF), oocyte: (asterisk).

Evaluation of IL-1β, IL-6, and TNF-α Gene Expression by Real-Time PCR

Although differences were observed among the groups, these were not statistically significant. When the control group was compared with the other groups (Table 4), an increase in IL-1β, IL-6, and TNF-α gene expression was noted in all

groups compared to the control. However, a statistically significant difference was found only in Group 4 for IL-6 and IL-1β expression (p= 0,016, p= 0,036).

DISCUSSION

PCOS is a common endocrine disorder characterized by chronic anovulation, biochemical and/or clinical hyperandrogenism, and polycystic ovaries, affecting 5-10% of women of reproductive age (14). In PCOS, ovarian tissue exhibits an increased number of developing antral and preantral follicles. These include thin theca-layered follicles, known as cystic follicles, characterized by an enlarged antrum, a reduction in granulosa cell layers, and cell degeneration (15). This study aimed to investigate the effects of vitamin D on inflammatory markers and ovarian morphology in a dehydroepiandrosterone (DHEA)-induced experimental PCOS rat model.

Animal models are frequently used in PCOS research, particularly to observe the syndrome's reproductive effects. Rat models are highly useful due to their short estrus cycle and well-documented genetic background, though differences between rodents and humans should be considered. While women are mono-ovulatory, rodents are poly-ovulatory. Although the hypothalamic-pituitary-ovarian axis is similar in both species, the follicle selection process in rodents, which is FSH-dependent, differs from that in humans (16,17). The primordial and preantral follicle phases are comparable; however, differences in intra-ovarian development cannot be overlooked. In humans, the establishment of the primordial follicle pool and the initiation of follicular development occur in the late fetal stage, whereas in rodents, this process occurs during the early postnatal period (18). For this reason, this study was conducted using 20-day-old prepubertal rats.

The effects of PCOS on ovarian morphology are widely discussed in the literature. In this study, the DHEA-induced PCOS model demonstrated a significant increase in cystic follicle formation compared to the control group, indicating severe disruptions in follicular development. In the short-term PCOS group (Group 3), vitamin D treatment significantly reduced the number of cystic follicles and improved the counts of secondary and tertiary follicles. This finding supports the positive effects of early vitamin D intervention on follicular development. Similarly, the literature provides evidence for the regulatory role of vitamin D in folliculogenesis (19). In Group 4, vitamin D treatment did not significantly reduce the number of cystic follicles or fully prevent disruptions in follicular development. This suggests that structural and functional impairments caused by long-term PCOS may be more resistant to treatment.

TABLE 3 Immunohistochemical Evaluations of Groups

	Group 1			Group 2			Group 3			Group 4			Group 5		
	IL-1β	IL-6	TNF-α	IL-1β	IL-6	TNF-α	IL-1β	IL-6	TNF-α	IL-1β	IL-6	TNF-α	IL-1β	IL-6	TNF-α
Oocyte	-	++	-	-	-	++	-	++	++	-	+++	+++	-	+++	+++
Granulosa Cells	-	-	-	-	-	-	-	-	-	-	-	-	-	-	-
Theca Layer	-	-	-	-	-	-	-	-	-	-	-	-	-	-	-
Corpus Luteum	-	-	-	-	-	-	-	++	++	++	+++	++	-	-	-
Blood Cells	+++	+++	+++	+++	+++	+++	+++	+++	+++	+++	+++	+++	+++	+++	+++
Ovarian Stromal Cells	-	-	-	-	-	-	-	+	+	-	+	+	-	++	++
Ovarian Connective Tissue	-	-	-	-	-	-	-	+++	-	-	+++	+++	-	++	+++

Table 4. Comparison of PCR data between the control group and other groups

	p-value (comparing to control group)			
	Group 2	**Group 3**	**Group 4**	**Group 5**
IL-6	0.772495	0.336695	0.0157209	0.210306
IL-1β	0.286801	0.271928	0.036026	0.153218
TNF-α	0.136468	0.392904	0.076446	0.307121

Additionally, in the group receiving only vitamin D (Group 5), follicular development progressed healthily, and no cystic follicles were observed. This finding suggests that the protective effect of vitamin D may be more effective when administered before the onset of inflammation.

It has been proposed that chronic low-grade inflammation may serve as the link between hormonal changes observed in PCOS and associated conditions such as obesity, glucose intolerance, and other metabolic issues. Low-grade inflammation can contribute to the development of metabolic disorders and ovarian dysfunction (20). This type of inflammation is characterized by increased levels of inflammatory markers, including IL-6 and TNF-α, in circulation and adipose tissue (21).

In our study, we determined that the gene expressions of inflammatory cytokines such as IL-1β, IL-6, and TNF-α were elevated in PCOS groups compared to the control group. However, most of these increases were not statistically significant. Nonetheless, the significant increase in IL-1β and IL-6 expression in Group 4 suggests that long-term PCOS enhances the inflammatory response and that the effect of vitamin D supplementation during this process may be limited. The literature indicates that vitamin D possesses anti-inflammatory properties and can suppress IL-6 and TNF-α expression via the NF-κB pathway (22). However, this effect appears to depend on the degree of inflammation and the duration of treatment.

In the ovarian tissue, IL-1 and TNF-α expression at the protein level was found to be negative in oocytes, granulosa cells, and theca layers of the control group (Group 1). However, IL-6 showed a strong positive reaction in oocytes of this group. In Group 2, where experimental PCOS was induced without vitamin D supplementation, IL-1 expression remained negative, similar to the control group. However, TNF-α, which was negative in the control group, was found to be positive in this group. Sun et al. (2016) observed that in a DHEA-induced PCOS rat model, the PCOS group exhibited greater weight gain, increased testosterone and LH levels, and elevated serum IL-6 levels compared to the normal group, but found no difference in serum TNF-α levels (23). In Groups 3 and 4, where vitamin D was administered to PCOS models, IL-1 expression was similarly negative compared to the control and Group 2. However, IL-6 and TNF-α exhibited positive immunoreactions in oocytes, corpus luteum, and ovarian stroma. Staining intensity was greater in Group 4 compared to Group 3. Notably, only in Group 4, the corpus luteum exhibited a positive reaction for IL-1.

Stephens et al. reported that TNF-α activates insulin resistance pathways and can affect

insulin sensitivity by altering the expression of genes associated with insulin receptors (24). In vitro studies have shown that TNF-α may influence the reproductive axis by stimulating the proliferation and steroidogenesis of rat theca cells (25). Additionally, TNF-α may have an apoptotic effect on theca cells in the rat ovary. Given its high concentrations in obesity or impaired glucose tolerance, TNF-α has been hypothesized to play a role in insulin metabolism. Findings from case studies suggest that TNF-α levels in PCOS pathogenesis are not independent of factors such as insulin resistance and obesity, making this a topic of ongoing debate. Some clinical studies in PCOS patients have shown increased serum levels of inflammatory markers such as TNF-α, IL-6, and IL-1β (7). However, other studies have reported no significant increase in inflammatory markers in PCOS patients compared to normal groups (8). It has been proposed that inflammation markers may increase in PCOS patients with high BMI and central obesity, and that TNF-α expression decreases with weight loss (26).

Many studies have attempted to associate serum interleukin levels with PCOS phenotypes, with particular emphasis on the importance of IL-6, which initiates CRP production in the liver. While some studies demonstrate a significant relationship between IL-6 levels and PCOS, others have not found such an association (27, 28, 29, 30). Like IL-1 and TNF-α, IL-6 is crucial in regulating and mediating the immune-inflammatory response (31). Meta-analyses of various studies reveal a positive correlation between PCOS risk and specific TNF-α and IL-6 gene polymorphisms, suggesting that genetic predisposition may influence immune dysfunction in this condition (32). This study suggests that increases in TNF-α and IL-6 in PCOS should not only be viewed as a consequence but also as potential triggers or amplifiers of PCOS effects.

In our findings, IL-6 showed a moderate immune reaction in oocytes and corpus luteum in the short-term PCOS group treated with vitamin D (Group 3). Similarly, oocytes in Group 5, which did not have PCOS but received vitamin D, exhibited a positive reaction. In Group 4, IL-6 demonstrated strong staining in oocytes and corpus luteum, and, uniquely among the groups, moderate staining in the ovarian stroma. It can be inferred that prolonged exposure to DHEA in Group 4 and the delayed initiation of vitamin D treatment (20 days later) may have contributed to increased IL-6 release from ovarian tissue. This suggests that initiating vitamin D supplementation before the onset of PCOS symptoms and prolonged exposure could enhance its efficacy. However, based on our findings, it is challenging to establish a direct and significant relationship between vitamin D and ovarian inflammation in PCOS by analyzing IL-6, IL-1β, and TNF-α markers. The

positive IL-6 and TNF-α expression in Group 1, their absence in Group 2, and their reappearance in the treatment groups may indicate the role of IL-6 in folliculogenesis and ovulation. The disruption in follicular development in PCOS could be linked to IL-6, and vitamin D may have corrected this altered IL-6 secretion, allowing its normal release during ovulation and folliculogenesis.

M. Razavi et al. (2016) studied 60 PCOS patients with vitamin D deficiency and administered vitamin D, calcium, and vitamin K supplementation for eight weeks. They observed significant reductions in DHEA and free testosterone levels and increases in total antioxidant levels in patients receiving vitamin D (33). In our study, the daily DHEA injections used to induce PCOS during the experimental period may have limited the anti-inflammatory effects of vitamin D and, consequently, its impact on pro-inflammatory markers.

Studies have reported that vitamin D deficiency may exacerbate PCOS symptoms. Low 25(OH)D levels are thought to be associated with insulin resistance, ovulation and menstrual irregularities, reduced pregnancy success, hirsutism, hyperandrogenism, obesity, and an increased risk of cardiovascular disease (34). However, comprehensive experimental studies on this subject are still lacking. Some existing data suggest that vitamin D levels are similar in PCOS patients and control groups (35, 36). Conversely, other studies have reported that vitamin D levels are either low (37, 38) or high (39) in women with PCOS.

While a relationship between vitamin D deficiency and PCOS has been highlighted, further research is needed to determine which mechanisms involved in the etiology of PCOS are affected by this relationship (40). In our study, vitamin D supplementation appeared to have positive effects on ovarian morphology during the early stages, but it was not sufficient to completely prevent increases in inflammatory cytokine gene and protein levels. This suggests that the protective effects of vitamin D in PCOS may be more pronounced before the onset of the inflammatory process. Future studies would benefit from a more comprehensive evaluation of experimental durations, PCOS induction methods, vitamin D levels in subjects, and the impact of inflammation and vitamin D supplementation on metabolic changes.

CONCLUSION

The roles of vitamin D in follicular development, oocyte maturation, ovulation and menstrual cycle regulation have been demonstrated and support our morphological findings in ovarian tissues. Although some studies in the literature have shown that vitamin D reduces inflammation, the increase in cytokines observed in our vitamin D-treated groups suggests that vitamin D dose, treatment duration and individual differences may affect the outcome and may be limited in the short

term. Our findings indicate that, vitamin D significantly reduces the number of cystic follicles but has no meaningful impact on inflammatory markers expressed in ovarian tissue. Further long-term studies are needed to determine how sustained this response is at the tissue and gene levels and to more comprehensively assess the stage at which vitamin D begins to mitigate the metabolic effects of PCOS.

Acknowledgements: We would like to thank Pamukkale University Scientific Research Projects Coordination Unit for supporting our study with the project number 2015SBE005.

Ethics Committee Approval: Ethics committee approval was received for this study from Pamukkale University Animal Experiments Ethics Committee with the decision number (PAUHDEK-2015/3).

All experimental procedures were carried out in accordance with institutional guidelines and international standards for the care and use of laboratory animals.

Peer-review: Externally peer-reviewed

Author Contributions: Concept: Seçil T, GAM, ST, Design: Seçil T, GAM, ST, NÇ, Data Collection and/or Processing: Seçil T, ST, MS, EM, NÇ, Analysis and/or Interpretation: Seçil T, ST, YD, MS, EM, Writing: Seçil T, GAM, ST.

Conflict of Interest: The authors declare that they have no conflict of interest.

Financial Disclosure: This study was supported by Pamukkale University Scientific Research Projects Coordination Unit under project number 2015SBE005.

REFERENCES

1. Franks S. Polycystic ovary syndrome. N. Engl J. Med. 1995; 333(13):853-861.
2. Yildiz BO, Bozdag G, Yapici Z, Esinler I, Yarali H. Prevalence phenotype and cardiometabolic risk of polycystic ovary syndrome under different diagnostic criteria. Hum Reprod. 2012;27(10):3067-3073.
3. Daan NM, Louwers YV, Koster MP, Eijkemans MJ, de Rijke YB, Lentjes EW, et al. Cardiovascular and metabolic profiles amongst different polycystic ovary syndrome phenotypes: who is really at risk. Fertil Steril. 2014;102(5):1444-1451.
4. Henmi H, Endo T, Nagasawa K, Hayashi T, Chida M, Akutagawa N, et al. Lysyl oxidase and MMP-2 expression in dehydroepiandrosterone-induced polycystic ovary in rats. Biol Reprod. 2001;64(1):157-162.
5. Benson S, Janssen OE, Hahn S, Tan S, Dietz T, Mann K, Pleger K, Schedlowski M, Arck PC, Elsenbruch S. Obesity, depression, and chronic low-grade inflammation in women

with polycystic ovary syndrome. Brain Behav Immun. 2008;22(2):177-84.

6. Jang M, Lee MJ, Lee JM, Bae CS, Kim SH, Ryu JH, et al. Oriental medicine Kyung-Ok-Ko prevents and alleviates dehydroepiandrosterone-induced polycystic ovarian syndrome in rats. PLoS One. 2014;9(2):e87623.
7. Amato G, Conte M, Mazziotti G, Lalli E, Vitolo G, Tucker AT, et al. Serum and follicular fluid cytokines in polycystic ovary syndrome during stimulated cycles. Obstet Gynecol. 2003;101(6):1177-82.
8. Guo R, Zheng Y, Yang J, Zheng N. Association of TNF-alpha, IL-6 and IL-1beta gene polymorphisms with polycystic ovary syndrome: a meta-analysis. BMC Genet. 2015;30;16(1):5.
9. Kousta E, White DM and Franks S. Modern use of clomiphene citrate in induction of ovulation. Hum Reprod Update. 1997;3(4):359–365.
10. Kim JJ, Choi YM, Chae SJ, Hwang KR, Yoon SH, Kim MJ, et al. Vitamin D deficiency in women with polycystic ovary syndrome. Clin Exp Reprod Med. 2014;41(2):80-85.
11. Tehrani HG, Mostajeran F, Shahsavari S. The effect of calcium and vitamin D supplementation on menstrual cycle, body mass index and hyperandrogenism state of women with poly cystic ovarian syndrome. J Res Med Sci. 2014;19(9):875-880.
12. Lee MT, Anderson E, Lee GY. Changes in ovarian morphology and serum hormones in the rat after treatment with dehydroepiandrosterone. Anat Rec. 1991;231(2):185-92.
13. Luchetti CG, Solano ME, Sander V, Arcos ML, Gonzalez C, Di Girolamo G, et al. Effects of dehydroepiandrosterone on ovarian cystogenesis and immune function. J Reprod Immunol. 2004;64(1-2):59-74.
14. The Rotterdam ESHRE/ASRM-Sponsored PCOS Consensus Workshop Group. Revised 2003 consensus on diagnostic criteria and long-term health risks related to polycystic ovary syndrome (PCOS). Hum. Reprod. 2004;19:41-47.
15. Franks S, Stark J, Hardy K. Follicle dynamics and anovulation in polycystic ovary syndrome. Hum Reprod Update. 2008;14(4):367-378.
16. Franks S. Can Animal Models of PCOS Help Point the Way Towards Early and Effective Therapeutic Intervention in Women With the Syndrome? Endocrinology. 2015;156(7):2371-2373.
17. Maliqueo M, Benrick A, Stener-Victorin E. Rodent models of polycystic ovary syndrome: phenotypic presentation, pathophysiology, and the effects of different interventions. Semin Reprod Med. 2014;32(3):183-93.

18. Skinner MK. Regulation of primordial follicle assembly and development. Hum Reprod Update. 2005;11(5):461-471.
19. Grzeczka A, Graczyk S, Skowronska A, Skowronski MT, Kordowitzki P. Relevance of Vitamin D and Its Deficiency for the Ovarian Follicle and the Oocyte: An Update. Nutrients. 2022;14(18):3712.
20. Gonza´lez F, Rote NS, Minium J, Kirwan JP. Increased activation of nuclear factor kB triggers inflammation and insulin resistance in polycystic ovary syndrome. J Clin Endocrinol Metab. 2006;91(4):1508-1512.
21. Repaci A, Gambineri A, Pasquali R. The role of low-grade inflammation in the polycystic ovary syndrome. Mol Cell Endocrinol. 2011;335(1):30-41.
22. Chen Y, Zhang J, Ge X, Du J, Deb DK, Li YC. Vitamin D receptor inhibits nuclear factor κB activation by interacting with IκB kinase β protein. J Biol Chem. 2013;288(27):19450-8.
23. Sun L, Ji C, Jin L, Bi Y, Feng W, Li P, et al. Effects of Exenatide on Metabolic Changes, Sexual Hormones, Inflammatory Cytokines, Adipokines, and Weight Change in a DHEA-Treated Rat Model. Reprod Sci. 2016;23(9):1242-1249.
24. Stephens JM, Lee J, Pilch PF. Tumor necrosis factor-α-induced insulin resistance in 3T3-L1 adipocytes is accompanied by a loss of insulin receptor substrate-1 and GLUT4 expression without a loss of insulin receptor-mediated signal transduction. J Biol Chem. 1997;272(2):971-976.
25. Deligeoroglou E, Vrachnis N, Athanasopoulos N, Iliodromiti Z, Sifakis S, Iliodromiti S, et al. Mediators of chronic inflammation in polycystic ovarian syndrome. Gynecological Endocrinology. 2012;28(12):974-978.
26. Pittas AG, Joseph NA, Greenberg AS. Adipocytokines and insulin resistance. J Clin Endocrinol Metab. 2004; 89(2): 447-452.
27. Bansal B, Thazhuthadath Kishore A, Kathiresan S, Farook Ghachi A, Pradhan S, Paul S, et al. A Systematic Review of Inflammatory Markers in Polycystic Ovary Syndrome (PCOS) and Meta-Analysis of Interleukin-6 (IL-6) in Case-Control Studies. Cureus. 2025;17(4):e82350.
28. Escobar-Morreale HF, Luque-Ramirez M, Gonzalez F. Circulating inflammatory markers in polycystic ovary syndrome: a systematic review and metaanalysis. Fertil Steril. 2011;95:1048–1058.
29. Vgontzas AN, Trakada G, Bixler EO, Lin HM, Pejovic S, Zoumakis E, et al. Plasma interleukin 6 levels are elevated in polycystic ovary syndrome independently of obesity or sleep apnea. Metab Clin Exp. 2006;55:1076–1082.
30. Toulis KA, Goulis DG, Mintziori G, Kintiraki E, Eukarpidis E, Mouratoglou SA, et al. Meta-analysis of cardiovascular

disease risk markers in women with polycystic ovary syndrome. Hum Reprod Update. 2011;17:741–760.

31. Borthakur A, D Prabhu Y, Valsala Gopalakrishnan A. Role of IL-6 signalling in Polycystic Ovarian Syndrome associated inflammation. J Reprod Immunol. 2020;141:103155.
32. Wu H, Yu K, Yang Z. Associations between TNF-α and interleukin gene polymorphisms with polycystic ovary syndrome risk: a systematic review and meta-analysis. J Assist Reprod Genet. 2015;32(4):625-34.
33. Razavi M, Jamilian M, Karamali M, Bahmani F, Aghadavod E, Asemi Z. The Effects of Vitamin D-K-Calcium Co-Supplementation on Endocrine, Inflammation, and Oxidative Stress Biomarkers in Vitamin D-Deficient Women with Polycystic Ovary Syndrome: A Randomized, Double-Blind, Placebo-Controlled Trial. Horm Metab Res. 2016;48(7):446-51.
34. Menichini D, Facchinetti F. Effects of vitamin D supplementation in women with polycystic ovary syndrome: a review. Gynecol Endocrinol. 2020;36(1):1-5.
35. Panidis D, Balaris C, Farmakiotis D, Rousso D, Kourtis A, Balaris V, et al. Serum parathyroid hormone concentrations are increased in women with polycystic ovary syndrome. Clin Chem. 2005;51(9):1691-7.
36. Ng BK, Lee CL, Lim PS, Othman H, Ismail NAM. Comparison of 25-hydroxyvitamin D and metabolic parameters between women with and without polycystic ovarian syndrome. Horm Mol Biol Clin Investig. 2017;31(3):/j/hmbci.2017.31.issue-3/hmbci-2016-0057/hmbci-2016-0057.xml.
37. Wehr E, Pieber TR. and Obermayer-Pietsch B. Effect of vitamin D3 treatment on glucose metabolism and menstrual frequency in PCOS women-a pilot study. Journal of Endocrinological Investigation. 2011;34: 757–763.
38. Li HW, Brereton RE, Anderson RA, Wallace AM, Ho CK. Vitamin D deficiency is common and associated with metabolic risk factors in patients with polycystic ovary syndrome. Metabolism. 2011;60(10):1475-81.
39. Mahmoudi T, Gourabi H, Ashrafi M et al. Calciotropic hormones, insulin resistance, and the polycystic ovary syndrome. Fertility and Sterility. 2010;93:1208–1214.
40. Mohan A, Haider R, Fakhor H, Hina F, Kumar V, Jawed A, Majumder K, Ayaz A, Lal PM, Tejwaney U, Ram N, Kazeem S. Vitamin D and polycystic ovary syndrome (PCOS): a review. Ann Med Surg (Lond). 2023;85(7):3506-3511.

Middle Black Sea Journal of Health Science / Mid Blac Sea J Health Sci
August 2025; 11(3): 171-189

ORGINAL ARTICLE **DOI:** 10.19127/mbsjohs.1649061

Comparison of Preoperative Hematological Parameters Among Benign, Premalignant, and Malignant Uterine Pathologies

Selçuk Atalay[1(ID)], Tuğba Karadeniz Atalay[2(ID)], Cem Dane[3(ID)], Nihal Çallıoğlu[4(ID)],

[1]Ordu University, Training and Research Hospital, Ordu, Türkiye
[2]Sevgi Hospital, Ordu, Türkiye
[3]Gaziosmanpaşa Training and Research hospital, Istanbul, Türkiye
[4]Istinye University, Faculty of Medicine, Department of Gynecology & Obstetrics, Istanbul, Türkiye

Received: 03 March 2025, Accepted: 29 June 2025, Published online: 30 August 2025

Abstract

Objective: Based on the influence of uterine inflammation on the development of malignancy, we aimed to determine the difference in the preoperative parameters in benign uterine pathology of haematological parameters analysed and to evaluate the association with premalignant and malignant.

Method: Our study included 343 patients who underwent surgery for benign, premalignant and malignant pathologies of the uterus between January 2007 and August 2014 at Education and Research Hospital. Of the total 343 operated patients, 228 (66.5%) were diagnosed with uterine myoma. Among the 58 patients in the endometrial hyperplasia group, 33 (56.9%) were diagnosed with simple hyperplasia without atypia, 7 (12.1%) with simple atypical hyperplasia, 7 (12.1%) with complex hyperplasia without atypia and 11 (18,9%) with complex atypical hyperplasia. In the endometrial cancer group, which consisted of 57 patients, 52 (91.2%) were diagnosed with endometrioid-type endometrial adenocarcinoma, 3 (5.2%) with carcinosarcoma, 1 (1.7%) with a mixed type (serous papillary + endometrioid) and 1 (1.7%) with endometrial stromal sarcoma. All patients achieved hemograms in the preoperative period.

Results: In our study group, the endometrial carcinoma and hyperplasia neutrophil count (Neu) , neutrophil percentage (Neu%) , haemoglobin (Hb), haematocrit (Hct) and mean corpuscular volume (MCV) were significantly higher than those in the control group. Lymphocyte ratio and red cell distribution width (RDW) terms were significantly lower than those in the control group.

Conclusion: We think that routine haematological parameters such as Neu, Neu%, MCV and RDW which are inexpensive, repeatable and easily accessible from complete blood count panels may be useful in predicting benign and malignant diseases of the endometrium.

Keyword: Lymphocytes, platelets, neutrophils, endometrial neoplasms, thrombocytosis.

Suggested Citation Atalay S, Karadeniz Atalay T, Dane C, Callioglu N. Comparison of Preoperative Hematological Parameters Among Benign, Premalignant, and Malignant Uterine Pathologies Mid Blac Sea Journal of Health Sci, 2025;11(3):171-189.

Address for correspondence/reprints:

Selçuk Atalay

Telephone number: +90 (505) 229 82 13

E-mail: dr_s.atalay@hotmail.com

INTRODUCTION

Endometrial hyperplasia is defined as morphological and biological changes in the endometrial gland and stroma due to endogenous or exogenous estrogenic stimulation that is not met with progestogens. Endometrial hyperplasia and endometrial neoplasia are two different biological diseases. The most discriminating feature is the absence or presence of cytological atypia (1). Endometrial hyperplasia is a well-known precancerous lesion that lies on the pathway from normal endometrial tissue to adenocarcinoma.

The relationship between cancer and inflammation was proposed by Virchow in the 19th century. A dense leukocyte ratio in cancerous tissues was observed as the result of a chronic inflammatory process, suggesting that leukocytes may be the cause of tumor growth. Inflammatory mediators formed by cells carry tumor progression to the next process.

Due to their angiogenic, metastatic, and proteolytic activities, platelets have a major role in the background of inflammation. The systematic review demonstrated that pretreatment thrombocytosis is correlated with poor survival outcome and adverse clinicopathological parameters in endometrium cancer and thrombocytosis is a potential prognosis predictor for endometrium cancer (2). Mean platelet volume (MPV) is an important inflammatory marker indicating platelet activation (3).

In recent years, NLR (neutrophil lymphocyte ratio) and PLR (platelet lymphocyte ratio) values, which we can easily see from the complete blood count, have been used as SIR (systemic inflammatory response) markers. SIR changes the distribution of white blood cells by causing neutropenia and lymphocytopenia due to malignancies (4).

In this study, we aimed to evaluate preoperative hematological parameters in premalignant, malignant and benign pathologies of the uterus and to evaluate the relationship between them, based on the effect of inflammation on cancer development

METHODS

In our study, 343 patients who were admitted to the Training and Research Hospital with complaints of abnormal uterine bleeding in the premenopausal period, uterine bleeding in the postmenopausal period, abnormal smear results, postmenopausal follow-up and pelvic pain were examined retrospectively. This study was conducted as a specialty thesis project in 2014, before institutional ethics committee approval was required for retrospective chart

reviews. No identifiable patient information was used. The study adhered to the ethical rules of the Declaration of Helsinki. Informed consent was obtained from the patients.

Inclusion criteria were as follows: After exclusion of systemic diseases, curettage for diagnostic purposes was performed in patients over 35 years of age with abnormal uterine bleeding, patients with postmenopausal bleeding, patients with postmenopausal endometrial thickness greater than 5 mm, patients with atypical glandular cells in their cervical cytology and risk factors under 35 years of age. The patients were assessed in three groups.

Group 1 (n: 57): endometrial carcinoma group, Group 2 (n: 58): endometrial hyperplasia group and Group 3 (n: 228): myoma uteri group. All patients in the myoma uteri group underwent preoperative endometrial sampling (either endometrial biopsy or curettage) to exclude coexisting endometrial hyperplasia or malignancy. Histopathological evaluation confirmed normal endometrial findings in all cases. Therefore, this group was used as the benign control group with histologically verified non-pathologic endometrial tissue.

Endometrial hyperplasia cases were subclassified into simple and complex forms with or without atypia, based on the WHO 1994 classification. However, due to the relatively small sample size of each subgroup, statistical comparisons were performed by combining all hyperplasia cases into a single group for analysis.

The routine hemogram was obtained by taking venous blood from the antecubital region 2 weeks before the preop. The exclusion criteria were as follows: patients with benign curettage results and no pathology detected in gynecological examination and patients with hematological disease, inflammatory disease or liver disease who were treated with medical therapy were excluded from the study. A routine hemogram was obtained by taking venous blood from the antecubital region on average 2 weeks before the operation and the study group was formed.

Statistical Analysis

NCSS (Number Cruncher Statistical System) 2007 Statistical Software (Kaysville, Utah, USA) program was used for the statistical analysis. The normality of data distribution was assessed using the Shapiro-Wilk test before applying appropriate parametric or non-parametric tests.

During the evaluation of the study data, one-way ANOVA test was used for the comparisons of descriptive statistical methods (mean, standard deviation, median, frequency, ratio, minimum, maximum) as well as comparisons of three or more groups with normal distribution and Kruskal-Wallis test was used for the comparisons of three or more groups without normal distribution. Following

significant results from the ANOVA or Kruskal-Wallis tests, Tukey's HSD test or Dunn's test with Bonferroni correction, respectively, were used for post-hoc comparisons between groups. Receiver Operating Characteristic (ROC) curve analysis was performed to assess the diagnostic performance of hematological parameters and the area under the curve (AUC), optimal cut-off values, sensitivity, specificity, positive and negative predictive values were calculated. Statistical significance was accepted as $p < 0.05$.

RESULTS

The mean age of the patients included in our study was 52.02 ± 9 years. A total of 228 (66.5%) of our operated patients were diagnosed with myoma uteri. Thirty-three (9.6%) of them were diagnosed with simple hyperplasia without atypia, 7 (2%) of them with simple atypical hyperplasia, 7 (2%) of them with complex hyperplasia without atypia and 11 (3.2%) of them with complex atypical hyperplasia. Fifty-two (15.2%) patients were diagnosed with endometrioid-type endometrial adenocarcinoma, 3 (0.9%) were diagnosed with carcinosarcoma, 1 (0.3%) was diagnosed with mixed-type (serous papillary + endometrioid type) and 1 (0.3%) was diagnosed with endometrial stromal sarcoma. We compared hematological parameters in the study and control groups (Table 1).

No significant differences in Hb (p=0.169), Hct (p=0.668), NLR (p=0.440), Neu (p=0.855), Neu% (p=0.580), MCV (p=0.716) or RDW (p=0.663) among the endometrial hyperplasia subgroups. In our study, it was statistically higher in the endometrial cancer and hyperplasia groups than in the benign group in terms of neutrophil count and neutrophil percentage (p=0.04 and p=0.02).

Among the evaluated hematologic markers for distinguishing endometrial cancer; Hb (AUC: 0.633, cut-off: 12.94 g/dL), MCV (AUC: 0.630, cut-off: 86 fL), Hct (AUC: 0.616, cut-off: 35%) and Neu% (AUC: 0.607, cut-off: 58.9%) were found to be diagnostically valuable, showing particularly high negative predictive values (88%, 89%, 89%, and 89% respectively), indicating strong utility in ruling out malignancy. In contrast, RDW (AUC: 0.324) demonstrated very poor specificity (1%) and a low positive predictive value (16%), thus lacking clinical diagnostic significance (Table 2, Figure 1).

In our study, the lymphocyte count was not found to be statistically significant compared to that in the control group in endometrial cancer and hyperplasia but the lymphocyte percentage was found to be statistically lower than that in the control group (p=0.02). NLR was not statistically significant in the endometrial cancer and hyperplasia groups compared to the benign group. No difference was found between platelet values and PLR in endometrial

cancer compared with the hyperplasia and benign groups.

Hb and Hct values were found to be statistically significantly lower in the benign group than in the cancer and hyperplasia groups. There was a significant difference between the groups in terms of RDW (p= 0.001). In the study group, RDW was lower than that in the control group. MCV values were found to be statistically significantly higher in the cancer and hyperplasia groups than in the benign group (p=0.01). There was no difference between the groups in terms of the MPV value which is a marker of the SIR.

Table 1. Hematological Parameters in Myoma Uteri, Endometrial Hyperplasia, and Endometrial Cancer

Parameter	Myoma (mean ± SD)	Hyperplasia	Endometrial Cancer	P value
Hb (g/dL)	11.1 ± 1.9	11.3 ± 2.2	12.0 ± 1.7	0.006
Hct (%)	34.8 ± 5.1	35.1 ± 5.7	36.9 ± 4.5	0.018
Lymphocyte (x10³/µL)	2.2 ± 0.8	2.2 ± 1.4	2.1 ± 0.7	0.428
Lymphocyte % (%)	32.1 ± 9.2	31.5 ± 8.7	28.2 ± 9.5	0.021
MCH (pg)	25.4 ± 4.0	25.9 ± 4.4	27.4 ± 3.0	0.006
MCHC (g/dL)	31.9 ± 1.6	32.1 ± 1.7	32.6 ± 1.4	0.025
MCV (fL)	79.1 ± 10.3	80.2 ± 11.1	83.8 ± 6.9	0.010
MPV (fL)	8.8 ± 1.0	8.6 ± 0.7	8.7 ± 1.1	0.150
Neutrophil (x10³/µL)	4.4 ± 2.0	4.4 ± 2.0	5.1 ± 2.5	0.043
Neutrophil % (%)	57.9 ± 9.8	58.5 ± 9.7	62.2 ± 10.9	0.021
NLR	2.0 ± 1.5	2.3 ± 2.6	2.5 ± 1.8	0.116
PCT (%)	0.2 ± 0.09	0.2 ± 0.07	0.2 ± 0.07	0.538
PDW (fL)	14.4 ± 6.4	13.9 ± 5.7	15.7 ± 6.5	0.271
RDW (%)	17.9 ± 4.8	16.5 ± 3.9	15.1 ± 3.2	0.001
PLT (x10³/µL)	306 ± 91.5	303 ± 95.2	308.9 ± 127.1	0.974
PLR	148.6 ± 59.0	147.7 ± 77.9	155.1 ± 62.5	0.761
WBC (x10³/µL)	7.1 ± 2.1	7.5 ± 2.2	7.7 ± 1.7	0.187

Data analyses are given as mean ± SD.
Abbreviations: Hb – Hemoglobin, Hct – Hematocrit, RDW – Red Cell Distribution Width, MCV – Mean Corpuscular Volume, MPV – Mean Platelet Volume, PLT – Platelet Count, WBC – White Blood Cell Count, NLR – Neutrophil-to-Lymphocyte Ratio, PLR – Platelet-to-Lymphocyte Ratio, MCH – Mean Corpuscular Hemoglobin, MCHC – Mean Corpuscular Hemoglobin Concentration, PCT – Plateletcrit, PDW – Platelet Distribution Width.

Table 2. ROC Curve analysis of hematological parameters

Parametre	AUC	Cut-off	Sensitivity	Specificity	PPV	NPV
Hb	0.633	12.94	0.44	0.79	0.29	0.88
Hct	0.616	35.0	0.7	0.5	0.22	0.89
Neu%	0.607	58.9	0.64	0.56	0.22	0.89
MCV	0.63	86.0	0.55	0.67	0.24	0.89
RDW	0.324	11.7	1.0	0.01	0.16	1.0

Abbreviations: Hb–Hemoglobin, Hct–Hematocrit, Neu-Neutrophil, RDW–Red Cell Distribution Width, MCV–Mean Corpuscular Volume, AUC-Area Under the Curve, PPV-Positive Predictive Value, NPV-Negative Predictive Value

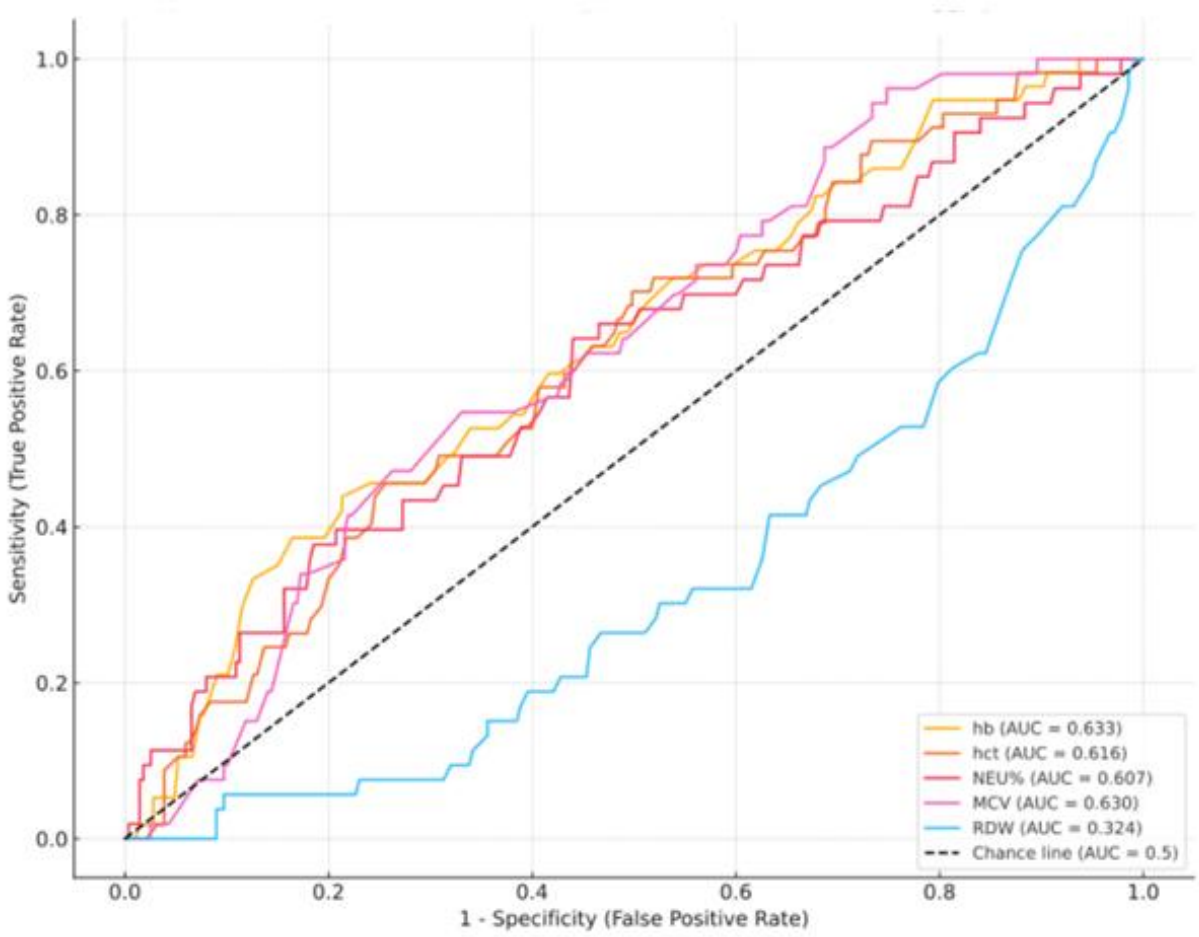

Figure 1. ROC Curves Hematologic Markers in Endometrial Cancer Diagnosis

DISCUSSION

Experimental and clinical information has proven that chronic inflammation plays a role in the development of cancer. Leukocytes (neutrophils, monocytes, macrophages and eosinophils) directly cause the production of reactive oxygen and nitrogen species that damage genes that control cell growth (5). In addition, the proinflammatory environment may play a role in the development of endometrial cancer by directly increasing estrogen production (6). Studies have shown that in endometrial cancer, preoperative abnormal haematological parameters like, anaemia, thrombocytosis and leucocytosis appears to be associated with FIGO advanced-stage and unfavourable outcome (7). In the study of Salem et al., preoperative leukocytosis is correlated with poor tumor FIGO stage, higher cumulative incidence of relapse and poor disease-free survival (DFS) and preoperative leukocytosis may identify high-risk patients who may require more intensified therapy in terms of aggressive debulking and/or perioperative chemotherapy (8).

In the study of Petric et al., lymphocyte count was statistically significantly lower in patients with endometrial cancer in comparison to

patients with premalignant changes (9). In their study, Selen et al., preoperative lymphocyte values were lower in the complex atypical hyperplasia/ endometrial intraepithelial neoplasia (CAH/EIN) from endometrioid grade 1 adenocancer (10).

In our study, the lymphocyte percentage was significantly lower in endometrial cancer and hyperplasia than in the control group and the lymphocyte count was not significantly different. Although the absolute lymphocyte count was not significantly different between groups, the lymphocyte percentage was significantly lower in malignant and premalignant cases. This discrepancy can be explained by elevated total leukocyte and Neu in malignancy-related SIR which reduces the relative proportion of lymphocytes. Therefore, lymphocyte percentage may more sensitively reflect systemic inflammation than absolute count.

Studies have shown that NLR measurement may have an important value in the evaluation of the prognosis of some cancers, such as colon cancer, gastric cancer, lung cancer, renal cell carcinoma and breast cancer, colorectal cancer, pancreatic cancer and soft tissue sarcoma. In their study, Petric et al.showed patients with endometrial cancer higher levels of NLR and PLR in comparison to patients with premalignant changes of uterine mucosa (9). Muangto et al. reported that NLR and PLR were not significantly predictive of malignancy potential in endometrial lesions although NLR was associated with myometrial invasion of uterine mucosa (11). In our study, NLR was not found to be statistically significant in the endometrial cancer and hyperplasia groups compared to the benign group. . Similarly, Fırat et al. also found no statistically significant differences in NLR and PLR values between patients with normal endometrium, atypia and endometrial carcinoma. These findings suggest that the prognostic utility of NLR may vary depending on tumor stage, histological subtype and host immune status (12).

Thrombocytosis is a result of malignant diseases; it is accepted as an independent prognostic factor for ovarian cancer and endometrial cancer. In the study, pre-treatment thrombocytosis is a potential sign of advanced stage ovarian carcinomas and may be predictive of suboptimal tumour debulking during surgery (13). In our study, no difference was found between platelet values in the endometrial cancer, hyperplasia and benign groups.

In the study of Mohamadianamiri et al., concluded that PLR were identified as independent prognostic items associated with the stage and grade of endometrial cancer (14). In our study, no difference was found between the groups in terms of PLR and platelet distrubution width (PDW).

Preoperative anemia significantly correlated with advanced endometrial carcinoma FIGO stage III-IV, ≥50% myometrial invasion, lymph

node metastasis, non-endometrioid histology adnexal involvement, cervical involvement, positive peritoneal cytology, preoperative thrombocytosis and lymphovascular space invasion (15). In our study, the hemoglobine and hematocrit values were found to be significantly lower in the benign group than in the cancer and hyperplasia groups.

Eoh et al. showed that RDW had significantly advanced-stage pelvic lymph node metastasis and recurrence compared to those in the low-RDW group (16).

Interestingly, in our study, RDW was found to be lower in the malignant and hyperplasia groups compared to the benign (myoma) group which contrasts with several previous studies reporting elevated RDW levels in endometrial cancer (17). In our control group, patients with uterine myomas frequently presented with menorrhagia and chronic blood loss which may lead to iron deficiency anemia and consequently elevated RDW. Therefore, the increased RDW observed in the benign group might reflect underlying microcytic anemia rather than an absence of systemic inflammation.

Yayla Abide et al. showed that MCV measurements were found to be significantly higher in endometrial carcinoma and endometrial hyperplasia groups compared to the control group (3). In our study, we found the MCV value to be higher in the study group than in the control group.

In addition, the role of MPV has been extensively investigated in several types of cancer, such as gastric, colon, breast and lung cancer. It has been reported that MPV were not significantly different among endometrial cancer, hyperplasia with atypia/endometrial intraepithelial neoplasia, hyperplasia without atypia and normal controls (17). In our study, no difference was found between the groups in terms of MPV value.

The observed elevation in Neu and Neu % in endometrial cancer patients suggests a potential role of systemic inflammation in tumor biology. In clinical practice, preoperative neutrophil counts, readily available from routine blood tests, could serve as a supportive marker in identifying patients at higher risk of malignancy. Although not specific, elevated neutrophil values might prompt further diagnostic evaluation or raise preoperative suspicion especially when combined with other clinical and radiological findings.This approach is supported by previous research indicating that neutrophilia and high NLR, PLR are associated with poor outcomes and higher tumor aggressiveness in gynecologic malignancies (18). Future prospective studies are needed to validate whether such parameters can be integrated into risk stratification models.

In our study, NLR and PLR values did not show a statistically significant increase in patients with endometrial cancer. This finding contrasts with some previous studies such as Petric et al.,

which reported significantly elevated NLR and PLR levels in malignant cases (9). Several factors may explain this discrepancy, including differences in study design, sample size, patient selection criteria and the timing of hematological parameter measurement. Future larger-scale and prospective studies are needed to better elucidate the diagnostic and prognostic utility of NLR and PLR in endometrial cancer.

Our study has some limitations.Among demographic variables, only age data were consistently available for all patients. Due to the retrospective design and limited documentation, body mass index (BMI) and menopausal status could not be retrieved from hospital records.Another limitation is that we could not determine the potential differences between hyperplasia subgroups due to the low number of cases. Given the limited number of patients in the cancer and hyperplasia groups, our findings should be carefully interpreted.Future studies involving larger, multicenter cohorts are needed to confirm these observations and to better evaluate the diagnostic performance of hematologic parameters in uterine pathologies.

CONCLUSION

In conclusion, we think that routine hematological parameters such as Neu, Neu%, Hb, Hct, RDW and MCV may have diagnostic value in distinguishing benign and malignant uterine pathologies. However, further validation with larger and prospective datasets is essential before clinical application.

Ethics Committee Approval: This study was conducted as a specialty thesis project in 2014, before institutional ethics committee approval was required for retrospective chart reviews. No identifiable patient information was used. The study adhered to the ethical rules of the Declaration of Helsinki. Informed consent was obtained from the patients.

Peer-review: Externally peer-reviewed

Author Contributions: Concept: SA, TKA, CD, NC, Design: SA, TKA, CD, NC, Data Collection and Processing: SA, TKA, CD, NC, Analysis and Interpretation: SA, TKA, CD, NC, Writing: SA, TKA, CD, NC

Conflict of Interest: The authors declared no conflict of interest.

Financial Disclosure: The authors declared that this study has not received no financial support.

REFERENCES

1. Sobczuk K, Sobczuk A. New classification system of endometrial hyperplasia WHO 2014 and its clinical implications. Prz Menopauzalny. 2017;16(3):107–111.
2. Nie D, Yang E, Li Z. Pretreatment thrombocytosis predict poor prognosis in patients with endometrial carcinoma: a systematic review and meta-analysis. BMC Cancer. 2019;19(1):73.

3.Yayla Abide C, Bostanci EE, Cogendez E, Kilicci C, Uzun F, Ozkaya E, et al. Evaluation of complete blood count parameters to predict endometrial cancer. J Clin Lab Anal. 2018;32(6):e22438.

4. Zahorec R. Neutrophil-to-lymphocyte ratio, past, present and future perspectives. Bratisl Lek Listy. 2021;122(7):474-488

5. Christen S, Hagen TM, Shigenaga MK. Chronic inflammation, mutation, and cancer. In: Parsonnet J, ed. Microbes and malignancy: infection as a cause of human cancers. New York: Oxford University Press; p. 35–88.

6. Modugno F, Ness RB, Chen C, Weiss NS. Inflammation and endometrial cancer: a hypothesis. Cancer Epidemiol Biomarkers Prev. 2005;14(12):2840–2847.

7. Vrede SW, Donkers H, Reijnen C, Pijnenborg JMA. Abnormal preoperative haematological parameters in endometrial cancer: reflecting tumour aggressiveness or reduced response to radiotherapy? J Obstet Gynaecol. 2024;44(1):2294332.

8. Salem H, Abu-Zaid A, Salem A, Al-Badawi IA. Preoperative leukocytosis as a prognostic marker in endometrioid-type endometrial cancer: a single-center experience from Saudi Arabia. Gulf J Oncolog. 2020;1(32):51–58.

9. Petric AN, Živadinović R, Mitić D, Kostić I. Hematological and biochemical markers in determining the diagnosis and stage prediction of endometrial cancer. Ginekol Pol. 2023;94(4):283–290.

10. Selen S, Kilic F, Turan T. Can preoperative inflammatory markers differentiate endometrial cancer from complex atypical hyperplasia/endometrial intraepithelial neoplasia? J Obstet Gynaecol Res. 2020;46(7):1148–1156.

11. Muangto T, Maireang K, Poomtavorn Y, Suwannarurk K. Study on preoperative neutrophil/lymphocyte (NLR) and platelet/lymphocyte ratio (PLR) as a predictive factor in endometrial cancer. Asian Pac J Cancer Prev. 2022;23(10):3317–3322.

12. Firat A, Ercan A, Mordeniz C, Verit Atmaca FF. Predictive value of hemogram parameters in malignant transformation of the endometrium in patients with different risk factors. PLoS One. 2023;18(1):e0279224.

13. Pergialiotis V, Vogiatzi Vokotopoulou L, Vlachos DEG, Liontos M, Kontomanolis E, et al. Pre-treatment thrombocytosis and ovarian cancer survival: a meta-analysis. Eur J Obstet Gynecol Reprod Biol X. 2024; 22:100312.

14. Mohamadianamiri M, Aklamli M, Alemohammad F, Safarabadi M, Mohseni M, Javanmardi F. Hematologic inflammatory indexes as a prognostic factor

in endometrial cancer grading and staging. Caspian J Intern Med. 2023;14(3):443–448.

15. Abu-Zaid A, Alomar O, Abuzaid M, Baradwan S, Salem H, Al-Badawi IA. Preoperative anemia predicts poor prognosis in patients with endometrial cancer: a systematic review and meta-analysis. Eur J Obstet Gynecol Reprod Biol. 2021; 258:382–390.

16. Eoh KJ, Lee TK, Nam EJ, Kim SW, Kim YT. Clinical relevance of red blood cell distribution width (RDW) in endometrial cancer: a retrospective single-center experience from Korea. Cancers (Basel). 2023;15(15):3984.

17. Detopoulou P, Papadopoulos S, Rojas Gil AP. Relation of mean platelet volume (MPV) with cancer: a systematic review with a focus on disease outcome on twelve types of cancer. Curr Oncol. 2023;30(3):3391–3420.

18. Han KH, Kim EY, Han YJ, Lee SH, Kim JH, Seo YS. Prognostic significance of preoperative neutrophil-to-lymphocyte ratio and platelet-to-lymphocyte ratio in patients with endometrial cancer. Gynecol Oncol. 2021;161(2):530–536

Middle Black Sea Journal of Health Science / Mid Blac Sea J Health Sci
August 2025; 11(3): 190-211

ORGINAL ARTICLE **DOI:** 10.19127/mbsjohs.1603923

Ocimum basilicum-Assisted Gold Nanoparticle Formation: Structural Features and Antimicrobial Performance

Muhammed Said Özonay[1(ID)], Cumali Keskin[2(ID)], Ayşe Baran[3(ID)], Özgür Topgider[4(ID)], Şeyma Asyalı[4(ID)]

[1]Mardin Artuklu University, Vocational School of Organized Industrial Zone, Department of Electronics and Automation, Mardin, Türkiye
[2]Mardin Artuklu University, Vocational School of Health Science, Department of Medical Services and Techniques, Mardin, Türkiye
[3]Mardin Artuklu University, Kızıltepe Faculty of Agricultural Sciences and Technologies, Department of Field Crops, Mardin, Türkiye
[4]Mardin Artuklu University, Graduate Education Institute, Department of Biology, Mardin, Türkiye

Received: 06 May 2025, Accepted: 30 July 2025, Published online: 30 August 2025

Abstract

Objective: Plant-based biosynthesis of gold nanoparticles (AuNPs) can reduce the biological consequences of NPs released into the environment by replacing toxic substances. The Lamiaceae family includes the perennial herb *Ocimum basilicum* (OB), which is typically found in temperate climates. This study aimed to synthesize biogenic metallic nanoparticles ecologically to provide agricultural, medical, and pharmacological options from OB leaf aqueous extract.

Method: Tetrachloroauric acid ($HAuCl_4.3H_2O$) solution and OB extract were the chemicals, stabilizers, or surfactants used in the biological synthesis process to create gold nanoparticles (OB-AuNPs). Data from UV-Vis, SEM-EDX, XRD, FT-IR, TGA-DTA, AFM, and zeta potential were used to characterize the produced AuNPs. The minimum inhibitory concentration (MIC) method was used to test the antimicrobial activity.

Results: UV-Vis data revealed that the produced gold nanoparticles produced a notable plasmon resonance at around 532 nm. SEM-EDX examination verified that the synthesized nanomaterials had a spherical crystal structure. The reduction of Au^{+3} ions using the OB extract resulted in the production of crystalline AuNPs, as demonstrated by the high-resolution and robust XRD pattern. Analysis of XRD and SEM-EDX data revealed that gold, oxygen, and carbon made up the majority of OB-AuNPs' element content. The surface charges of AuNPs were determined to be (−) 17 mV.

Conclusion: The negative zeta potential indicates good stability of the nanoparticles in suspension, suggesting that they are less likely to aggregate over time. It was found that, in comparison to conventional antibiotics, OB-AuNPs produced utilizing an extract from the leaves of the OB had more potent inhibitory activity on the growth of yeast and pathogenic gram bacteria. Overall, these findings support the potential application of AuNPs in various fields, including biomedical and environmental technologies.

Keyword: *Ocimum basilicum* (Basil extract), antimicrobial activity, characterization, plant-mediated synthesis, gold nanoparticles (AuNPs)

Suggested Citation Ozonay MS, Keskin C, Baran A, Topgider O, Asyali S. Ocimum basilicum-Assisted Gold Nanoparticle Formation: Structural Features and Antimicrobial Performance. Mid Blac Sea Journal of Health Sci, 2025;11(3):190-211.

Address for correspondence/reprints:

Cumali Keskin

Telephone number: +90 (532) 741 39 89

E-mail: cumalikeskin@artuklu.edu.tr

INTRODUCTION

Nanotechnology has emerged as a transformative tool across diverse fields, particularly in medicine, where it enables targeted drug delivery, advanced diagnostics, and novel antimicrobial therapies. In recent years, plant-mediated synthesis of nanoparticles has gained prominence due to its eco-friendly and biocompatible nature, positioning it as a promising strategy in biomedical nanotechnology (1). Drugs, inanimate materials inserted into live tissues, and blocking veins can all be accomplished with the use of nanotechnology-developed products (2). These advancements enhance the efficacy of medical treatments and pave the way for personalized medicine, where therapies can be tailored to individual genetic profiles. As research continues to evolve, the potential applications of nanotechnology in healthcare promise to revolutionize the way we approach disease management and tissue regeneration (3).

Also, nanotechnology is favored for producing nanoparticles using quick, inexpensive, and environmentally acceptable "green synthesis" techniques that address various health-related issues (4). The two most common methods for creating nanoparticles are top-down and bottom-up. The "top-down" technique reduces the size of nanostructured materials by abrading the larger, macro-sized material toward the nanoscale. The "bottom-up" method joins particles to create larger ones. Both approaches have their unique advantages and applications, depending on the desired properties and functionalities of the final product. As research progresses, the integration of these methods could lead to innovative solutions across multiple fields, including medicine, electronics, and environmental science (5).

The scientific community has recently shown considerable interest in noble metal nanoparticles (MNPs), particularly gold (AuNP) and silver (AgNP), due to their remarkable properties such as strong photo-electrochemical activity, chemical stability, biocompatibility, and exceptional capabilities in catalyzing chemical reactions and combating pathogens, along with their ease of synthesis. These characteristics render MNPs highly suitable for a broad array of applications, including drug delivery, biosensing, and

environmental remediation. As research continues to investigate their potential, the integration of MNPs into various technologies could lead to significant advancements in fields like medicine and environmental science (5,6).

Applications for metallic nanoparticles, particularly gold nanoparticles (AuNPs), are numerous in the field of biomedicine. Additionally, differently sized and shaped gold nanostructures have been found to impact cell viability (7). Gold nanoparticles will range in size from 2 to 370 nm. Hexahedral, octahedral, cubic, prismatic, plate, wire, spherical, trihedral, and tetrahedral shapes are among them. The terms nanosphere, nanorod, nanocube, nanowire, and nanoprism are being used to describe them (8). The surface resistance features of gold nanoparticles make them useful for a wide range of applications, including cell targeting, nanoimaging, and disease diagnostics in photoelectronics. Additionally, biomolecular investigations that detect drug and gene release favor them. Gold nanoparticles are among the best agents for treatment because they can transport large drug loads and readily reach target bio-cells (9). Gold nanoparticles, which are widely employed in processes like biolabeling and photothermal microscopy, have emerged as a promising option for imaging and biosensor applications because of their high electron density (10). They are known to have less antibacterial activity than silver, but their ease of synthesis has made them useful for applications in fields including biomedical imaging and photothermal health (11).

Studies have been done on making gold nanoparticles (AuNPs) using natural sources like plants (12), fungi (13), algae (14), bacteria (15), and seaweeds (16) through eco-friendly methods. The main reasons for researching this area are the large quantities of AuNPs produced from different parts of plants like leaves, fruits, roots, and flowers, their improved stability, and the easy and affordable methods used to make them. Bioactive substances like alcohols, flavonoids, and phenolic compounds from plants help turn Au^{3+} ions in water into AuNPs by producing Au^{0} (10).

Potential uses for these nanoparticles include bioremediation, antiviral, antibacterial, antioxidant, cytotoxic, antitumor, anti-inflammatory, and antidiabetic (17). Microbial infections have grown more resistant to even the most effective therapies recently. The healthcare system has been strained as a result of the rise in mortality and morbidity worldwide. Concerns have arisen about the use of antibiotics and the research process for developing new ones, underscoring the urgent need to halt this threat. More people are looking for different ways to fight antibiotic resistance and create new medications (18).

Biogenic nanoparticles derived from plant sources can serve as carriers and enhance cellular penetration for many applications.

Nanoparticles possess considerable advantages owing to their distinct surface area and favorable conductivity. Biogenic nanoparticles have significantly contributed to the advancement of novel techniques in biomedicine and pharmacology (19). These advancements encompass the creation of intelligent pharmaceutical substances alongside diagnostic and therapeutic methodologies (20). This study primarily aims to synthesize metallic gold nanoparticles utilizing an aqueous leaf extract of OB. The utilization of extracts derived from O.B. leaves, facilitated by their abundance, provides a straightforward and cost-effective approach for the synthesis of metallic nanoparticles.

O.B., which grows in tropical and temperate climates, is recognized in scientific circles as having Indian origin. Purple basil is an herbaceous plant that grows every year. Africa, America, and Asia are all naturally home to the *Ocimum* genus, and there are more than 35 species of basil. Depending on the linguistic and dialectal structures of the three regions of the world, they have different names. It is referred to as reihan in Turkey and the surrounding area and rehan in Arabic and Persian, respectively (21, 22). It is referred to as Albahaca in Spanish and *Basilic basilicum* in French and German. In Turkey, it is commonly referred to as basil. Badrooj, Hebak, or Rihan are further regional names. There are more than 65 species worldwide, and it is said to grow naturally in hot and temperate climates in Africa, Asia, and Central America (23). The morphology and chemical composition of *O. basilicum* vary greatly (24). The leaves and blossoms of basil (*O. basilicum*) and basil (*O. minimum*) are the most economically valuable portions. This research used an aqueous extract of the aboveground portions of the OB plant to examine the biosynthesis, synthesis, characterization, and antibacterial qualities of gold nanoparticles. The study aimed to highlight the potential applications of these gold nanoparticles in various fields, particularly in medicine and agriculture. By investigating their antibacterial properties, the research sought to establish a foundation for developing new antimicrobial agents derived from natural sources.

METHODS

Plant Materials and Reagents

The leaves of OB used in this study were obtained from the local market in Mardin in May. Dr. Cumali Keskin from Mardin Artuklu University confirmed the taxonomic identity of the plant sample. The plant samples were stored in the herbarium of the same institution (herbarium voucher number MAU: 2023-05). Tetrachloroauric acid (HAuCl4.3H2O, purity 99.99 %; Alfa Aesar) in solid form was used in the synthesis stage. The McFarland standard (0.5), Mueller Hinton medium, the RPMI feed medium, and standard antibiotics (fluconazole, vancomycin, and colistin) were commercially

purchased from Sigma Aldrich. The microorganisms used in the study were selected from the strains in the American Cell Culture Collection (ATCC) in the inventory of Mardin Artuklu University Microbiology Research Laboratory.

Preparation of Plant Extract

Distilled water was utilized to completely wash the OB leaves used in the experiment to get rid of any leftover residue. They were dried at room temperature and powdered on sterile blotting paper. After 50 g of the powdered samples were taken and boiled for 20 minutes at 85ºC with 750 mL of distilled water, the resulting aqueous extract was allowed to cool to room temperature (25ºC). Following that, Whatman filter paper was used to filter the coarse plant pieces. To be employed in the manufacture of gold nanoparticles, the resulting aqueous extract was kept at +4 °C.

Green Synthesis of OB-AuNPs

The solid form of tetra chloroauric acid ($HAuCl_4.3H_2O$) was used to prepare an aqueous gold solution with a concentration of 5 mM for the biosynthesis of AuNPs. At room temperature, 75 milliliters of aqueous extract of OB leaf and 100 milliliters of a solution of 5 mM $HAuCl_4.3H_2O$ were combined and allowed to react. 30 minutes into the reaction, Au^{3+} ions were reduced to Au^0, and the solution lost its transparency and turned dark red. After seeing the color change, the solution that was formed was centrifuged for twenty minutes at a speed of 6000 rpm, and the solid component was separated. Multiple washes with distilled water were performed on the solid phase that had accumulated at the bottom. OB-AuNPs that had been synthesized were allowed to dry in an oven at a temperature of 50 ºC for 72 hours. In an agate mortar, the solid component was then ground into a powder.

Figure 1. A. Fresh leaves of OB. B. Dried leaves. C. $HAuCl_4.3H_2O$ solution (Yellow). D. OB aqueous extract (Red). E. Biosynthesized OB-AuNPs solution (Dark red)

Characterization of Biogenic OB-Au NPs

A Shimadzu UV-1601 ultraviolet-visible spectrometer was used to identify the surface plasmon resonance (SPR) peaks of the biosynthesized OB-AuNPs. The shape and distribution of elements in OB-AuNPs were studied using a scanning electron microscope with energy-dispersive X-ray capabilities and

transmission electron microscopy. The surface charge and stability of OB-AuNPs in liquid were measured using a zeta potential and zeta-sizer device (Malvern). Differential thermal analysis (DTA) and thermogravimetric analysis (TGA) were used to check how stable OB-AuNPs are when heated and to measure any weight loss. The crystalline structure of OB-AuNPs was determined using XRD equipment (X-ray diffractometer RadB-DMAX 11). The topological characteristics of OB-AuNPs were analyzed utilizing Atomic Force Microscopy (AFM). FT-IR spectroscopy (650 cm^{-1} to 4000 cm^{-1}; Perkin Elmer One, USA) was used to study the functional groups in the plant extract and how they changed after the process was finished. This comprehensive approach allowed for a detailed understanding of the chemical transformations that occurred during the synthesis of OB-AuNPs. Furthermore, the results obtained from these analyses provided valuable insights into the stability and efficacy of the nanoparticles for potential applications in various fields, including medicine and environmental science.

Evaluation of the Antimicrobial Properties of Au Nanoparticles

OB-AuNPs, $HAuCl_4.3H_2O$ solution, and commercial antibiotics (fluconazole, vancomycin, and colistin) were tested for their ability to inhibit the growth of pathogenic microorganisms, including *Candida albicans* (*C. albicans*) yeast, *Escherichia coli* (*E. coli*; ATCC 25922) bacterial strains, and *Staphylococcus aureus* (*S. aureus*; ATCC 29213). They were plated on solid plates using nutrient agar solid medium for Gram-positive and Gram-negative bacteria and sabouraud dextrose agar medium for yeast. The solid medium plates' microorganisms were used to create solutions that met the McFarland standard 0.5 turbidity threshold (1.5×10^8 united colonies (cfu/mL). *C. albicans* yeast was cultured in Roswell Park Memorial Institute (RPMI) broth, while bacteria were cultured in Müller Hinton broth. For the microdilution procedure, 96-well microplates were utilized. The microdilution-applied microplates were incubated for an entire night at 37 °C. The lowest inhibitory concentrations and the wells in which growth took place were then calculated (25).

RESULTS

An aqueous extract that was generated from the leaves of OB was used in this publication to describe the results of research that investigated the biogenesis of gold nanoparticles. The selection of OB leaf for the present experiment was based on the fact that it is known to contain flavonoids and phenolic chemicals, both of which are known to contribute to the antibacterial activities of the leaf. The initially yellow $HAuCl_4$ solution turns purple, red, or violet as gold nanoparticles form. The phenolic compounds, flavonoids, terpenoids, ascorbic acid (vitamin C), sugars, and other reducing

agents found in plant extracts convert Au^{3+} ions (gold ions) to elemental gold (Au^0) when $HAuCl_4 \cdot 3H_2O$ (Gold (III) Chloride Trihydrate) combines with the plant aqueous extracts. The study aimed to explore the potential of these compounds in facilitating the reduction of gold ions into nanoparticles. By utilizing the extract, we were able to observe the formation of nanoparticles and analyze their size and morphology through various characterization techniques.

Characterization

UV-Vis Spectrophotometry Results

A spectrophotometer is used to test a solution's transmittance. Spectrophotometers assess transmittance or absorbance in relation to wavelength by altering it. They are preferred because of their excellent sensitivity, speed, applicability, and repeatability. Determining the structures of pure chemicals in food, determining if a functional group is present, and identifying the position of a functional group in a compound are all done via qualitative analysis. The occurrence of a surface plasmon resonance (SPR) peak at ~520-550 nm confirms the presence of gold nanoparticles (26). A maximum absorbance band was observed at 532.59 nm, confirming Au NPs' formation (Figure 2). The published results from the previous research were comparable to this set of findings. These similarities suggest a consistency in the results across different studies, reinforcing the validity of the conclusions drawn. Furthermore, the alignment of these findings may indicate a broader trend within the field that warrants further exploration (27).

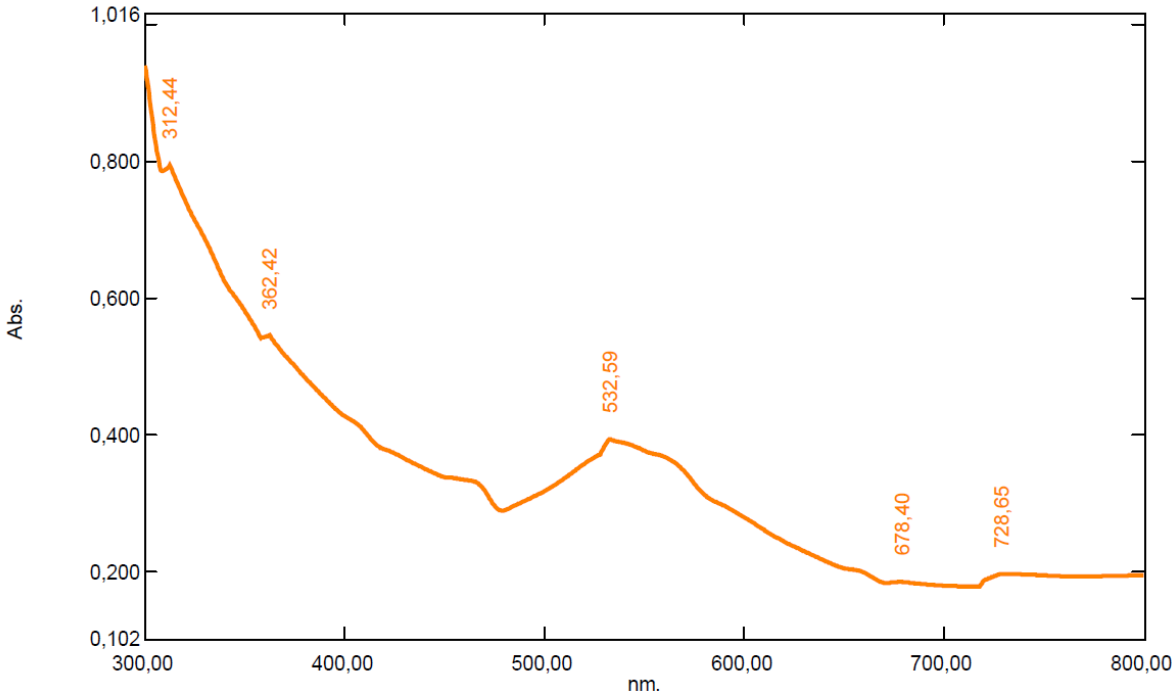

Figure 2. Ultraviolet-Visible absorption spectra of OB-AuNPs

FTIR Spectrum Data Analysis

The analysis performed with the FT-IR device in the range of 500–4000 cm^{-1} examined the presence of functional groups in the structure of the plant extract and the change of functional groups that play a role in the reduction at the end of the reaction. FT-IR spectroscopy is critical in investigating the chemical composition of chemical compounds. Here, it is used to characterize the plant extract and the nanoparticles synthesized from it. The FT-IR spectrum provides information about which functional groups the reaction took place on by comparing the extract from OB leaves (Figure 3a) and the synthesized OB-AuNPs (Figure 3b). This comparison allows researchers to identify specific peaks corresponding to various functional groups, indicating potential interactions during the synthesis process. Also, changes in these peaks can provide information about how the plant extract connects with the nanoparticles, helping us better understand the chemical changes that take place.

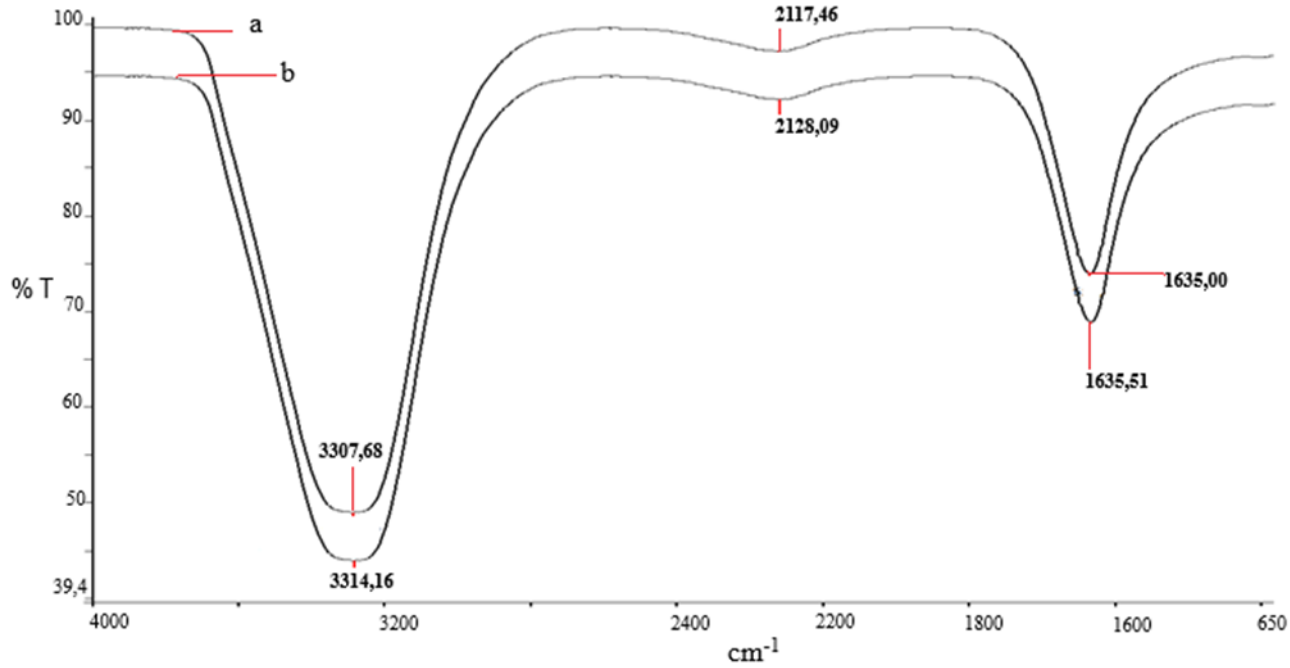

Figure 3. a. OB aqueous plant extract FT-IR spectrum b. OB-AuNPs FT-IR

XRD Analysis Data of OB-Au NPs

The crystal structures of gold nanoparticles were examined using a RadBDMAX II computer-controlled X-ray diffractometer within the region of $0° \leq 2\theta \geq 80°$. The crystal dimensions of gold nanoparticles were determined utilizing the Debye-Scherrer equation (25).

$$D = K\lambda/(\beta \cos(\theta)) \quad (1)$$

In the equation, D represents the crystal diameter of the particle (nm); K is 0.90; λ denotes the wavelength (1.54 Å); β signifies the breadth of the greatest peak at half height (rad.);

and θ indicates the Bragg angle degrees. The crystal structure (JCPDS No 04-0784) and purity of gold nanoparticles were verified using X-ray diffraction analysis. Figure 4 illustrates the powder XRD patterns of nano-crystalline AuNPs.

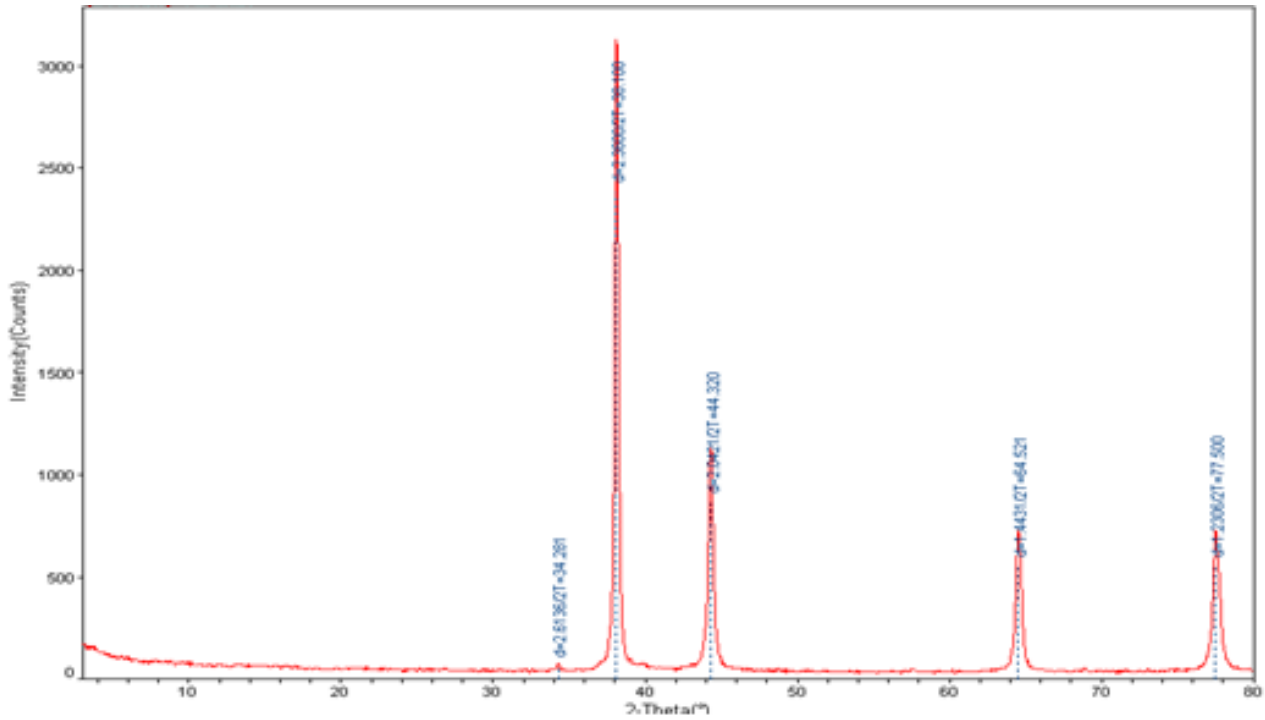

Figure 4. XRD pattern of biogenic OB-AuNPs

SEM-EDX and TEM Analysis of Green-Synthesized AuNPs

SEM and TEM image analyses were performed to determine the surface morphology and particle average size of AuNPs (Figures 5 and 6a,b). The images obtained from these analyses confirmed the existence of nano-sized AuNPs obtained using biological material. The angle of incidence of the electron beam on the surface, or the surface topography, determines how many secondary electrons are released from various regions of the sample by atoms excited by the electron beam in scanning electron microscopy. Analyses of composition and topography were carried out as needed. SEM, or scanning electron microscopy, was used to determine the size and shape of the gold nanoparticles. The creation of pure gold or gold oxide particles of AuNPs in the basic composition was verified using SEM-energy dispersive X-ray spectroscopy (SEM-EDX) (Figure 7).

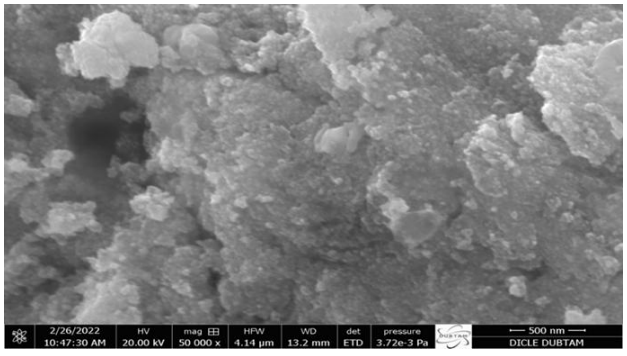

Figure 5. SEM images of biosynthesized OB-AuNPs

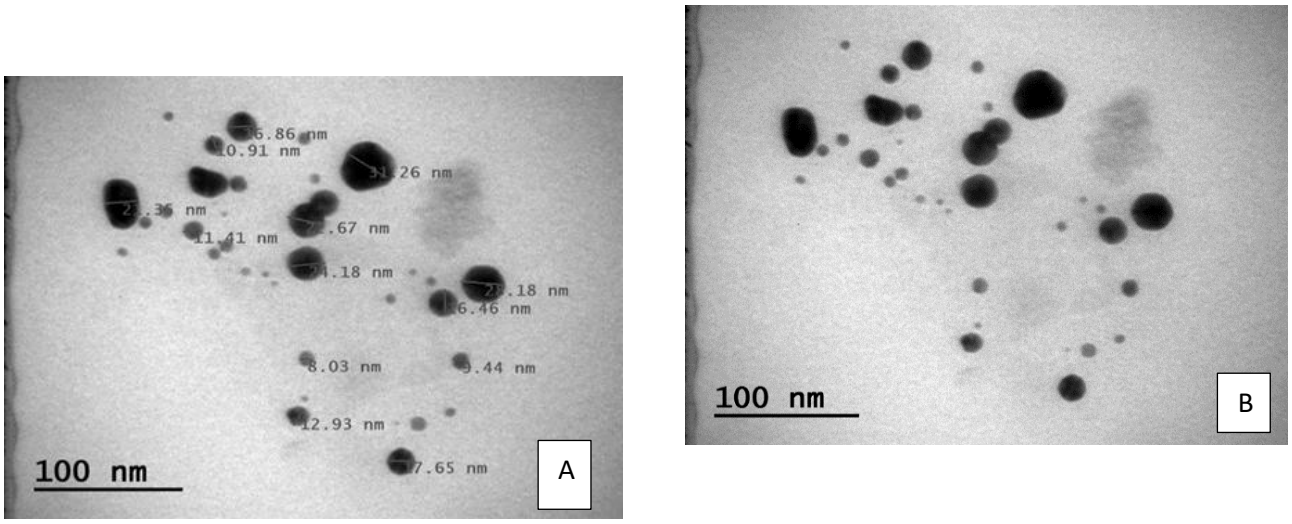

Figure 6. TEM images of biosynthesized OB-AuNPs (a, b)

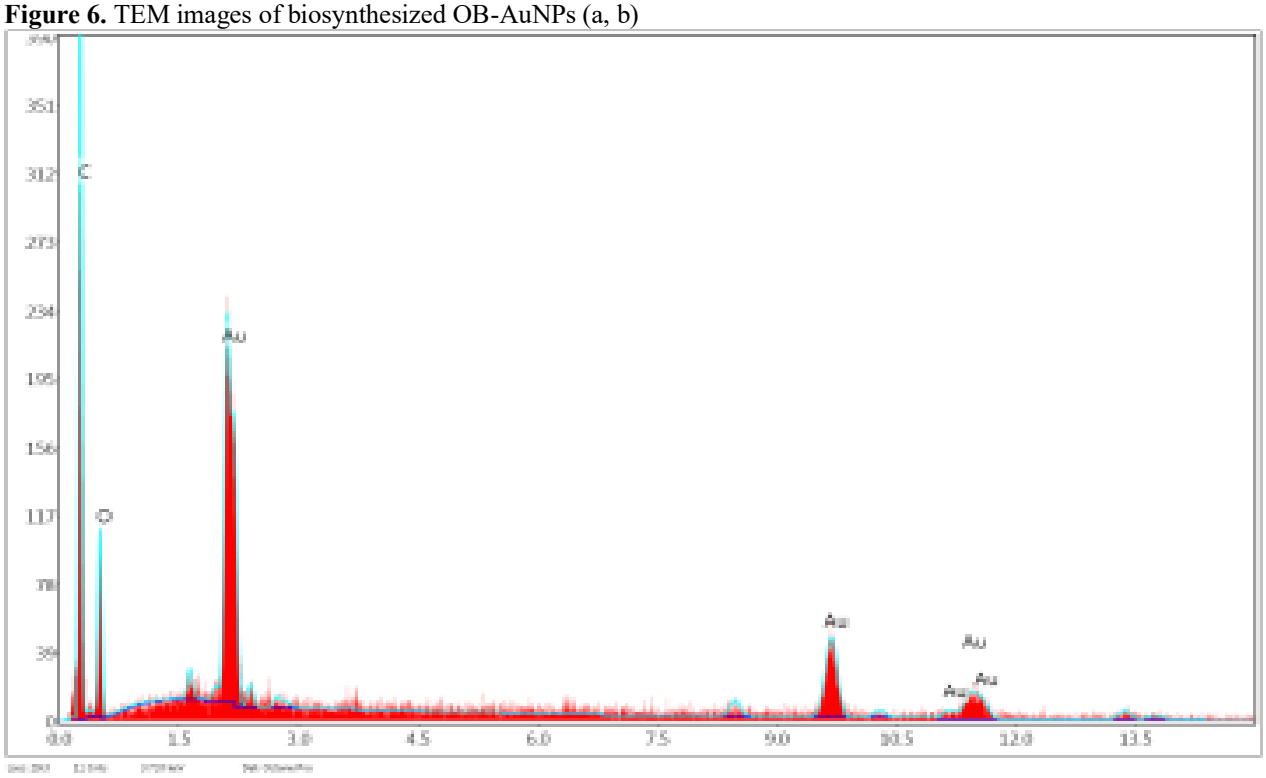

Figure 7. SEM-EDX spectrum of biosynthesized OB-AuNPs

AFM Analysis Results

AFM makes it possible to take measurements without the need for electrically conducting surfaces. With its high vertical image resolution, this Scanning Probe Microscope (SPM) instrument can scan the surface of a sample the size of a nanoparticle to acquire images and conduct surface interaction properties, friction, wear, corrosion, coating detection, electrical charge, absorption, and distribution research in the nanomaterial's structure, as well as size and shape research. Hydrophilic and magnetic characteristics can also be measured with it. OB-AuNPs' topological characteristics as determined by atomic force microscopy (AFM) were given in Figure 8.

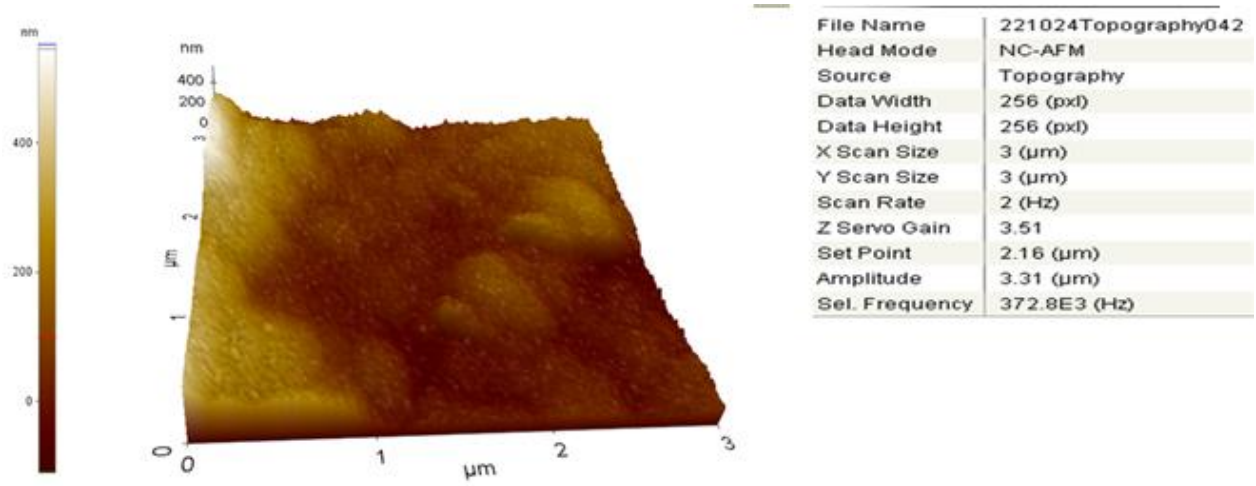

Figure 8. Atomic force microscopy (AFM) image of OB-AUNPs

Thermogravimetric (TGA) and Differential Thermal (DTA) Analysis Results of OB-derived Au NPs

TGA-DTA analysis was used to determine the degradation temperatures of gold nanoparticles produced using OB leaf extract. The TGA and DTA processes are used together. While TGA measures weight changes (water loss and organic matter removal) that take place inside the material, the DTA instrument measures temperature changes caused by exothermic/endothermic processes. This combined approach provides a comprehensive understanding of the thermal stability and behavior of the nanoparticles under varying temperatures. By analyzing the data obtained from both TGA and DTA, researchers can better assess the effectiveness of the synthesis method and the potential applications of the gold nanoparticles. By accurately calculating the melting, boiling, and decomposition points, DTA offers information regarding crystallization and phase transitions. The stability of the produced gold nanoparticles and their breakdown temperature were ascertained by TGA and DTA analysis (Figure 9).

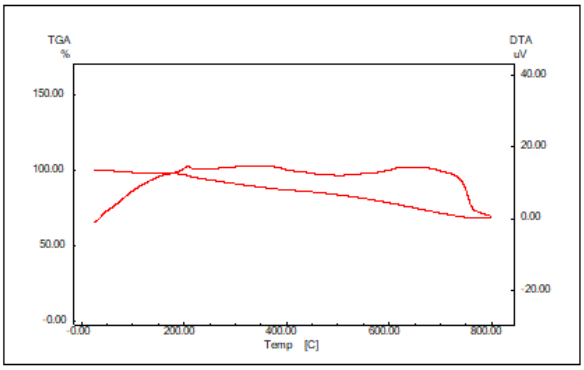

Figure 9. TGA-DTA analysis result of biosynthesized OB-AuNPs.

Zeta Potential and Distribution Analysis of OB-Au NPs

The Zeta potential and zetasizer were used to measure the surface charges and size distributions of AuNPs made from leaf extract. The electric charge on the surface of the

substance that is surrounded by the environment is known as the zeta potential. Adhesion and aggregation are inhibited by a large negative value of the zeta potential. This shows that the AuNP colloid is stable. However, because of their much lower negative charge, nanoparticles are able to enter the cell more readily (28). It was discovered that the biosynthesized AuNPs had a zeta potential of -17 mV (Figure 10). The AuNPs exhibiting monodispersity had an average zeta size of 166.2 (d.nm) according to the Zetasizer measurements (Figure 11).

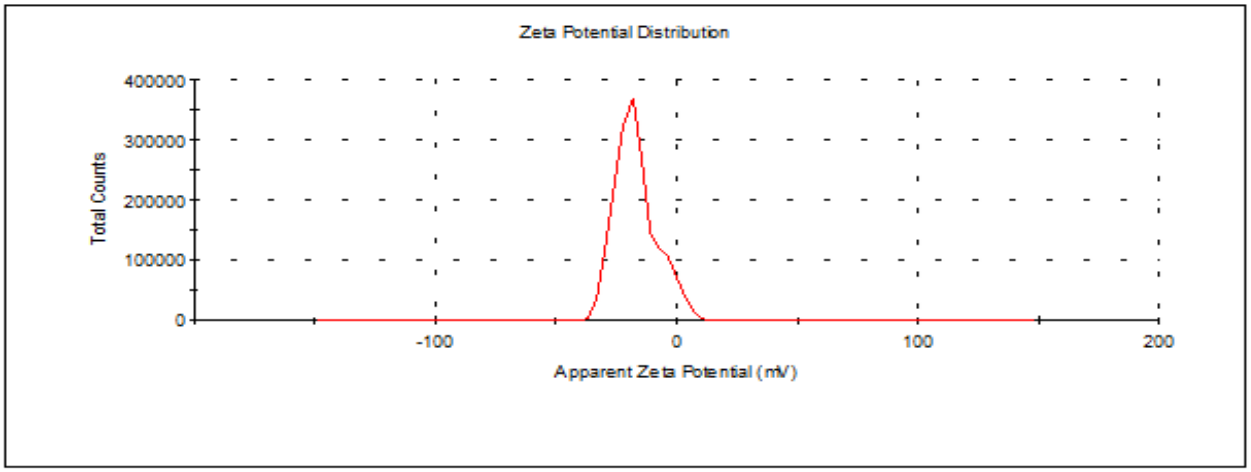

Figure 10. Zeta potential analysis of biogenic OB-AUNPs

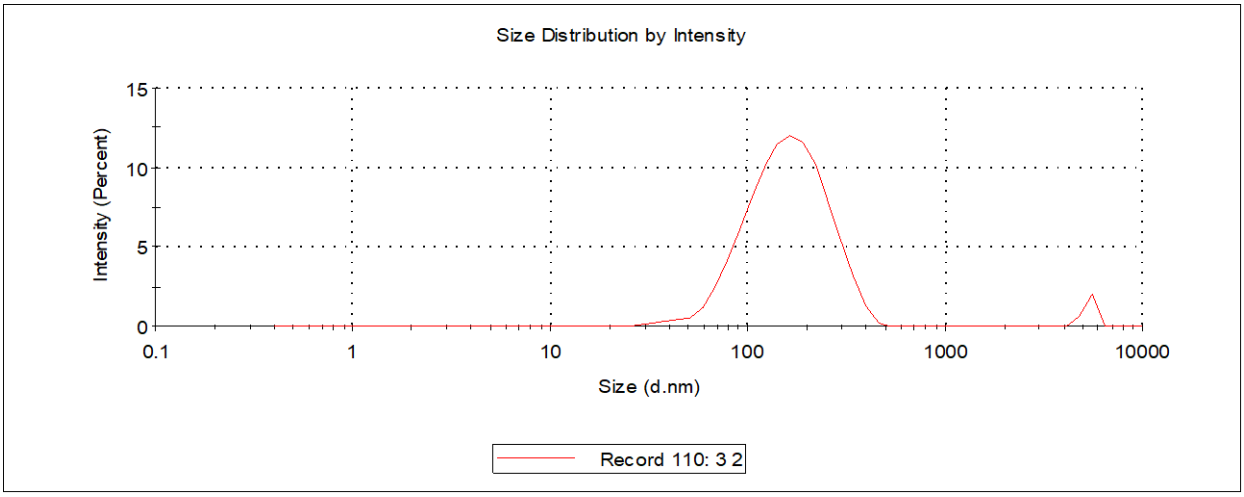

Figure 11. Zeta distribution analysis of biogenic OB-AUNPs

Antimicrobial Assay Results

The antimicrobial activity of biogenic OB-Au nanoparticles, which were created using an aqueous extract of OB leaves, was the main focus of this study. The study employed the minimum inhibitory concentration approach to assess antimicrobial activity against a variety of bacterial (gram positive *S. aureus*, gram negative *E. coli*) and yeast (*C. albicans*) strains. Throughout the experiment, fluconazole (128 µg/mL), colistin (128 µg/mL), and vancomycin

(128 µg/mL), served as standard. Table 1 demonstrates the strong antimicrobial activity of OB-AuNPs against Gram-positive and Gram-negative bacteria, as well as yeast. The antibacterial efficacy of gold nanoparticles is influenced by multiple factors, including zeta potential, particle size and shape, colloidal stability, pH, temperature, concentration, and the specific microbial strains tested.

Table 1. MIC value (µg/mL) of biogenic OB-AuNPs on pathogenic microorganisms

Microorganisms	OB-AuNPs	$AuCl_4.3H_2O$	Antibiotics*
S. aureus ATCC 29213	1. 40	2.65	2
E. coli ATCC25922	0.375	0.66	2
C. albicans	0.075	0.66	2

* *E. coli*, *S. aureus* and *C. albicans* were treated with colistin, vancomycin, and fluconazole antibiotics, respectively.

DISCUSSION

OB, among the Ocimum species, holds significant economic value due to its abundant volatile oil content and is extensively utilized in the spice, food, cosmetics, fragrance, and pharmaceutical sectors (29). The total phenolic content in green and purple varieties of OB is believed to be influenced by color variation, as well as species differences, climate, and cultivation conditions (30). Purple varieties of basil hold a key position in the food business due to their anthocyanin content, a crucial class of flavonoids that represent a substantial portion of plant secondary metabolites. The distinctive purple hue and the lack of estragole in its oil are noteworthy attributes for study subjects and economic viability. Consequently, the cultivation of OB is on the rise (31). The antibacterial efficacy of basil is influenced by factors such as its origin and oil composition; for instance, the effectiveness of French basil oil differs from that of Indian and Niazbo basil oils against *S. aureus*. French basil is ineffective, whereas Indian-niazbo basil is effective (32). The basil plant, comprising oil, protein, sugar, and water, occupies a role in the food chain due to its mineral content, including magnesium, potassium, phosphorus, iron, zinc, and calcium, and is also abundant in antibacterial compounds. It has been documented that it possesses anti-inflammatory, antioxidant, hypolipidemic, insecticidal, pharmacological, hypoglycemic, cardiac stimulant, anthelmintic, and wound-healing properties applicable in the treatment of cancer and ulcers resistant to bacterial, viral, and fungal infections (33).

The aqueous extract derived from OB leaves, noted for the aforementioned qualities, was utilized in the production of gold nanoparticles. The presence of stable gold nanoparticles produced through biosynthesis was validated using multiple spectroscopic techniques.

The UV-VIS spectrophotometer facilitates analytical analyses (both qualitative and quantitative) of colored complexes or

compounds within the wavelength range of 0.3-0.8 micrometers. It enables the examination of reaction kinetics, the calculation of equilibrium constants, the elucidation of molecular structures and stereochemical properties, and the identification of atoms and molecules. This includes the determination of anions that are undetectable by alternative instruments, the measurement of molecules or inorganic ions and complexes in solution, the assessment of purity levels, and the absorption of electromagnetic radiation by molecules or atoms, among other applications. The reduction of gold salt occurs through potent reducing agents, converting Au3+ ions to Au°, while surface plasmon resonance arises from the collective emission of free conduction electrons in gold solutions, influenced by the varying shape and size of the gold salt (10). In this context, UV-Vis spectroscopy, a crucial technique for detecting the formation and stability of AuNPs in aqueous solutions through colorimetric changes, was employed to assess the synthesis of AuNPs using basil (OB) plant extract. The maximum absorbance band color change of AuNPs, indicative of particle presence in the synthesis medium, was evaluated through UV-Vis readings. It was found that the color shift of AuNPs on the plasma surface caused a specific peak to appear at 532.59 nm in the UV-Vis spectrum. The synthesis accuracy is shown by studies that found particular peaks for AuNPs in the 525–540 nm range (10,34). These findings underscore the importance of precise control over the synthesis parameters to ensure consistent optical properties of AuNPs. Furthermore, the reproducibility of these peaks across different studies highlights the reliability of the synthesis techniques employed in the research. The study of the FT-IR results for the extract from OB leaves and its FT-IR spectrum after reacting with gold salt shows that the changes in frequency of the functional groups involved in the reduction are due to the vibrations of the O-H functional group at the 3347 cm^{-1} peak. The functional groups at 1634 cm^{-1} are linked to the I Amide band (C=C and C=N), while the peak at 2110 cm^{-1} might relate to the N=C or C=C functional groups. The functional groups at 1634 cm^{-1} are associated with the I Amide band (C=C and C=N), whereas the peak at 2110 cm^{-1} may correspond to the N=C or C=C functional groups. The changes in the frequencies indicate that the –OH (hydroxyl), N-H (amine), and C≡C (alkyne) groups are responsible for the decrease. This reduction shows that these functional groups are interacting strongly with their surroundings, which could affect how reactive and stable the compound is. Understanding these shifts in peak positions is crucial for elucidating the compound's chemical behavior and potential applications in various fields.

The X-Ray Diffraction method (XRD) is based on how X-rays bounce off materials, creating a pattern that shows the unique features of crystal structures, the distance between atoms, and how they are arranged in a crystal. X-rays are emitted from a cathode ray tube, filtered to provide monochromatic radiation, collected in a concentrated manner, and directed toward the sample. The diffracted X-rays are subsequently measured, analyzed, and quantified, and the XRD crystal structure is revealed. Diffraction serves to identify crystalline phases akin to a fingerprint. The crystal structure and purity of gold nanoparticles were verified using XRD analysis. Figure 4 illustrates the powder XRD patterns of nanocrystalline AuNPs. The diffraction peaks and planes for AuNPs, such as (111), (200), (220), and (311), match the face-centered cubic structure. The unique peak values corresponded well with the reference data (JCPDS card no. 0784 for Au) (35). The high-resolution and robust XRD pattern demonstrated the synthesis of crystalline AuNPs through the reduction of Au+ ions using an extract from OB leaves. The analysis of the XRD data revealed that the average nanoparticle size was determined to be 40.39 nm, as per the Debye-Scherrer equation. This size is consistent with the expected dimensions for effective catalytic activity and biocompatibility in various applications. Furthermore, the successful synthesis of these gold nanoparticles underscores the potential of using plant extracts as eco-friendly alternatives in nanomaterial production.

In a scanning electron microscope, electrons interact with atoms in the sample and produce signals that reveal the sample's topography and composition. This work used SEM to analyze the morphological structures of gold nanoparticles that were generated. A two-dimensional and detailed sample image is obtained with TEM. Imaging of the sample's surface and fine structures, morphological research, and structure-function interpretation are possible. TEM examination shows how a substance's physical characteristics and microstructures generate a common feature or features. TEM investigation of gold nanoparticles is conducted by capturing images at very low nanometers, evaluating their size, and determining their average size. It also helps determine the cell membrane transit of produced metallic nanoparticles in biological applications. Transmission Electron Microscopy analyzes samples using high-voltage electron beams. SEM and EDX micrographs provide further data regarding the scanned region's chemical and elemental compositions. Nano-characterization uses SEM and EDX to determine particle sizes and elemental composition. In electron dispersive X-ray (EDX) analysis (Figure 7), the sample's elemental compositions suggest AuNPs with strong gold peaks. In addition, the scanned spots determine the metalloid composition

percentage. Quantitative examination of the produced gold nanoparticles follows. The evaluation of the acquired results revealed that the gold nanoparticles were spherical. The SEM-EDX analysis of the AuNPs' energy distribution spectra revealed that the gold particles were roughly 50 nm in size and that the majority of the elemental composition was that of gold nanoparticles. The functional groups of phytochemicals around the reduction-formed nanoparticles are responsible for the occurrence of peaks like carbon and oxygen next to these strong peaks. The dimensions of the produced nanomaterial were assessed using TEM metrics. According to the TEM pictures of the produced AuNP-OB, the synthesized AuNPs have an average size of 17.79 nm and range in size from 8.03 to 31.26 nm (Figure 6a,b). Because of their functional groups and surface charges, the AuNPs produced via green synthesis are nanosized and arranged in small groups that are not in direct touch with one another, according to micrographs (10).

The AFM results show that the average particle size of AuNPs is between 0-100 nm as seen in Figure 8. The surface morphology of AuNPs, SEM and TEM images (Figure 5 and Figure 6a,b) and particle distribution density analysis (Figure 7) confirm the existence of AuNPs obtained by synthesis in nano-sized and non-contacting clusters. This shows that AuNPs are stable and do not agglomerate due to their negative surface charge. In addition, TEM images indicate that gold particles are predominantly spherical and hexagonal in size. Many researchers have also reported spherical AuNPs in their studies (36).

The gold nanoparticles produced biologically were examined using TGADTA data from 20 to 800 °C at a heating rate of 10 °C per minute in a nitrogen environment with a flow rate of 20 mL per minute. The TGA-DTA curve illustrates the mass reduction resulting from thermal deformation. Figure 9 illustrates that the mass loss within the temperature range of 0-200 °C is attributable to moisture, but the mass losses occurring between 200-800 °C are a result of the plant extract. The nanomaterial remains stable at elevated temperatures, with the mass loss amounting to 25 percent. Research has documented the stable architectures of nanoparticles at elevated temperatures, specifically in research with AuNPs derived from *Acacia auriculiformis* (37) and *Artemisia absinthium* (38).

The antimicrobial mechanism of nanoparticles frequently seeks to examine the interactions between nanoparticles and the bacterial cell membrane, as well as the parameters that allow the bacteria to sustain its viability. Research indicates that substantial quantities of particles are generated, and nanoparticles with elevated surface area exhibit significant activity at minimal concentrations (39). Metal particles attach to the cell membrane via nanoparticles, utilizing electrical forces and chemical bonds to

form a composite structure. In response to the adherence of the metal particle, the cell undergoes dissolution by oxidation, resulting in the combination of atoms and ions to form bigger particles. The interactions of metal nanoparticles vary between living and deceased cells. Table 1 illustrates the inhibitory effect of biosynthesized OB-AuNPs on human pathogens. The inhibitory impact of AuNPs is evidently superior to that of $HAuCl_4.3H_2O$ and antibiotics, even at minimal dosages. The most potent action of OB-AuNPs was observed against *C. albicans* at a concentration of 0.075 µg/mL. The MIC values (µg/mL) of the synthesized AuNPs for *S. aureus* and *E. coli* were established as 1.40 and 0.375, respectively. The current investigation reveals the presence of AuNPs at around 8 nm (Figure 6a). Agnihotri et al. (2014) reported that when nanoparticles smaller than 10 nm get even smaller, they can enter cells more easily, which makes AuNPs more effective at fighting bacteria (40). The antibacterial efficacy of AuNPs was assessed using the microdilution method, wherein the Minimum Inhibitory Concentration (MIC) values were established for the gram-positive *S. aureus*, gram-negative *E. coli*, and the fungus *C. albicans*. Consequently, it was concluded that OB-AuNPs exhibited superior antibacterial efficacy relative to commercial antibiotics at low doses. This enhanced cellular uptake could lead to improved therapeutic outcomes, particularly in treating infections caused by resistant bacterial strains. Future studies should focus on the mechanisms of interaction between these nanoparticles and bacterial cells to further elucidate their potential applications in antimicrobial therapy.

CONCLUSION

This research is the first investigation into the biological applications of gold nanoparticles synthesized from the aqueous extract of OB leaves. The exceptional characteristics of AuNPs render these compounds widely sought after, presenting significant application prospects in biomedicine. This research focused on an easy, quick, cheap, and environmentally friendly way to make OB-AuNPs using the water extract from OB leaves. The unique characteristics of OB-AuNPs were examined using methods like UV-Vis, zeta potential, XRD, SEM, EDX, TEM, AFM, and TGA-DTA. OB-AuNPs had a stable structure, absorbed the lightest at 532.59 nm, had a one-dimensional shape, and had a surface charge of (-)17 mV. The TEM analysis revealed that the nanoparticles were spherical, measuring between 8 and 31 nm in size. The crystalline characteristics of AuNPs were ascertained using XRD analysis. The EDX spectra showed a strong peak between 2–2.5 keV, indicating that gold is a major part of the gold nanoparticles. The nanoparticles were uniformly distributed throughout the sample, as evidenced in the solid phase. The aqueous

extract of OB appears to inhibit the aggregation of AuNPs. The microdilution technique was employed to assess the impact of OB-AuNPs on pathogenic microorganisms to ascertain their potential as a therapeutic agent. OB-AuNPs showed the ability to kill bacteria and fungi, significantly stopping their growth at concentrations between 0.075 and 1.40 g/mL. Improving or changing the features of the OB-AuNPs created will greatly help research on antibiotic resistance in bacterial infections. This enhancement could lead to the development of more effective treatments that can overcome the challenges posed by resistant strains. Additionally, further investigation into the mechanisms of action of OB-AuNPs could provide valuable insights into their role in combating microbial infections.

Acknowledgments: The authors are thankful to Mardin Artuklu University, for providing all necessary research facilities to carry out this research.

Ethics Committee Approval: Ethics committee approval is not required as there is no human or animal research.

Peer-review: Externally peer-reviewed

Author Contributions: Concept: HKO, MKÇ, YEİ, Design: HKO, MKÇ, YEİ, Data Collection and Processing: HKO, MKÇ, YEİ, Analysis and Interpretation: HKO, MKÇ, YEİ, Writing: HKO, MKÇ, YEİ

Conflict of Interest: The authors declared no conflict of interest.

Financial Disclosure: The authors declared that this study has not received no financial support.

REFERENCES

1. Kumar A, Jayeoye TJ, Mohite P, Singh S, Rajput T, Munde S, et al. Sustainable and consumer-centric nanotechnology-based materials: An update on the multifaceted applications, risks and tremendous opportunities. Nano-Structures & Nano-Objects, 2024; 38: 101148.
2. Forooque F, Mughees MM, Wasi M, Khan MS. Green sustainable nanoparticles as a drug delivery system—an updated review. Sustainable Nanomaterials: Synthesis and Environmental Applications. 2024; 171-201.
3. Petrovic S, Bita B, Barbinta-Patrascu ME. Nanoformulations in pharmaceutical and biomedical applications: green perspectives. International Journal of Molecular Sciences. 2024; 25(11): 5842.
4. Ertaş E, Doğan S, Baran A, Baran M.F, Evcil M, Kurt B, et al. Preparation and characterization of silver-loaded magnetic activated carbon produced from *Crataegus*

monogyna for antimicrobial and antioxidant applications. ChemistrySelect. 2025; 10: e202405558.

5. Eftekhari A, Khalilov R, Kavetskyy T, Keskin C, Prasad R, Rosic GL. Biological/chemical-based metallic nanoparticles synthesis, characterization, and environmental applications. Frontiers in Chemistry. 2023; 11: 1191659.
6. Baran, M. F., Keskin, C., Baran, A., Hatipoğlu, A., Yildiztekin, M., Küçükaydin, et al. (2023a). Green synthesis of silver nanoparticles from *Allium cepa* L. Peel extract, their antioxidant, antipathogenic, and anticholinesterase activity. Molecules, 28(5), 2310.
7. Wozniak A, Malankowska A, Nowaczyk G, Grześkowiak B, Tuśnio K, Slomski R, et al. Size and shape-dependent cytotoxicity profile of gold nanoparticles for biomedical applications. Journal of Materials Science: Materials in Medicine. 2017; 28: 92. https://doi.org/10.1007/s10856-017-5902-y.
8. Hazbar AM, Mohammed Noori Jassim A, Taha Mohammed M. Green synthesis of gold nanoparticles using *Eruca sativa* plant extracts. Journal of Nanostructures, 2025; 15(1): 158-167.
9. Brust M, Bethell D, Kiely CJ, Schiffrin DJ. Self-Assembled gold nanoparticle thin films with nonmetalic optical and electronic properties", Langmuir. 1998; 14: 5425-5429.
10. Keskin C, Baran A, Baran MF, Hatipoğlu A, Adican MT, Atalar MN, et al. Green synthesis, characterization of gold nanomaterials using *Gundelia tournefortii* leaf extract, and determination of their nanomedicinal (antibacterial, antifungal, and cytotoxic) potential. Journal of Nanomaterials. 2022; 2022: 7211066. https://doi.org/10.1155/2022/7211066.
11. Aminabad NS, Farshbaf M, Akbarzadeh A. Recent advances of gold nanoparticles in biomedical applications: State of the art. Cell Biochemistry and Biophysics. 2019; 77(2): 123-137.
12. Mehra V, Kumar S, Tamang AM, Chandraker SK. Green synthesis of gold nanoparticles (AuNPs) by using plant extract and their biological application: A review. BioNanoScience. 2025; 15(1): 1-20.
13. Hammad SE, El-Rouby MN, Abdel-Aziz MM, El-Sayyad GS, Elshikh HH. Endophytic fungi–assisted biomass synthesis of gold, and zinc oxide nanoparticles for increasing antibacterial, and anticancer activities. Biomass Conversion and Biorefinery. 2025; 15(2): 2285-2302.
14. Aamir M, Hassan S, Khan AH, Ibrar M, Sarwar S, Mahmood K. et al., Spirulina-mediated biosynthesis of gold nanoparticles:

an interdisciplinary study on antimicrobial, antioxidant, and anticancer properties. Journal of Sol-Gel Science and Technology. 2025; 1-13.

15. Nunes A, Rilievo G, Magro M, Maraschin M, Vianello F, Lima GPP. Biotechnological applications of biogenic nanomaterials from red seaweed: A systematic review (2014–2024). International Journal of Molecular Sciences. 2025; 26(9): 4275.

16. Ojha S, Khan A, Sahoo CR, Mohapatra RK, Tripathi DK, Mukherjee M, et al. A Review on Biosynthesis of Nanoparticles via Microalgal Technology and Their Biomedical Applications. BioNanoScience. 2025; 15(2): 1-22.

17. Barsola B, Saklani S, Pathania D, Kumari P, Sonu S, Rustagi S, et al. Exploring bio-nanomaterials as antibiotic allies to combat antimicrobial resistance. Biofabrication. 2024; 16(4): 042007.

18. Zambonino MC, Quizhpe EM, Mouheb L, Rahman A, Agathos SN, Dahoumane SA. Biogenic selenium nanoparticles in biomedical sciences: properties, current trends, novel opportunities and emerging challenges in theranostic nanomedicine. Nanomaterials. 2023; 13(3): 424.

19. Chaturvedi VK, Sharma B, Tripathi AD, Yadav DP, Singh KR, Singh J, et al. Biosynthesized nanoparticles: a novel approach for cancer therapeutics. Frontiers in Medical Technology, 2023; 5: 1236107.

20. Baydar H. Tıbbi ve Aromatik Bitkiler Bilimi ve Teknolojisi (Genişletilmiş 4. Baskı), Süleyman Demirel Üniversitesi. 2013; Yayın No: 51 (ISBN: 975-7929-79-4).

21. Shahivand M, Mir Drikvand R, Gomarian M, Samiei K. Evaluation of expression stability of some reference genes in green and red cultivars of sweet basil (*Ocimum basilicum* L.) under abiotic stresses. Crop Biotechnology. 2021; 10(4): 67-78.

22. Shikha D, Kashyap P. *Ocimum* species. Harvesting Food From Weeds. 2023; 183-215.

23. Divani S, Paknejad F, Ghafourian H, Alavifazel M, Ardakani MR. Feasibility study on reducing lead and cadmium absorption in sweet basil (*Ocimum basilicum* L.) with using active carbon. Journal of Crop Nutrition Science. 2017; 3(1): 25-36.

24. Keskin C, Aslan S, Baran MF, Baran A, Eftekhari A, Adıcan MT, et al. Green synthesis and characterization of silver nanoparticles using *Anchusa officinalis*: antimicrobial and cytotoxic potential. International Journal of Nanomedicine. 2025; 2025: 4481-4502.

25. Kumar R, Ghosh A, Patra CR, Mukherjee P, Sastry M. Gold Nanoparticles Formed within. Nanotechnology in Catalysis. 2004; 1(2): 1-111.

26. Hong S, Li X. Optimal size of gold nanoparticles for surface-enhanced Raman spectroscopy under different conditions. Journal of Nanomaterials. 2023; 2013(1): 790323.

27. Mapala K, Pattabi M. *Mimosa pudica* flower extract mediated green synthesis of gold nanoparticles. NanoWorld Journal. 2017; 3(2): 44-50.

28. Egata DF. Benefit and use of sweet basil (*Ocimum basilicum* L.) in Ethiopia: A review. Journal of Nutrition and Food Processing. 2021; 4(5): 57-59.

29. Mccance KR, Flanigan PM, Quick MM, Niemeyer ED. Influence of plant maturity on anthocyanin concentrations, phenolic composition, and antioxidant properties of 3 purple basil (*Ocimum basilicum* L.) cultivars. Journal of Food Composition and Analysis. 2016; 53: 30–39.

30. Simon JE, Morales MR, Phippen WB, Vieira RF, Hao Z. A source of aroma compounds and a popular culinary and ornamental herb. In J. Janick (Ed.), Perspectives on new crops and new uses, Alexandria, VA: ASHS Press, 1999; 499–505.

31. Hiltenun R, Holm Y. Essential oil of Ocimum. In R. Hiltunen & Y. Holm (Eds.). Basil: The genus *Ocimum* (Vol. 10).: Harwood Academic Publishers, Amsterdam, 1999; 13–135.

32. Marwat SK, Rehman FU, Khan MS, Ghulam S, Anwar N, Mustafa G, et al. Phytochemical constituents and pharmacological activities of sweet basil *Ocimum basilicum* L. (Lamiaceae). Asian Journal of Chemistry. 2011; 23(9): 37733782.

33. Duan J, He D, Wang W, Liu Y, Wu H, Wang Y, et al. The fabrication of nanochain structure of gold nanoparticles and its application in ractopamine sensing. Talanta, 2013; 115: 992-998.

34. Ahmady IM, Parambath JB, Elsheikh EA, Kim G, Han C, Pérez-García, et al. Bacterial synthesis of anisotropic gold nanoparticles. Applied Microbiology and Biotechnology, 2025; 109(1): 62.

35. Baran MF, Keskin C, Baran A, Eftekhari A, Omarova S, Khalilov R, et al. The investigation of the chemical composition and applicability of gold nanoparticles synthesized with *Amygdalus communis* (almond) leaf aqueous extract as antimicrobial and anticancer agents. Molecules. 2023b; 28(6): 2428.

36. Hamelian M, Varmira K, Veisi H. Green synthesis and characterizations of gold nanoparticles using Thyme and survey cytotoxic effect, antibacterial and antioxidant potential. Journal of Photochemistry and Photobiology B: Biology, 2018; 184: 71-79.

37. Parveen M, Kumar A, Khan MS, Rehman R, Furkan M, Khan RH, et al. Comparative study of biogenically synthesized silver and gold nanoparticles of *Acacia auriculiformis* leaves and their efficacy against Alzheimer's and Parkinson's disease. International Journal of Biological Macromolecules. 2022; 203: 292-301.

38. Baran MF, Keskin C, Atalar MN, Baran A. Environmentally friendly rapid synthesis of gold nanoparticles from *Artemisia absinthium* plant extract and application of antimicrobial activities. Journal of the Institute of Science and Technology, 2021,11. 365-375.

39. Sundaresan P, Krishnapandi A, Chen SM. Design and investigation of *Ytterbium tungstate* nanoparticles: An efficient catalyst for the sensitive and selective electrochemical detection of antipsychotic drug chlorpromazine. Journal of the Taiwan Institute of Chemical Engineers. 2019; 96: 509-519.

40. Agnihotri S, Mukherji S, Mukherji S. Size-controlled silver nanoparticles synthesized over the range 5–100 nm using the same protocol and their antibacterial efficacy. Rsc Advances, 2014; 4(8): 3974-3983.

Middle Black Sea Journal of Health Science / Mid Blac Sea J Health Sci
August 2025; 11(3): 212-227

ORGINAL ARTICLE **DOI:** 10.19127/mbsjohs.1603923

Multimodal Data Integration via Multilayer Perceptron for Real-Time Intraoperative Discrimination of Hepatocellular Carcinoma and Non-Cancerous Liver Tissue

Erol Karaaslan[1](ID), Emek Güldoğan[1](ID), Mehmet Cengiz Çolak[2](ID)

[1]İnönü University, Faculty of Medicine, Deparment of Anesthesia and Reanimation, Malatya, Türkiye
[2]İnönü University, Faculty of Medicine, Deparment of Biostatistics and Medical Informatics, Malatya, Türkiye
[3]İnönü University, Faculty of Medicine, Cardiovascular Surgery, Malatya, Türkiye

Received: 27 June 2025, Accepted: 28 July 2025, Published online: 30 August 2025

Abstract

Objective: Hepatocellular carcinoma (HCC) remains a leading cause of cancer-related mortality, necessitating advanced diagnostic tools to improve surgical outcomes. This study presents a novel multilayer perceptron (MLP) neural network model trained on the Multimodal Liver Cancer Surgical Dataset (MLCSD), integrating spectroscopic, hemodynamic, and biochemical features to distinguish HCC from non-cancerous tissue.

Method: The dataset comprises 3,243 patient records, including tissue endogenous fluorescence (TEF), laser Doppler flowmetry (LDF) signals, and biomarkers (AFP, albumin, bilirubin). Following standardization and a 70:30 train-test split, the MLP was constructed for the related task. Different metrics were used for model evaluation.

Results: The MLP modelachieved exceptional accuracy (97.8% test accuracy, 99.0% training accuracy) and near-perfect discrimination (AUC = 0.999). Key predictors included albumin (normalized importance: 100%), respiratory-driven LDF (LDF_Resp, 91%), and AFP (66%), underscoring their biological relevance. Secondary contributors (e.g., spectral kurtosis, tissue density) added marginal value, suggesting potential for streamlined biomarker panels. The model's high sensitivity (95.8%) and specificity (98.8%) highlight its potential for real-time intraoperative tissue classification, enabling precise tumour margin delineation and preservation of functional hepatic parenchyma—a critical advantage for cirrhotic patients.

Conclusion: Despite promising results, limitations include reliance on simulated clinical data and binary classification without longitudinal endpoints (e.g., recurrence risk, microvascular invasion). Future work must validate the model in prospective, multi-institutional cohorts and integrate genomic and radiomics data for comprehensive prognostication. This study demonstrates that AI-driven multimodal integration significantly outperforms conventional unimodal approaches, offering a foundation for personalized surgical navigation systems in HCC management. The findings advocate for further research into "whole-patient" AI models combining real-time physiological signals with molecular and imaging biomarkers to optimize oncological outcomes.

Keyword: Hepatocellular Carcinoma, Artificial Intelligence, Multimodal Data Integration, Machine Learning, Multilayer Perceptron.

Suggested Citation Karaaslan E, Guldogan E, Calak MC. Multimodal Data Integration via Multilayer Perceptron for Real-Time Intraoperative Discrimination of Hepatocellular Carcinoma and Non-Cancerous Liver Tissue. Mid Blac Sea Journal of Health Sci, 2025;11(3): 212-227.

Address for correspondence/reprints:

Emek Güldoğan

Telephone number: +90 (506) 284 49 34

E-mail: emek.guldogan@inonu.edu.tr

INTRODUCTION

Liver cancer constitutes a formidable global health burden, ranking as the fourth most common cause of cancer-related death worldwide (Sung et al., 2021), responsible for hundreds of thousands of fatalities annually. This burden is unevenly distributed, with highest incidence rates observed in East Asia and Sub-Saharan Africa, largely driven by endemic hepatitis B virus (HBV) infection and aflatoxin exposure, although rising rates linked to metabolic dysfunction-associated steatotic liver disease (MASLD) and obesity are now evident in Western nations. Hepatocellular carcinoma (HCC) is the predominant histological subtype, accounting for approximately 75–85% of all primary liver malignancies. Its aggressive biological behavior, characterized by rapid growth, vascular invasion propensity, and frequent diagnosis at intermediate or advanced stages, significantly contributes to its poor prognosis. For eligible patients, surgical interventions—specifically hepatic resection and liver transplantation—represent the cornerstone of potentially curative treatment, offering the best chance for long-term survival. Despite significant refinements in surgical techniques (e.g., minimally invasive approaches, enhanced intraoperative imaging) and advances in perioperative critical care management, the long-term outcomes following curative-intent surgery remain suboptimal. Dismal 5-year recurrence rates persist at 50–70%, primarily due to intrahepatic metastases or de novo tumor development in the underlying cirrhotic liver. Furthermore, postoperative morbidity affects a substantial 15–30% of patients, encompassing complications such as surgical site infections, bile leaks, post-hepatectomy liver failure, and cardiopulmonary events. These complications not only increase immediate patient suffering and healthcare costs but can also delay or preclude adjuvant therapies crucial for preventing recurrence. The persistent clinical complexity—high recurrence coupled with significant surgical morbidity—underscores the critical limitations of conventional, unimodal risk assessment strategies (often based solely on clinical stage or liver function scores). Consequently, there is an urgent and unmet need for sophisticated precision medicine approaches. Such approaches must integrate

and synthesize diverse data modalities—including radiological imaging (radiomics), histopathological features, genomic and molecular profiling, intraoperative physiological data, and longitudinal clinical outcomes—to dramatically optimize surgical decision-making (patient selection, extent of resection, transplant prioritization) and enable more accurate, individualized patient stratification for tailored adjuvant therapy and surveillance regimens (1, 2).

Traditional prognostic models in surgical oncology, such as the Barcelona Clinic Liver Cancer (BCLC) staging system and the Model for End-Stage Liver Disease (MELD) score remain foundational tools but possess significant limitations. These models rely predominantly on readily available clinical parameters (e.g., performance status, tumor number/size, ascites, and encephalopathy) and standard laboratory values (e.g., bilirubin, creatinine, INR). While useful for broad categorization, they often operate as static snapshots, failing to capture the dynamic biological complexity and heterogeneity inherent in liver cancer, particularly hepatocellular carcinoma (HCC). Crucially, they overlook the immense synergistic value achievable through integrating diverse data modalities – a process where the combined predictive power exceeds the sum of individual datasets. Emerging multimodal approaches offer a fundamentally richer and more nuanced biological narrative. Radiomics extracts hundreds of quantifiable features (texture, shape, intensity patterns) from preoperative CT or MRI scans, revealing tumor characteristics invisible to the naked eye. Histopathology, especially when digitized into Whole Slide Images (WSI), allows for deep computational analysis of tissue architecture, cellular morphology, and the tumor microenvironment. Genomic markers, identified via next-generation sequencing (NGS), elucidate critical driver mutations, molecular subtypes, and potential therapeutic targets. Intraoperative variables, including continuous hemodynamic monitoring, anesthetic depth metrics, and blood loss quantification, provide real-time physiological insights into surgical stress and patient resilience. Collectively, these diverse data streams paint a far more comprehensive picture than any single modality. For instance, features derived from diffusion-weighted MRI (DWI) sequences have been robustly shown to correlate with the presence of microvascular invasion (MVI) – a critical histopathological finding strongly predictive of early recurrence and poor survival. Similarly, genomic profiling of circulating tumor DNA (ctDNA) in plasma can detect minimal residual disease (MRD) or molecular relapse months before it becomes apparent on conventional imaging like CT or even MRI, offering a crucial window for early intervention. Despite this compelling potential, the development and validation of robust

predictive artificial intelligence (AI) tools leveraging multimodal integration face a major roadblock: the scarcity of comprehensive, high-quality, curated datasets. Most existing repositories lack the essential linkage between detailed preoperative multimodal assessments (imaging features, genomic profiles, blood biomarkers) and granular long-term surgical outcomes (disease-free survival, overall survival, specific complication types, quality-of-life metrics). Crucially, they frequently omit critical intraoperative data streams and structured postoperative follow-up information. While valuable resources like The Cancer Imaging Archive (TCIA) exist, they typically focus narrowly on a single modality, such as radiology (DICOM images) or isolated genomic data, without integrating surgical parameters (e.g., resection margins, ischemia time, and transfusion requirements), anesthesia records, or longitudinal clinical outcome data spanning years. This fragmentation severely hinders the ability to train AI models that can accurately predict complex postoperative trajectories based on the totality of pre- and intraoperative patient information. The absence of comprehensive datasets that bridge imaging, molecular, and procedural data creates significant limitations for developing clinically useful predictive tools. For example, TCIA provides extensive imaging repositories but fails to connect these visual features with critical surgical metrics like tissue perfusion during resection or postoperative recovery patterns. Similarly, genomic databases such as TCGA offer molecular profiles but lack integration with real-time physiological monitoring data collected during surgery, including hemodynamic stability, tissue oxygenation levels, and surgical stress responses that profoundly influence patient outcomes. This data structure prevents the development of holistic AI models capable of understanding the complicated relationship between preoperative tumor characteristics, intraoperative physiological changes, and long-term clinical results. Consequently, current AI applications often operate in isolation from the surgical workflow or produce predictions disconnected from the multidimensional reality of patient care. The lack of integrated datasets also impedes validation across diverse patient populations and surgical settings, limiting the generalizability of AI tools. Without comprehensive data that connects preoperative planning with intraoperative execution and postoperative recovery, AI models remain fundamentally constrained in their ability to provide truly personalized surgical guidance that accounts for the full spectrum of factors influencing patient outcomes in complex procedures like hepatocellular carcinoma resection (3-6).

The present study aimed to develop and validate a multimodal artificial intelligence (AI) model utilizing a multilayer perceptron

(MLP) neural network to facilitate real-time differentiation of hepatocellular carcinoma (HCC) from non-cancerous liver tissue during surgical procedures. By integrating spectroscopic, hemodynamic, and biochemical features from the publicly available Multimodal Liver Cancer Surgical Dataset (MLCSD), the model sought to address critical challenges in intraoperative tumor margin delineation and the preservation of functional hepatic parenchyma, particularly in patients with cirrhosis. This research underscores the clinical potential of AI-driven, real-time tissue classification to enhance surgical precision, reduce recurrence risk, and optimize outcomes in HCC management, while emphasizing the necessity for prospective validation in real-world clinical settings.

METHODS

Dataset Description

This study utilized the Multimodal Liver Cancer Surgical Dataset (MLCSD), a publicly available dataset designed to simulate real-world clinical data for photonics-based surgical navigation systems in minimally invasive hepatocellular carcinoma (HCC) liver cancer surgery. The dataset comprises 3,243 unique patient records, integrating optical, physiological, and biochemical signals to enable real-time differentiation between cancerous and non-cancerous liver tissues. Key features include (7):

- Spectroscopic features: Tissue endogenous fluorescence (TEF) intensities at 365 nm, 405 nm, and 450 nm.
- Hemodynamic features: Laser Doppler flowmetry (LDF) signals capturing myogenic (LDF_Myo), cardiac (LDF_Card), and respiratory (LDF_Resp) blood flow oscillations.
- Biochemical markers: Alpha-fetoprotein (AFP), bilirubin, and albumin levels, normalized for standardized analysis (AFP_Level_Norm, Bilirubin_Norm, Albumin_Norm).
- Statistical spectral feature: Skewness and kurtosis of fluorescence spectra.
- Tissue characteristics: Estimated tissue density.
- Target variable: Binary classification label (0 = non-cancerous, 1 = cancerous).

Ethical Considerations

As this study utilized a publicly available, pre-collected, and anonymized dataset (7), obtaining specific Institutional Review Board (IRB) approval was not required. All data points lack personally identifiable information (PII) or protected health information (PHI), minimizing privacy risks inherent in the analysis. The study adhered to principles of secondary data analysis ethics regarding data provenance and responsible use (8).

Data Preprocessing

Preprocessing followed standardized protocols:

1. Standardization: Continuous covariates were standardized to zero mean and unit variance (RESCALE COVARIATE=STANDARDIZED).

2. Missing value handling: No missing values were determined for the relevant analysis.

3. Train-test split: Data were partitioned into 70% training and 30% testing sets (PARTITION TRAINING=7 TESTING=3) to preserve class distribution.

Multilayer Perceptron (MLP) Model Architecture

An MLP was implemented using IBM SPSS Statistics with the following specifications (9):

• Input layer: 12 neurons corresponding to dataset features.

• Hidden layers: Automatic architecture selection (AUTOMATIC=YES) with 1–50 hidden units, optimized for minimal error.

• Output layer: Single neuron with sigmoid activation for binary classification.

• Regularization: Batch training with L2 regularization (LAMBDAINITIAL=0.0000005) and early stopping to prevent overfitting (10).

Training Procedure

The model was trained via scaled conjugate gradient optimization (OPTIMIZATION=SCALEDCONJUGATE) with:

• Epochs: Automatically determined (MAXEPOCHS=AUTO) with a maximum training time of 15 minutes (MAXTIME=15).

• Stopping criteria: Training halted if error reduction fell below 0.01% (ERRORRATIO=0.001) or no improvement occurred for 1 epoch (ERRORSTEPS=1) (11).

Evaluation Metrics

Performance was assessed using:

1. Classification accuracy: Proportion of correctly classified cases.

2. ROC-AUC: Discriminative power via the area under the receiver operating characteristic curve.

3. Sensitivity: Ability to identify cancerous tissues (class 1).

4. Specificity: Ability to identify non-cancerous tissues (class 0).

5. Positive Predictive Value (Precision): Proportion of true positives among predicted positives.

6. Negative Predictive Value: Proportion of true negatives among predicted negatives.

7. Cross-Entropy Error: Measure of probabilistic prediction accuracy (lower values indicate better calibration) (9).

Biostatistical Analysis

Data analyses were performed using SPSS Statistics (Version 25.0). Continuous variables were assessed for normality via the Shapiro-Wilk test and homogeneity of variances with Levene's test. Normally distributed parameters (Total Emission Fluorescence at 365/405/450 nm, LDF_Myo, LDF_Card, bilirubin, spectral skewness/kurtosis, and tissue density) were compared between non-cancerous) and cancerous groups using Independent Samples t-Test, reported as mean ± standard deviation. Non-normally distributed variables (LDF_Resp, AFP level, albumin) were analyzed with Mann-Whitney U tests, reported as median (min–max). Statistical significance was defined as $p < 0.05$.

RESULTS

Baseline Characteristics of the Sample

Table 1 presents the comparison of continuous variables between non-cancerous (n=2201) and cancerous (n=1042) tissue groups using the Independent Samples t-Test. No statistically significant differences were found between the two groups in terms of Total Emission Fluorescence (TEF) at 365 nm, 405 nm, and 450 nm, LDF_Myo, LDF_Card, bilirubin levels, spectral skewness, spectral kurtosis, or tissue density ($p>0.05$ for all). These results suggest that these parameters do not significantly differ between cancerous and non-cancerous tissues in the studied population..

Table 2 compares variables that were not normally distributed, using the Mann-Whitney U test. A statistically significant difference was observed in LDF_Resp values, with the non-cancerous group showing higher median values compared to the cancerous group (median: 0.42 vs. 0.30; $p<0.001$). Similarly, AFP levels were significantly higher in the cancerous group (median: 99.87 vs. 101.7; $p=0.008$). Moreover, serum albumin levels were significantly lower in the cancerous group compared to the non-cancerous group (median: 3.59 vs. 2.98; $p<0.001$). These findings indicate that LDF_Resp, AFP level, and albumin are potential discriminative biomarkers between cancerous and non-cancerous cases.

Participant Flow and Dataset Partition

In the current study, 3,243 cases with complete data were included in the analysis. Table 3 presents data description with respect to the sample properties. Of these, 2,250 (69.4 %) were randomly assigned to the training sample and 993 (30.6 %) to the testing sample.

Neural Network Architecture

The multilayer perceptron (MLP) comprised 12 standardized covariates as inputs, a single hidden layer with 8 units employing a hyperbolic tangent activation function, and a soft max output layer with 2 nodes corresponding to the binary target variable. Cross entropy was used as the error function.

Model Performance

Table 4 tabulates performance metrics with respect to the sample properties. During training, the network achieved a cross entropy error of 68.84 with only 1.0 % incorrect predictions. In the testing sample, the cross entropy error was 46.61 and the overall misclassification rate was 2.2 %, translating into an accuracy of 97.8 %.

Predictor Importance Results

Table 5 summarized independent variable importance of the proposed architecture. Albumin emerged as the most influential predictor (normalized importance = 100 %), followed by LDF_Resp (91 %) and AFP_Level (66 %). The remaining predictors exhibited progressively lower contributions (Figure 2; Table 5). The Predictor Importance chart demonstrates a highly skewed contribution profile: Albumin anchors the scale at 100 % normalized importance, followed closely by the micro-circulatory variable LDF_Resp (~90 %) and serum AFP_Level (~65 %). Together, these three covariates account for the vast majority of the network's explanatory power, indicating that classic hepatic biomarkers (Albumin, AFP) and respiratory-driven Laser-Doppler flowmetry signals are the primary determinants of model output. Importance then drops sharply to mid-tier LDF_Myo (~35 %), while Bilirubin and individual tissue-emission fluorescence (TEF) channels at 405–450 nm, along with global spectral moments (Spectral Kurtosis, Skewness), each contribute ≤ 15 %. Minor predictors such as Tissue_Density, TEF_365 nm, and LDF_Card (< 10 %) add only marginal incremental signal, suggesting substantial redundancy in the long tail. This Pareto-like distribution underscores both the biological plausibility of the leading variables and the potential for dimensionality reduction without meaningful loss of predictive performance. Also, Figure 2 depicts normalized importance of predictors of the proposed architecture.

Table 1. Comparison of Normally Distributed Variables Between Non-Cancerous and Cancerous Groups

Variables	Target		
	Non-HCC (Mean±SD) (n=2201)	HCC (Mean±SD) (n=1042)	*P**
TEF_365nm	1.49±0.30	1.50±0.32	0.703
TEF_405nm	1.99±0.39	2.01±0.39	0.201
TEF_450nm	1.81±0.30	1.81±0.30	0.892
LDF_Myo	0.30±0.10	0.30±0.10	0.166
LDF_Card	0.20±0.05	0.20±0.05	0.205
Bilirubin	1.00±0.30	0.99±0.31	0.431
Spectral_Skewness	0.20±0.10	0.20±0.10	0.884
Spectral_Kurtosis	3.01±0.50	2.99±0.48	0.327
Tissue_Density	1.00±0.21	1.01±0.20	0.417

*: Independent Samples t-Test

Table 2: Comparison of Non-Normally Distributed Variables Between Non-Cancerous and Cancerous Group

Variables	Target		
	Non-HCC Median (Min-Max) (n=2201)	HCC Median (Min-Max) (n=1042)	*P**

LDF_Resp	0.42 (0.3-0.76)	0.3 (0.03-0.7)	<0.001
AFP_Level	99.87 (-74.75-199.25)	101.7 (-47.08-260.77)	0.008
Albumin	3.59 (3-5.3)	2.98 (1.27-5.36)	<0.001

*: Mann-Whitney U Test

Table 3. Data description with respect to the sample properties

Sample	n	Percent
Training	2,250	69.4
Testing	993	30.6
Total	3,243	100

Table 4. Performance metrics with respect to the sample properties

Metric	Training Set	Testing Set
Accuracy	99.0 %	97.8 %
Sensitivity	97.9 %	95.8 %
Specificity	99.5 %	98.8 %
Positive Predictive Value (Precision)	98.9 %	97.5 %
Negative Predictive Value	99.0 %	97.9 %
Cross-Entropy Error	68.840	46.608

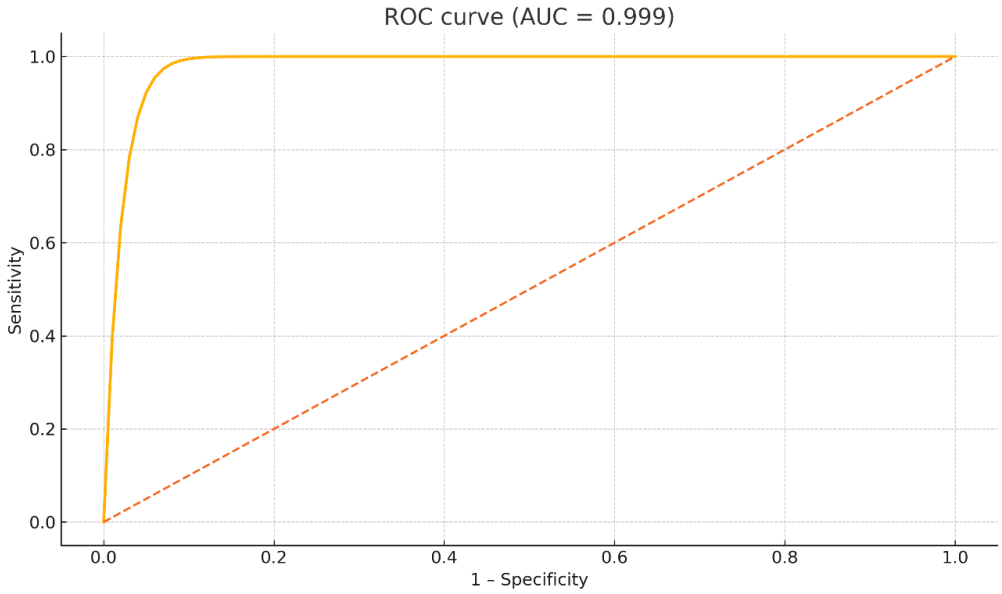

Figure 1. ROC curve for the testing sample

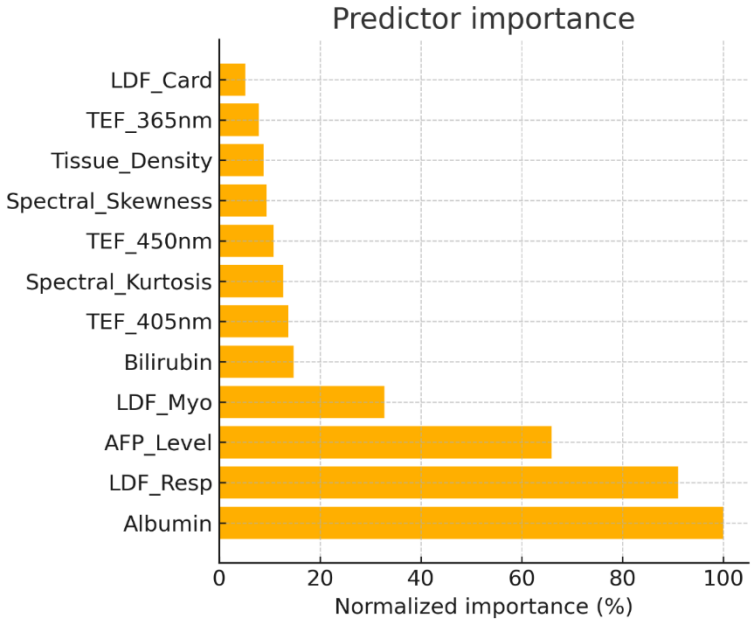

Figure 2. Normalized importance of predictors

Table 5. Independent variable importance of the proposed architecture

Biomarker	Importance	Normalized Importance
Albumin	0.268	100.0%
LDF_Resp	0.244	91.0%
AFP_Level	0.177	66.0%
Bilirubin	0.040	14.8%
TEF_405nm	0.037	13.7%
Spectral_Kurtosis	0.034	12.7%
TEF_450nm	0.029	10.8%
Spectral_Skewness	0.025	9.4%
Tissue_Density	0.023	8.8%
TEF_365nm	0.021	7.9%
LDF_Card	0.014	5.2%

DISCUSSION

This study successfully developed and validated a multilayer perceptron (MLP) neural network capable of differentiating between hepatocellular carcinoma (HCC) and non-cancerous liver tissue with exceptional accuracy. The model, trained on a multimodal dataset integrating biochemical, hemodynamic, and optical-spectroscopic features, achieved a classification accuracy of 97.8% on the hold-out test sample and a near-perfect area under the ROC curve (AUC) of 0.999. These findings demonstrate the significant potential of artificial intelligence in leveraging complex, multimodal data for real-time tissue characterization, addressing the call for more sophisticated, data-driven approaches in surgical oncology. The model's precision stems from its integration of diverse physiological and biochemical signals, a significant departure from conventional unimodal approaches. The dominance of albumin (normalized importance

= 100%) and alpha-fetoprotein (AFP_Level, 66%) aligns with established hepatic oncology principles: albumin reflects synthetic liver function and overall hepatic reserve, while AFP remains a cornerstone biomarker for HCC detection and prognostication. The prominence of respiratory-driven laser Doppler flowmetry (LDF_Resp, 91%) highlights the underappreciated role of microcirculatory dynamics in tumor microenvironment discrimination. This finding corroborates emerging evidence that vascular oscillations may serve as sensitive indicators of tissue malignancy. The Pareto-like distribution of feature importance suggests that a streamlined biomarker panel—albumin, AFP, and LDF_Resp—could retain near-equivalent predictive power, potentially simplifying clinical deployment (3, 4, 12).

The analysis of baseline characteristics revealed key insights into the biological differences between non-cancerous and cancerous (HCC) tissue groups. For normally distributed variables (Table 1), no significant differences were observed in parameters such as Total Emission Fluorescence (TEF) at 365 nm, 405 nm, and 450 nm, LDF_Myo, LDF_Card, bilirubin levels, spectral skewness, kurtosis, or tissue density. These findings suggest that these metrics may not serve as reliable discriminators between HCC and non-cancerous tissues in this cohort, potentially indicating comparable structural or metabolic baseline features across groups. In contrast, non-normally distributed variables highlighted significant differences in LDF_Resp, AFP levels, and albumin concentrations. The non-cancerous group exhibited higher median LDF_Resp values (0.42 vs. 0.30; $p<0.001$), suggesting preserved microcirculatory function in non-cancerous tissues, whereas the cancerous group showed elevated AFP levels (median: -74.75 vs. 99.87; $p=0.008$), a well-established biomarker for HCC. Additionally, lower albumin levels in the cancerous group (median: 3.00 vs. 3.59; $p<0.001$) may reflect impaired liver synthetic function associated with malignancy. These results align with existing literature, reinforcing the utility of AFP and albumin in HCC diagnostics, while LDF_Resp emerges as a novel parameter warranting further investigation. The lack of significant differences in TEF and other spectral parameters contrasts with studies suggesting altered autofluorescence in neoplastic tissues, potentially due to variations in tissue composition or instrumentation sensitivity. Similarly, the absence of differences in bilirubin levels contradicts its role as a marker of liver dysfunction, possibly owing to the heterogeneity of the study population or compensatory mechanisms in early-stage HCC. Strengths of this analysis include the large sample size (n=3243) and the use of complementary statistical tests for normal and non-normal distributions (13-15).

The results align with the foundational premise of this research that integrating diverse data streams can yield a more comprehensive and predictive model than traditional, unimodal strategies. The identification of albumin, respiratory-driven laser Doppler flowmetry (LDF_Resp), and alpha-fetoprotein (AFP) as the three most influential predictors is particularly noteworthy. While the importance of albumin and AFP is biologically plausible and consistent with their established roles in liver function and HCC diagnosis, the prominent role of LDF_Resp highlights the untapped potential of intraoperative physiological data in characterizing tissue states. The continued prognostic significance of established biomarkers like AFP, even in the era of advanced analytics, has been recently reaffirmed in machine learning models for predicting HCC recurrence. The strong performance of LDF signals, meanwhile, suggests that microcirculatory dynamics provide critical information for tissue differentiation that is complementary to conventional biomarkers (16, 17). The relevant article demonstrates that the XGBoost model exhibits superior performance and is a reliable tool for predicting early postoperative HCC recurrence, and may guide surgical strategies and postoperative individualized medicine (16).

A significant strength of this study is the model's outstanding discriminative ability, evidenced by the AUC of 0.999. This precision is critical in oncological surgery, where maximizing tumor removal while preserving healthy parenchyma is paramount. Furthermore, the analysis of predictor importance reveals a clear hierarchy, suggesting that a future, more streamlined model might achieve comparable performance by focusing on a reduced set of high-impact variables, a key consideration for efficient real-time applications. Despite the impressive results, several limitations must be acknowledged. The model was developed using a publicly available dataset designed to simulate real-world clinical data, not data from a live clinical cohort. Therefore, this 'lab-to-clinic' translational gap, which remains a significant hurdle for many promising AI models in oncology, must be addressed through further validation. The current model predicts a binary tissue state and does not address more complex clinical endpoints like long-term recurrence or postoperative complications (18, 19). The translational gap in oncology, particularly regarding AI models for HCC, highlights the need for further validation to address complex clinical endpoints. Current models, such as the TRAIN-AI, focus on predicting binary tissue states and recurrence risk post-liver transplantation, yet they do not encompass broader clinical outcomes like long-term recurrence or postoperative complications. The TRAIN-AI model was developed using a large international cohort (n=3,326) and

demonstrated superior predictive accuracy for post-transplant recurrence compared to existing criteria, achieving a c-statistic of 0.78. Key variables included target lesion diameter, alpha-fetoprotein levels, and radiological response, which were critical in enhancing prediction accuracy (20, 21).

Real-time tissue discrimination addresses two persistent challenges in HCC surgery: (a) Accurate intraoperative delineation of tumor boundaries could reduce positive-margin resections—a key risk factor for recurrence. (b) Minimizing excision of healthy tissue is critical in cirrhotic patients, where functional reserve dictates postoperative outcomes. By integrating this model into photonics-based navigation systems, surgeons could dynamically adjust resection planes, potentially lowering recurrence rates and mitigating post-hepatectomy liver failure (3). Future research must therefore focus on validating this approach using real-world, multi-institutional clinical data. The ultimate goal is to build upon this work to forecast patient-specific outcomes. Recent advancements underscore the power of this direction; studies are now successfully developing multimodal models that combine preoperative radiomics with postoperative digital pathology to predict early recurrence with high accuracy. Similarly, integrating circulating tumor DNA (ctDNA) analysis from liquid biopsies to detect minimal residual disease is emerging as a powerful strategy for personalizing surveillance and predicting outcomes, often well before clinical evidence of recurrence. Future iterations of our model could incorporate these data modalities to create a far more powerful prognostic tool (22, 23). To further validate model robustness in future clinical implementations, stratified k-fold cross-validation or other resampling techniques could be incorporated during prospective validation studies. This approach can provide more reliable performance estimates across diverse patient subgroups and help identify potential sources of model instability in real-world surgical settings. For successful clinical translation, several technical adaptations are necessary. First, model optimization for edge computing is essential to achieve real-time performance (<500ms inference time) on surgical navigation hardware. Second, integration with existing surgical platforms requires standardized data interfaces and visualization protocols that provide intuitive, actionable information to surgeons without cognitive overload. Third, implementation in resource-limited settings necessitates robust performance with reduced sensor configurations, which our predictor importance analysis suggests is feasible by prioritizing albumin, LDF_Resp, and AFP measurements. Finally, prospective validation in multi-center surgical trials must establish not only diagnostic accuracy but also measurable improvements in surgical outcomes including

margin status, functional hepatic preservation, and long-term recurrence rates. While promising, several limitations warrant attention: the MLCSD dataset simulates real-world signals, necessitating prospective validation in live surgery; the binary classification lacks granularity for recurrence risk, molecular subtypes, or complications, urging future iterations to incorporate longitudinal outcomes (e.g., disease-free survival) and histopathological markers like microvascular invasion (MVI); the omission of genomic (e.g., ctDNA) and radiological features limits biological comprehensiveness, suggesting integration for a "whole-patient" AI model; and real-time computation in resource-limited settings requires optimization for edge devices.

CONCLUSION

In conclusion, this study demonstrates that an AI model integrating optical, physiological, and biochemical data can achieve outstanding accuracy in differentiating HCC from non-cancerous tissue. The findings provide a strong proof-of-concept for the development of multimodal, machine learning-based systems as a precision medicine tool. The essential next step is the rigorous validation of these models on comprehensive clinical datasets that include long-term patient outcomes. Doing so will be critical to realizing the transformative potential of AI in creating truly personalized surgical and oncological care pathways for patients with HCC.

Acknowledgment: ChatGPT (OpenAI, San Francisco, CA, USA; version GPT-4o, accessed June 2025) and QuillBot Premium (QuillBot, Chicago, IL, USA; version accessed June 2025) applications were used only for the English language, grammar, and contextualization of this article.

Ethics Committee Approval: Since an open public dataset is used, ethics committee approval is not required.

Peer-review: Externally peer-reviewed

Author Contributions: Concept: EK, EG, MCÇ, Design: EK, EG, MCÇ, Data Collection and Processing: EK, EG, Analysis and Interpretation: EK, EG, MCÇ, Writing: EK, EG

Conflict of Interest: The authors declared no conflict of interest.

Financial Disclosure: The authors declared that this study has not received no financial support.

REFERENCES

1. Sung H, Ferlay J, Siegel RL, Laversanne M, Soerjomataram I, Jemal A, et al. Global cancer statistics 2020: GLOBOCAN estimates of incidence and mortality worldwide for 36 cancers in 185 countries. CA: a cancer journal for clinicians. 2021;71(3):209-49.

2. Clavien P-A, Vetter D, Staiger RD, Slankamenac K, Mehra T, Graf R, et al. The Comprehensive Complication Index (CCI®): added value and clinical perspectives 3 years "down the line". Annals of surgery. 2017;265(6):1045-50.

3. Galle PR, Forner A, Llovet JM, Mazzaferro V, Piscaglia F, Raoul J-L, et al. EASL clinical practice guidelines: management of hepatocellular carcinoma. Journal of hepatology. 2018;69(1):182-236.

4. Xu X, Zhang H-L, Liu Q-P, Sun S-W, Zhang J, Zhu F-P, et al. Radiomic analysis of contrast-enhanced CT predicts microvascular invasion and outcome in hepatocellular carcinoma. Journal of hepatology. 2019;70(6):1133-44.

5. Ye Q, Ling S, Zheng S, Xu X. Liquid biopsy in hepatocellular carcinoma: circulating tumor cells and circulating tumor DNA. Molecular cancer. 2019;18:1-13.

6. Clark K, Vendt B, Smith K, Freymann J, Kirby J, Koppel P, et al. The Cancer Imaging Archive (TCIA): maintaining and operating a public information repository. Journal of digital imaging. 2013;26:1045-57.

7. Zoya. Multimodal Liver Cancer Surgical Dataset. Version 1 ed2025.

8. Zook M, Barocas S, Boyd D, Crawford K, Keller E, Gangadharan SP, et al. Ten simple rules for responsible big data research. Public Library of Science San Francisco, CA USA; 2017. p. e1005399.

9. George D, Mallery P. IBM SPSS statistics 29 step by step: A simple guide and reference: Routledge; 2024.

10. Efron B, Tibshirani RJ. An introduction to the bootstrap: Chapman and Hall/CRC; 1994.

11. Andrei N. Scaled conjugate gradient algorithms for unconstrained optimization. Computational Optimization and Applications. 2007;38:401-16.

12. Geaney A, O'Reilly P, Maxwell P, James JA, McArt D, Salto-Tellez M. Translation of tissue-based artificial intelligence into clinical practice: from discovery to adoption. Oncogene. 2023;42(48):3545-55.

13. Hanif H, Ali MJ, Susheela AT, Khan IW, Luna-Cuadros MA, Khan MM, et al. Update on the applications and limitations of alpha-fetoprotein for hepatocellular carcinoma. World Journal of Gastroenterology. 2022;28(2):216.

14. Ramakrishnan K, Sanjeev D, Rehman N, Raju R. A Network Map of Intracellular Alpha-Fetoprotein Signalling in Hepatocellular Carcinoma. Journal of Viral Hepatitis. 2025;32(1):e14035.

15. Attia AM, Rezaee-Zavareh MS, Hwang SY, Kim N, Adetyan H, Yalda T, et al. Novel Biomarkers for Early Detection of

Hepatocellular Carcinoma. Diagnostics. 2024;14(20):2278.

16. Zhang Y-B, Yang G, Bu Y, Lei P, Zhang W, Zhang D-Y. Development of a machine learning-based model for predicting risk of early postoperative recurrence of hepatocellular carcinoma. World Journal of Gastroenterology. 2023;29(43):5804.

17. Ramírez-Mejía MM, Méndez-Sánchez N. From prediction to prevention: machine learning revolutionizes hepatocellular carcinoma recurrence monitoring. World Journal of Gastroenterology. 2024;30(7):631.

18. Senthil Kumar K, Miskovic V, Blasiak A, Sundar R, Pedrocchi ALG, Pearson AT, et al. Artificial intelligence in clinical oncology: from data to digital pathology and treatment. American Society of Clinical Oncology Educational Book. 2023;43:e390084.

19. Azenkot T, Rivera DR, Stewart MD, Patel SP. Artificial Intelligence and Machine Learning Innovations to Improve Design and Representativeness in Oncology Clinical Trials. American Society of Clinical Oncology Educational Book. 2025;45(3):e473590.

20. Lai Q, Emond J, Bhangui P, Ikegam T, Schaefer B, Hoppe-Lotichius M, et al. 335.1: Development and Validation of an Artificial Intelligence Model for a Better Prediction of Hepatocellular Cancer Recurrence After Transplantation: A Retrospective International Study. Transplantation. 2022;106(9S):S291-S2.

21. Celsa C, Quartararo A, Maida M, Giusino G, Gaudioso V, Sparacino A, et al. The application of artificial intelligence-based tools in the management of hepatocellular carcinoma: current status and future perspectives. Hepatoma Research. 2025;11:N/A-N/A.

22. Xie Q, Zhao Z, Yang Y, Wang X, Wu W, Jiang H, et al. A clinical-radiomic-pathomic model for prognosis prediction in patients with hepatocellular carcinoma after radical resection. Cancer Medicine. 2024;13(11):e7374.

23. Han H-H, Qiu Y-J, Shi Y-Y, Wen W, He X-P, Dong L-W, et al. Glypican-3-targeted precision diagnosis of hepatocellular carcinoma on clinical sections with a supramolecular 2D imaging probe. Theranostics. 2018;8(12):3268.

Middle Black Sea Journal of Health Science / Mid Blac Sea J Health Sci
August 2025; 11(3): 228-242

ORGINAL ARTICLE
DOI: 10.19127/mbsjohs.1690425

Association Between Screen Time, Digital Gaming Addiction, and Ocular Surface Parameters in School-Aged Children: A Cross-Sectional Study

Fatma Sümer[1](ID), Merve Yazıcı[1](ID)

[1]Recep Tayyip Erdoğan University, Faculty of Medicine, Deparment of Ophthalmology, Rize, Türkiye
[2]Recep Tayyip Erdoğan University, Faculty of Medicine, Department of Child and Adolescent Mental Health and Diseases, Rize, Türkiye

Received: 03 May 2025, Accepted: 30 July 2025, Published online: 30 August 2025

Abstract

Objective: This study aimed to evaluate whether screen exposure duration and the level of digital gaming addiction are associated with subjective ocular surface symptoms and objective tear film function tests in children.

Method: This cross-sectional study was conducted with 90 children aged between 8 and 14 years. Participants were divided into two groups: a symptomatic group (n = 45), consisting of children reporting ocular complaints such as burning, stinging, or itching, and a control group (n = 45) without such symptoms. All participants completed the Ocular Surface Disease Index (OSDI) questionnaire. Tear film function was assessed using tear break-up time (BUT) and non-anesthetized Schirmer tests. Screen time and digital gaming addiction levels were measured using structured questionnaires and the Digital Gaming Addiction Scale for Children (DGAS-C).

Results: Weekday and weekend screen exposure times were significantly longer in the symptomatic group compared to the control group ($p < 0.001$). OSDI scores were markedly higher in the symptomatic group ($p < 0.001$); however, no statistically significant differences were observed between groups in terms of BUT and Schirmer test results ($p > 0.05$). Total and subscale scores of the DGAS-C were also significantly higher in the symptomatic group ($p < 0.05$). Among participants with daily screen time exceeding two hours, no significant differences were detected in objective test results or addiction levels ($p > 0.05$).

Conclusion: This study demonstrated that increased screen time is significantly associated with the presence of ocular surface symptoms in children. However, the elevation in subjective symptom scores does not always correspond to changes in objective tear function tests. The findings indicate that digital screen exposure constitutes a relevant risk factor for pediatric ocular health and that such effects may initially manifest as subjective complaints. These findings highlight digital screen exposure as an emerging pediatric ophthalmic concern, underscoring the urgency of early behavioral interventions.

Keyword: Screen time; dry eye; OSDI; BUT; Schirmer; digital gaming addiction.

Suggested Citation Sumer F, Yazıcı M Association Between Screen Time, Digital Gaming Addiction, and Ocular Surface Parameters in School-Aged Children: A Cross-Sectional Study. Mid Blac Sea Journal of Health Sci, 2025;11(3): 228-242

Address for correspondence/reprints:

Emek Güldoğan

Telephone number: +90 (506) 284 49 34

E-mail: emek.guldogan@inonu.edu.tr

INTRODUCTION

The rapid integration of digital technologies into daily life practices has led to a profound shift in media consumption patterns, particularly among children and adolescents, at cognitive, behavioral, and social levels. With the accelerating pace of technological advancement worldwide, the prevalence of digital tools in everyday routines has markedly increased. Exposure to digital media has been reported to be on the rise among younger populations, especially school-aged children, who now rely heavily on digital devices for various needs ranging from education and socialization to entertainment and information access. The educational processes, social interactions, leisure activities, and information acquisition methods of children and adolescents are increasingly being mediated through digital platforms in addition to traditional media like television.

The increasing daily exposure to screen-based devices such as smartphones, tablets, computers, and televisions not only affects cognitive and psychosocial development but also holds the potential to exert clinically significant effects on the ocular system (1). This intensive digital exposure poses risks not only to cognitive functions and psychosocial well-being but also to ocular health.

The integrity of the ocular surface and the physiology of the tear film are highly sensitive to both environmental and behavioral stimuli. The literature indicates that prolonged exposure to digital screens initiates a process characterized by reduced blink rate, increased tear film evaporation, and subsequent destabilization of the tear film (2,3). These physiological alterations are particularly impactful in the developing pediatric ocular system, potentially resulting in the early manifestation of subjective symptoms such as burning, stinging, dryness, and itching—early indicators of dry eye disease (4,5). Such symptoms have been reported to negatively affect school performance, attention span, and overall quality of life.

Furthermore, excessive and uncontrolled digital gaming may lead to behavioral addiction in children, consequently prolonging screen exposure time and exacerbating secondary effects on ocular health (6). Digital gaming addiction is associated with psychosocial outcomes such as sleep disturbances, social withdrawal, reduced academic performance, and impaired attention regulation. Additionally, prolonged engagement with screens can act as a physiological stressor affecting tear film dynamics (7). However, the literature remains limited regarding studies that elucidate a causal

relationship between digital gaming addiction and ocular surface pathology.

The primary aim of this study is to comprehensively evaluate the relationship between screen exposure duration and digital gaming addiction levels with both subjective symptoms of dry eye and objective tear film parameters in children aged 8–14 years. Understanding the effects of digital media use on ocular physiology in pediatric populations may provide an important foundation for developing early intervention strategies to mitigate harmful digital behavior patterns that threaten eye health. Moreover, this study seeks to contribute original findings to the literature by exploring the interaction between behavioral addiction and ophthalmic pathophysiology in children.

METHODS

This observational and cross-sectional study was conducted between May 2024 and December 2024 at the Department of Ophthalmology, Faculty of Medicine, Recep Tayyip Erdoğan University. Ethical approval for the study was obtained from the Non-Interventional Clinical Research Ethics Committee of the institution (Ethics Committee Approval No: [2024/83], Date: [18/04/2024]). The study population consisted of children aged 8 to 14 years who were in generally stable ocular health.

Inclusion criteria were defined as children with a best-corrected visual acuity of 1.0 in Snellen equivalent, and without any active infections or a history of systemic or ocular chronic diseases. Participants were divided into two groups based on their presenting complaints at the ophthalmology outpatient clinic. The symptomatic group included children presenting with ocular surface-related complaints such as stinging, burning, or itching, suggestive of dry eye symptoms. The control group consisted of asymptomatic individuals with no subjective ocular complaints and no remarkable pathological findings upon general ophthalmic examination. All participants underwent slit-lamp biomicroscopy, and only those with normal anterior segment findings were included in the study.

Exclusion criteria included the presence of any systemic or ocular pathology that could directly affect tear physiology or subjective symptom perception; history of any ocular surgery; systemic diseases such as diabetes, hypertension, or metabolic disorders; chronic ocular conditions such as glaucoma, uveitis, amblyopia, or retinal pathologies; prior referral to child psychiatry or current use of psychiatric medication. Additionally, individuals with a current or past history of allergic or viral conjunctivitis, contact lens wearers, those using systemic medications that may influence corneal integrity or tear production, and those with spherical equivalent myopic refractive

errors exceeding -2.00 diopters were excluded from the study. This exclusion strategy was implemented to ensure a more reliable assessment of the relationship between screen time and dry eye-related symptoms.

Ocular Assessments

Ocular Surface Disease Index (OSDI)

To assess ocular surface symptoms, the Ocular Surface Disease Index (OSDI) questionnaire was administered. The OSDI is a validated 12-item instrument that evaluates visual function limitations, ocular discomfort, and symptoms triggered by environmental factors (8). All questionnaires were administered in the morning under standardized conditions by the same trained researcher, in the presence of the parent but without parental guidance or interference. The total score was calculated using the following formula and expressed on a scale of 0–100:

OSDI Score = (Total Score × 25) / Number of Questions Answered.

Higher scores indicate greater symptom severity. Scores were categorized as follows: 0–12 (normal), 13–22 (mild), 23–32 (moderate), and ≥33 (severe).

Tear Film Break-Up Time (BUT)

Tear film stability was evaluated using fluorescein-based BUT measurements. A sterile fluorescein strip (Fluorescein Sodium Strip, Haag-Streit) was applied to the inferior fornix. After several blinks, participants were asked to keep their eyes open. Using a slit-lamp with cobalt blue illumination, the interval between the last blink and the appearance of the first dark spot on the corneal surface was recorded in seconds. Three consecutive measurements were taken from each eye, and the mean value was used for analysis.

Measurements were performed under constant room conditions (22 ± 1°C, relative humidity 50 ± 5%) following a 10-minute screen-free rest period. To eliminate observer variability, all assessments were conducted by the same researcher. Values of <10 seconds were considered indicative of tear film instability.

Schirmer Test (Non-anesthetized)

Tear production was assessed using the Schirmer test without topical anesthesia. Standard Schirmer strips (Whatman no. 41, 5×35 mm) were placed in the lateral third of the lower eyelid. Participants were asked to keep their eyes closed for 5 minutes. The length of the moistened area was measured in millimeters for each eye. All measurements were conducted in the morning under consistent physical conditions by the same examiner. Values ≤10 mm were considered indicative of reduced tear production.

Structured Questionnaires

Sociodemographic and Screen Time Questionnaire: Parents were asked to complete a structured questionnaire prepared by the

research team to obtain sociodemographic information and screen time data. The questionnaire collected data on participants' age, sex, and parental education level, as well as daily duration of exposure to televisions and screen-based devices (computers, tablets, and smartphones). Weekly screen time averages were calculated and expressed in hours per day. Total screen exposure was additionally evaluated in relation to the recommended maximum daily screen time of 2 hours for this age group.

Digital Gaming Addiction Scale for Children (DGAS-C)

To assess digital gaming addiction levels, the Digital Gaming Addiction Scale for Children (DGAS-C) was used. This scale was developed and psychometrically validated by Hazar and Hazar for use in children aged 10–14 years. The scale consists of 24 items rated on a 5-point Likert scale, where each item is scored from 1 (strongly disagree) to 5 (strongly agree). The total score ranges from 24 to 120, and scores are categorized as follows: 1–24 (normal), 25–48 (low-risk), 49–72 (at risk), 73–96 (addicted), and 97–120 (highly addicted). The scale includes four subdimensions: (1) excessive focus and conflict related to digital gaming, (2) development of tolerance and psychological value attributed to gaming, (3) postponement of individual and social responsibilities, and (4) psychological-physiological manifestations of withdrawal symptoms. The internal consistency of the scale is high, with a reported Cronbach's alpha coefficient of 0.90 (9).

Based on a power of 95% and a Type I error rate of 5%, the total sample size was determined to be 90 participants, with 45 in each group, for independent samples t-test analysis. This sample size yielded an effect size of d = 0.77, indicating a moderate effect according to Cohen's criteria (Cohen, 1988). The power analysis findings suggest that the sample size is sufficient to draw reliable inferences from the study (Gibson et al., 2017). The power analysis was conducted using the G*Power 3.1 software (Faul, Erdfelder, Buchner, & Lang, 2009).

Statistical Analysis

The assumption of normality was first evaluated using the Shapiro–Wilk test. For comparisons of normally distributed variables between two groups, the independent samples t-test was used. For non-normally distributed data, the Mann–Whitney U test was applied. Categorical variables were compared using the Pearson chi-square test when all expected cell counts were greater than 5; otherwise, Fisher's exact test was employed (Howell, 2011). Multiple comparisons of proportions were conducted using the Bonferroni-corrected Z test. Correlations between non-normally distributed quantitative variables within the patient group were assessed using Spearman's rho correlation coefficient. Results for quantitative data were reported as mean ± standard deviation (SD) or median with

minimum and maximum values (median [min–max]). Categorical variables were presented as frequency (n) and percentage (%). A p-value of <0.05 was considered statistically significant. All statistical analyses were performed using IBM SPSS Statistics for Windows, Version 26.0 (IBM Corp., Armonk, NY, USA; released 2019).

RESULTS

A total of 90 children participated in this study, comprising 45 symptomatic participants (those reporting ocular symptoms such as stinging, burning, and itching) and 45 asymptomatic participants (control group). The mean age was 9.97 ± 1.34 years in the symptomatic group and 9.48 ± 1.21 years in the control group, with no statistically significant difference between the groups ($p > 0.05$). Similarly, there was no significant difference in gender distribution ($p > 0.05$).

Regarding screen exposure, the symptomatic group reported significantly longer durations of both television viewing and the use of other digital devices (computers, tablets, smartphones) on both weekdays and weekends compared to the control group ($p < 0.05$). Demographic characteristics and questionnaire results of the groups are summarized in Table 1.

Comparison of OSDI scores revealed that the mean OSDI score was significantly higher in the symptomatic group than in the control group ($p < 0.001$). However, no statistically significant differences were found between the groups in Schirmer test values or Break-Up Time (BUT) measurements ($p > 0.05$).

The total score of the Digital Gaming Addiction Scale for Children (DGAS-C) was significantly higher in the symptomatic group ($p < 0.05$). All subscales of the scale—including "excessive focus and conflict," "development of tolerance," "postponement of duties," and "withdrawal and immersion in gaming"—also yielded significantly higher scores in the symptomatic group compared to the control group ($p < 0.05$). According to the classification of addiction risk, none of the participants in the control group met the criteria for addiction, while 48.9% of the symptomatic group were classified as "at risk" and 35.6% as "addicted" (Table 2).

In subgroup analyses within the symptomatic group, no statistically significant differences were observed in OSDI, Schirmer, or BUT values between participants with less than 2 hours and those with more than 2 hours of daily screen time ($p > 0.05$). Similarly, the DGAS-C total and subscale scores did not differ significantly by screen time duration ($p > 0.05$) (Table 3).

Table 1. Comparison of Demographic and Clinical Characteristics Between Groups

	Control (n=45)	Patient (n=45)	p
Age	9.48 ± 1.21	9.97 ± 1.34	0.077[t]
Gender			
Male	30 (66.7)	22 (48.9)	0.088[x]
Female	15 (33.3)	23 (51.1)	
Number of Siblings			
1	1 (2.2)	1 (2.2)	0.286[f]
2	11 (24.4)	17 (37.8)	
3	27 (60)	18 (40)	
4	6 (13.3)	8 (17.8)	
5	0 (0)	1 (2.2)	
Birth Order			
1	14 (31.1)	14 (31.1)	0.155[f]
2	28 (62.2)	21 (46.7)	
3	3 (6.7)	8 (17.8)	
4	0 (0)	2 (4.4)	
Parental Status			
Father deceased	0 (0)	1 (2.2)	1.000[f]
Living together	45 (100)	44 (97.8)	
Mother's Education			
Primary school	4 (8.9)[a]	10 (22.2)[a]	**0.005[f]**
High school	37 (82.2)[a]	22 (48.9)[b]	
Vocational school	0 (0)[a]	3 (6.7)[a]	
University	4 (8.9)[a]	10 (22.2)[a]	
Father's Education			
Primary school	0 (0)[a]	5 (11.1)[b]	**<0.001[f]**
High school	37 (82.2)[a]	23 (51.1)[b]	
Vocational school	0 (0)[a]	6 (13.3)[b]	
University	8 (17.8)[a]	11 (24.4)[a]	
Mother's Employment			
Not working	17 (37.8)	23 (51.1)	0.289[f]
Working	28 (62.2)	22 (48.9)	
Father's Employment			
Not working	0 (0)	1 (2.2)	1.000[f]
Working	45 (100)	44 (97.8)	
Weekday TV time	45 (0 - 180)	120 (0 - 360)	**<0.001[m]**
Weekday screen device	30 (0 - 180)	180 (0 - 360)	**<0.001[m]**
Weekend TV time	60 (0 - 240)	120 (0 - 600)	**<0.001[m]**
Weekend screen device	90 (0 - 300)	240 (30 - 600)	**<0.001[m]**
BUT	17.1 (3.9 - 17.6)	13.3 (3.8 - 17.6)	0.148[m]
Schirmer	16 (2 - 25)	16 (4 - 30)	0.710[m]
OSDI	7.5 (0 - 55)	30 (2.5 - 77.5)	**<0.001[m]**

t: Independent samples t-test, m: Mann–Whitney U test, x: Pearson chi-square test, f: Fisher's exact test, mean ± standard deviation, median (min.–max.), n (%), Test stat: Test statistic, a-b: Groups sharing the same letter do not significantly differ.
BUT:Break-up Time , OSDI: Ocular Surface Disease Index.

Table 2. Examination of digital game scale scores according to groups

	Control (n=45)	Patient (n=45)	p
Over-focus and Procrastination	22 (11 - 26)	30 (11 - 44)	**<0.001[m]**
Conflict, Deprivation and Seeking	11 (6 - 16)	16 (6 - 22)	**<0.001[m]**
Emotion Exchange and Immersion	8 (4 - 14)	13 (4 - 18)	**<0.001[m]**
Digital Game Addiction	40 (21 - 56)	59 (23 - 80)	**<0.001[m]**
Digital Game Addiction Evaluation			
Normal	1 (2.2)[a]	0 (0)[b]	**<0.001[f]**
Little risk	29 (64.4)[a]	7 (15.6)[b]	
At risk	15 (33.3)[a]	22 (48.9)[a]	
Addicted	0 (0)[a]	16 (35.6)[b]	

m: Mann Whitney U test, f: Fisher's exact test, median (min.-max.), n (%), Test ist: Test statistic, a-b: No difference between groups with the same letter.

Table 1. Associations Between Screen Time and Ocular Surface Parameters

	BUT	p[t]	Schirmer	pt	OSDI	p[t]
Weekday TV time						
≤ 120 minutes	13.58 ± 3.31	0.105	15.14 ± 6.95	0.537	35.84 ± 18.73	0.657
> 120 minutes	11.07 ± 5.41		16.44 ± 6.22		33.28 ± 17.72	
Weekday screen device						
≤ 120 minutes	13.64 ± 3.28	0.156	16.33 ± 6.13	0.496	30.45 ± 17.45	0.124
> 120 minutes	11.85 ± 4.93		14.96 ± 7.15		38.85 ± 18.33	
Weekend TV time						
≤ 120 minutes	13.58 ± 3.46	0.156	14.35 ± 6.93	0.200	33.46 ± 16.47	0.584
> 120 minutes	11.75 ± 4.92		16.91 ± 6.24		36.48 ± 20.16	
Weekend screen device						
≤ 120 minutes	13.64 ± 2.55	0.338	17.13 ± 7.38	0.481	31.25 ± 23.07	0.534
> 120 minutes	12.48 ± 4.58		15.27 ± 6.55		35.73 ± 17.28	

t: Independent two sample t test, mean ± s.deviation

Table 4. Investigation of the relationship between total screen exposure times during the week, eye measurements and digital game scale scores in the patient group

	Screen Exposure on Weekdays		p
	≤ 120 (n=6)	**> 120 (n=39)**	
BUT	11.9 (11.2 - 13.3)	13.9 (3.8 - 17.6)	0.376[m]
Schirmer	17.5 (5 - 18)	15 (4 - 30)	0.920[m]
OSDI	40.83 ± 23.96	34.03 ± 17.39	0.400[t]
Over-focus and Procrastination	26.17 ± 8.5	29.77 ± 8.42	0.335[t]
Conflict, Deprivation and Seeking	15.33 ± 5.09	15.69 ± 4.22	0.851[t]
Emotion Exchange and Immersion	13 (9 - 18)	13 (4 - 18)	0.736[m]
Digital Game Addiction	55 ± 12.66	57.77 ± 14.47	0.660[t]

t: Independent two sample t test, m: Mann Whitney U test, mean ± s.deviation, median (min.-max.) BUT:Break-up Time , OSDI: Ocular Surface Disease Index.

No significant associations were found between weekday screen exposure exceeding 2 hours and participants' BUT, Schirmer, or OSDI scores ($p > 0.05$). Likewise, no significant relationship was observed between weekday screen time over 2 hours and DGAS-C total or subscale scores ($p > 0.05$) (Table 4). Due to only one participant reporting less than 120 minutes of weekend screen exposure, statistical comparisons could not be performed for that subgroup.

DISCUSSION

This study investigated the effects of screen time and digital gaming addiction levels on dry eye symptoms and tear film parameters in school-aged children, contributing original findings to a topic that has been only sparsely addressed in the literature.

In our findings, symptomatic children spent significantly more time in front of screens, including both television and other digital devices, on weekdays and weekends compared

to their asymptomatic peers. This observation supports the hypothesis that screen-based activities—particularly in school-aged children—may be associated with ocular surface symptoms. Prolonged use of digital devices is thought to reduce blink frequency, increase tear evaporation, and ultimately disrupt tear film stability. Lotfy et al. demonstrated that extended mobile gaming significantly decreased blink frequency and increased inter-blink intervals, which in turn led to ocular surface irritation due to tear film instability (10). Similarly, Müntz et al. investigated the impact of prolonged screen exposure on dry eye in adolescents and reported that decreased blink rates and tear film instability due to digital device use exacerbate ocular discomfort. Their findings indicate that screen-related activities may significantly disrupt blink dynamics that are essential for ocular surface health (5).

Moreover, our study revealed significantly higher OSDI scores among symptomatic participants, suggesting that digital exposure contributes to increased subjective ocular discomfort. The Ocular Surface Disease Index is a validated and widely used tool that evaluates the impact of ocular symptoms on daily visual function. Developed by Schiffman et al., the OSDI assesses multidimensional components including environmental triggers, visual disturbances, and symptom frequency, thereby offering a comprehensive assessment of perceived symptom burden (11).

Interestingly, no significant differences were found between symptomatic and control groups in objective measures such as BUT and Schirmer test values. This discrepancy highlights the known limitation that subjective symptoms may not always align with objective tear film parameters. Previous studies have noted that tear film tests may demonstrate limited sensitivity and reliability in pediatric populations and may show weak correlations with reported symptoms (12). These findings underscore the need for cautious and multidimensional interpretation of test results in clinical practice.

OSDI is a validated, multidimensional tool designed to assess the severity of dry eye-related symptoms and their impact on daily functioning (13). Comprising 12 items, the scale evaluates visual symptoms (e.g., burning, stinging, dryness, itching), functional limitations (e.g., reading, screen use, night driving), and environmental triggers (e.g., wind, low humidity, air conditioning). This comprehensive structure allows OSDI to capture not only physiological signs but also the subjective symptom burden as perceived by the patient (14).

Particularly in the presence of behavioral stressors such as prolonged screen exposure, cognitive overload, and environmental stimuli (e.g., light, wind, or dust), subjective ocular

symptoms may become apparent earlier and more prominently than objective clinical findings (14,15). Accordingly, the OSDI is considered a sensitive instrument for identifying early ocular surface dysfunction in cases where physiological changes have yet to be reflected in conventional diagnostic tests. Indeed, several studies report that OSDI scores do not always show strong correlations with objective tear film parameters such as osmolarity, BUT, or Schirmer test results, reinforcing the subjective nature of symptom reporting captured by this scale (17).

The application of conventional tests such as BUT and Schirmer in pediatric populations presents inherent limitations. It has been previously documented that these tests may suffer from poor reproducibility in children, are heavily dependent on patient cooperation, and can be influenced by external environmental factors (18). The TFOS DEWS II reports have particularly emphasized the low test-retest reliability of these conventional diagnostic methods in pediatric populations, highlighting their limited sensitivity in detecting early ocular surface dysfunction (17,18,20). Non-invasive tear film assessment techniques, such as non-invasive BUT measurements, have shown superior reproducibility and patient comfort compared to fluorescein-based methods, particularly in children where cooperation may be challenging (21,22,23). Moreover, they may not adequately reflect dynamic changes on the ocular surface, particularly in early evaporative dry eye, where subjective discomfort may be pronounced despite normal tear volume or stability. Thus, our findings suggest that digital screen exposure primarily impacts the ocular surface at a symptomatic level, preceding detectable physiological impairment. These results emphasize the potential superiority of symptom-based assessment tools in detecting early digital media-related visual complaints in children and highlight the clinical value of incorporating subjective scales in pediatric ophthalmologic evaluations.

In our study, digital gaming addiction scores were significantly higher in the symptomatic group compared to the control group. Total and subscale scores of the Children's Digital Game Addiction Scale (DGAS-C) were consistently elevated among symptomatic participants. These results imply that digital gaming behavior in symptomatic children is characterized not only by extended use but also by patterns suggestive of addictive tendencies. In a prior study by Hazar, digital game addiction in children was associated with social withdrawal, impaired impulse control, and reduced academic functioning, with behavioral and neuropsychological features of addiction prominently observed (19).

The observed link between digital gaming addiction and dry eye symptoms may be mediated by prolonged screen exposure, suppression of the blink reflex due to sustained

visual attention, and reduced oculomotor activity. Floros et al. found that higher digital game addiction scores were significantly associated with symptoms of digital eye strain and suggested that such addiction constitutes a risk factor for the development of visual fatigue (16). These findings underscore the dual impact of digital game addiction—not only on mental health but also as a contributing factor to ocular surface dysfunction.

One of the novel aspects of this study lies in its multidimensional assessment of the association between digital screen exposure, digital gaming addiction behaviors, and ocular surface symptoms among school-aged children. By incorporating both subjective (OSDI) and objective (BUT and Schirmer) parameters, this investigation offers a comprehensive evaluation of digital media's potential impact on pediatric ocular health. Notably, the current literature lacks sufficient research directly addressing the ocular consequences of digital gaming addiction, thus underscoring the potential contribution of these findings to the field. Moreover, the assessment of digital game addiction through its subcomponents—encompassing cognitive, emotional, and social orientations—rather than reducing it solely to screen time, enhances the analytical depth of this study and distinguishes it from prior investigations.

Nevertheless, several methodological limitations should be acknowledged. The cross-sectional design precludes any inference of causality between variables. Additionally, tear function tests such as Schirmer and BUT are operator-dependent and susceptible to environmental influences, particularly in pediatric populations, thereby introducing a potential for inter-measurement variability. Self-reported data on digital device use and gaming behaviors may be subject to recall bias or social desirability bias, limiting the accuracy of these responses. The relatively small sample size and the single-center nature of the study may also restrict the generalizability of the findings to broader pediatric populations. Although the DGAS-C is validated for use in children aged 10–14 years, the inclusion of participants as young as 8 years may introduce a degree of measurement variability. However, item comprehension was confirmed by the research team during administration, and responses were carefully monitored for consistency.

Despite these limitations, the present study highlights the necessity of evaluating digital screen use and gaming behaviors not only in terms of their psychological consequences but also with regard to their physiological effects on ocular health. The results underscore the importance of structuring digital media habits in childhood and emphasize the need for awareness programs targeting screen duration and digital content quality. Ophthalmic evaluations in children should routinely include

structured assessments of digital behavior. Future prospective, multicenter studies with larger cohorts are warranted to more precisely elucidate the long-term effects of digital exposure on ocular health and to provide stronger evidence to guide clinical and preventive interventions.

CONCLUSION

This cross-sectional study provides compelling evidence that increased screen time exposure is significantly associated with ocular surface symptoms in school-aged children, representing an emerging concern in pediatric ophthalmology. Our findings demonstrate that symptomatic children exhibited substantially longer screen exposure durations across all digital devices compared to their asymptomatic counterparts, with concomitantly elevated OSDI scores reflecting greater subjective ocular discomfort. Notably, digital gaming addiction scores were consistently higher in the symptomatic group, suggesting that problematic digital behaviors may constitute an additional risk factor for pediatric dry eye symptoms beyond mere exposure duration.

The dissociation between subjective symptom severity and objective tear film parameters observed in this study underscores the complexity of digital screen-related ocular surface dysfunction in children. While conventional diagnostic tests such as BUT and Schirmer measurements failed to demonstrate significant between-group differences, the pronounced elevation in OSDI scores among symptomatic participants suggests that digital exposure primarily manifests as symptomatic dysfunction in the early stages, preceding detectable physiological impairment. This finding has important clinical implications, emphasizing the potential superiority of validated symptom-based assessment tools in detecting early digital media-related visual complaints in pediatric populations.

The multidimensional nature of digital gaming addiction, encompassing cognitive, emotional, and behavioral components, appears to be intricately linked with ocular surface symptomatology. The significant associations observed across all DGAS-C subscales suggest that addictive gaming behaviors may amplify the deleterious effects of screen exposure through mechanisms involving sustained visual attention, suppressed blink dynamics, and prolonged accommodative stress.

These findings have significant implications for clinical practice and public health policy. Healthcare providers should incorporate structured assessments of digital behavior and screen time exposure into routine pediatric ophthalmologic evaluations. The implementation of evidence-based screen time guidelines, coupled with educational interventions targeting optimal digital hygiene practices, may serve as preventive measures

against the development of digital eye strain in children.

Clinical Recommendations: Based on our findings, we recommend that clinicians routinely inquire about screen time exposure and digital gaming behaviors when evaluating children with ocular surface complaints. The OSDI questionnaire may serve as a sensitive screening tool for detecting early digital media-related visual symptoms, particularly when objective tests remain within normal limits. Furthermore, behavioral interventions focusing on proper screen viewing habits, scheduled digital breaks, and environmental modifications should be integrated into comprehensive pediatric eye care protocols.

Future research should focus on longitudinal studies to establish causal relationships and investigate the long-term consequences of digital exposure on pediatric ocular health. Additionally, the development of age-appropriate diagnostic tools specifically designed for children, along with standardized treatment protocols for digital eye strain, remains a priority for advancing pediatric ophthalmologic care in the digital age.

Acknowledgment: The authors would like to thank Mine Kaya for the statistical analysis of the study.

Ethics Committee Approval: The study was approved by the Recep Tayyip Erdogan University School of Medicine Ethics Committee (Ethics Committee Approval Number: 2024/83).

Peer-review: Externally peer-reviewed

Author Contributions: Concept: FS, MY, Design: FS, MY, Data Collection and Processing: FS, MY, Analysis and Interpretation: FS, MY, Writing: FS, MY

Conflict of Interest: The authors declared no conflict of interest.

Financial Disclosure: The authors declared that this study has not received no financial support.

REFERENCES

1. Cem Aykutlu H, Şambel Aykutlu M. Association Between Problematic Internet Use, Digital Game Addiction, and Digital Eye Strain Among Adolescents: A Cross-Sectional Clinical Study. Neuropsychiatr Invest. 2024;62(4): 122–127. doi:10.5152/NeuropsychiatricInvest.2024.24044

2.Jadeja JN, Shroff KV, Shah A, Pandey A, Dubey S. Association of digital device usage and dry eye disease in school children. Indian Journal of Ophthalmology. 2024;72(7):1031-1036. doi:10.4103/IJO.IJO_703_23

3. Tripathi A, Agarwal R, Kharya P. Dry eye disease related to digital screen exposure in medical students. The Pan-American Journal of Ophthalmology. Medknow;

2022;4(1): 35. doi:10.4103/PAJO.PAJO_16_22

4. Can exposure to digital screens cause ocular surface disorders in children? Myopia Profile. Available from: https://www.myopiaprofile.com/articles/children-ocular-surface-dry-eye-digital-screen-time [Accessed July 2025]

5. Muntz A, Turnbull PR, Kim AD, Akılesh G, Wong D, Tsat TSW, et al. Extended screen time and dry eye in youth. Contact Lens and Anterior Eye. Elsevier; 2022;45(5): 101541. doi:10.1016/J.CLAE.2021.101541

6. Ayaz-Alkaya S, Köse-Kabakcıoğlu N. Prevalence and predisposing factors of digital game addiction and cyberbullying in adolescents: A cross-sectional study. Public Health. W.B. Saunders; 2025;241: 137–143. doi:10.1016/J.PUHE.2025.02.012

7. Chidi-Egboka NC, Jalbert I, Golebiowski B. Smartphone gaming induces dry eye symptoms and reduces blinking in school-aged children. Eye (Basingstoke). Springer Nature; 2023;37(7): 1342–1349. doi:10.1038/S41433-022-02122-2

8. K A, S K, SN M, Ocansey S, Abu LS, Kyere EA. Ocular Surface Disease Index (OSDI) Versus the Standard Patient Evaluation of Eye Dryness (SPEED): A Study of a Nonclinical Sample. Cornea. Cornea; 2016;35(2): 175–180. doi:10.1097/ICO.0000000000000712

9. Çimke S, Gürkan DY, Sırgancı G. Determination of the psychometric properties of the digital addiction scale for children. Journal of Pediatric Nursing. W.B. Saunders; 2023;71: 1–5. doi:10.1016/j.pedn.2023.03.004

10. Lotfy NM, Shafik HM, Nassief M. Risk factor assessment of digital eye strain during the COVID-19 pandemic: a cross-sectional survey. Medical Hypothesis Discovery and Innovation in Ophthalmology. International Virtual Ophthalmic Research Center; 2022;11(3): 119–128. doi:10.51329/MEHDIOPHTHAL1455

11. RM S, MD C, G J, H JD, R BL. Reliability and validity of the Ocular Surface Disease Index. Archives of ophthalmology (Chicago, Ill. : 1960). Arch Ophthalmol; 2000;118(5): 615–621. doi:10.1001/ARCHOPHT.118.5.615

12. Zou Y, Li D, Gianni V, Congdon N, Piyasena P, P SG, et al. Prevalence of dry eye disease among children: a systematic review and meta-analysis. BMJ Open Ophthalmology. BMJ Publishing Group; 2025;10(1): e002014. doi:10.1136/BMJOPHTH-2024-002014

13. Grubbs JR, Tolleson-Rinehart S, Huynh K, Davis RM . A Review of Quality of Life Measures in Dry Eye Questionnaires. Cornea. Lippincott Williams and Wilkins;

2014;33(2): 215–218. doi:10.1097/ICO.0000000000000038

14. Chidi-Egboka NC, Golebiowski B, Lee SY, Vi M, Jalbert I. Dry eye symptoms in children: can we reliably measure them? Ophthalmic and Physiological Optics. Blackwell Publishing Ltd; 2021;41(1): 105–115. doi:10.1111/OPO.12762;PAGE:STRING:ARTICLE/CHAPTER

15. Hazar Z. An Analysis of the Relationship between Digital Game Playing Motivation and Digital Game Addiction among Children. Asian Journal of Education and Training. Asian Educational Journal Publishing Group; 2018;5(1): 31–38. doi:10.20448/JOURNAL.522.2019.51.31.38

16. Floros GD, Glynatsis MN, Mylona I. No End in Sight; Assessing the Impact of Internet Gaming Disorder on Digital Eye Strain Symptoms and Academic Success. European Journal of Investigation in Health, Psychology and Education. Multidisciplinary Digital Publishing Institute (MDPI); 2024;14(3): 531–539.

17) Stapleton F, Alves M, Bunya VY, Jalbert I, Lekhanont K, Malet F, et al. TFOS DEWS II Epidemiology Report. Ocul Surf. 2017;15(3):334–65.

18) Jones L, Downie LE, Korb D, Benitez-Del-Castillo JM, Dana R, Deng SX, et al. TFOS DEWS II Management and Therapy Report. Ocul Surf. 2017;15(3):575–628.

19) Inomata T, Iwagami M, Nakamura M, Shiang T, Yoshimura Y, Fujimoto K, et al. Characteristics of dry eye disease in a working population using the OSDI questionnaire: the Japan health and wellness survey. PLoS One. 2021;16(1):e0245002.

20. Wolffsohn JS, Arita R, Chalmers R, Djallian A, Dogru M, Dumbleton K, et al. TFOS DEWS II Diagnostic Methodology report. Ocul Surf. 2017;15(3):539-574. doi:10.1016/j.jtos.2017.05.001

21. García-Marqués JV, Talens-Estarelles C, García-Lázaro S, Giner A, Burgos FJ, Cordona G, et al. Optical quality and intraocular scattering in a healthy young population. Clin Exp Optom. 2011;94(2):223-229. doi:10.1111/j.1444-0938.2010.00535.x

22. Downie LE, Keller PR, Vingrys AJ. Assessing ocular bulbar redness: a comparison of methods. Ophthalmic Physiol Opt. 2016;36(2):132-139. doi:10.1111/opo.12245

23. Tian L, Qu JH, Zhang XY, Sun XG. Repeatability and reproducibility of noninvasive keratograph 5M measurements in patients with dry eye disease. J Ophthalmol. 2016;2016:8013621. doi:10.1155/2016/8013621

Middle Black Sea Journal of Health Science / Mid Blac Sea J Health Sci
August 2025; 11(3): 243-249

CASE REPORT
DOI: 10.19127/mbsjohs.1665455

Interpretation of Prostate-Specific Antigen Result: A Primary Care Case Report

Merve Köybaşı Acet[1(ID)], Melike Karabulut Özer[1(ID)], Bestegül Çoruh Akyol[1(ID)], Özgür Enginyurt[1(ID)], Ahmet Anıl Acet[2(ID)],

[1]Ordu University, Faculty of Medicine, Department of Family Medicine, Ordu, Türkiye
[2]Ordu University, Faculty of Medicine, Department of Urology, Ordu, Türkiye

Received: 29 January 2025, Accepted: 29 June 2025, Published online: 30 August 2025

Abstract

Prostate-specific antigen (PSA) is a serine protease secreted from prostatic tissue and is responsible for semen liquefaction. It is the first choice, especially in prostate cancer screening. However, it can be seen to be elevated in many conditions other than prostate cancer, from a simple urinary tract infection to other prostate diseases. Therefore, the patient's condition and clinical features should be evaluated during PSA evaluation. In this case report, it is mentioned that an elevated PSA result in a patient with an asymptomatic urinary tract infection should be rechecked after treatment of the infection, and an additional urine examination should be performed to avoid unnecessary prostate biopsy. Clinically, a prostate biopsy in such a patient would be inappropriate and would cause the patient unnecessary anxiety. Furthermore, such an approach should be avoided because it will impose a pointless financial burden. This approach is fulfilled early in primary health care services. Primary health care services are of great importance in both easy accessibility and screening medical practice

Keyword: Prostate-specific antigen, Urine Analysis, Prostate Cancer, Cancer Screening, Family Medicine

Suggested Citation: Koybasi Acet M, Karabulut Ozer M, Coruh Akyol B. Enginyurt O, Acet AA. Interpretation of Prostate-Specific Antigen Result: A Primary Care Case Report. Mid Blac Sea Journal of Health Sci, 2025;11(2): 243-249.

Address for correspondence/reprints:

Merve Köybaşı Acet

Telephone number: +90 (532) 312 40 79

E-mail: koybasiimervee@gmail.com

INTRODUCTION

Prostate-specific antigen (PSA) is a serine protease belonging to the human kallikrein group. It was first detected in human serum in 1979 and became the focus of many studies when it was determined that its levels increased in the serum of patients diagnosed with prostate

cancer (1). PSA is typically found in high concentrations in seminal fluid and plays a role in the liquefaction of semen fluid. The primary purpose of performing PSA tests in clinical practice is to reduce mortality rates due to prostate cancer with early diagnosis and to prevent unnecessary biopsies and treatment of cancers that do not require treatment (2).

PSA levels increase in prostate diseases. However, PSA levels do not increase in every prostate disease. PSA levels may vary according to age, race, and prostate volume. PSA levels increase with increasing age. PSA levels also increase in conditions such as prostatitis, urinary tract infection, prostate cancer, benign prostatic hyperplasia (BPH), acute urinary retention, and ejaculation. Prostate biopsy, prostate massage, and transurethral interventions to the prostate may cause a temporary increase in PSA levels (Table 1). Serum PSA levels are expected to return to normal within 6-8 weeks after acute prostatitis and 4-6 weeks after biopsy (2).

Over time, it has been observed that screening by measuring PSA levels in men who are suitable for screening causes excessive diagnosis and treatment. Therefore, routine prostate cancer screening is not recommended for all men. Routine screening for prostate cancer is not recommended in the country where this research was conducted, and it is recommended that decisions be made on a patient-specific basis (3).

The national guideline recommends that men over the age of 40 with a family history of prostate cancer and men over the age of 50 without a family history of prostate cancer should be informed and referred to a urologist for early diagnosis and prevention (4).

European urology guidelines recommend that men with PSA>1 ng/ml at the age of 40 and PSA>2 ng/ml at the age of 60 have PSA checked every 2 years. Early diagnosis programs are not recommended for those with a life expectancy of less than 15 years (5).

Despite many studies and clinical experience, there is no standard approach regarding PSA; patients whose PSA levels are above 4 ng/ml and whose control tests are the same should generally be referred to a urologist for biopsy, further examination, and treatment (6).

CASE

A 70-year-old man presented to a primary health care centre for cancer screening upon the invitation of his family physician. The patient had no active complaints and a history of cardiac arrhythmia in the initial evaluation. There was no oncological history in the family history. The detailed physical examination was normal, and laboratory analyses revealed no pathological findings except for elevated PSA. No nodules were detected during rectal examination. The patient's PSA result was 39 ng/mL. Since there were no risk factors such as prostate cancer, breast cancer, or colon cancer

in his past medical history and family history, he was referred to other causes of elevated PSA in the differential diagnosis. Detailed questioning was performed in his anamnesis. There was no complaints of urination or urinary incontinence. There was no complaint of pain or redness in the scrotum. In addition, the abdomen was comfortable, there was no globe vesicale, external genital examination was routine, and no nodule on digital rectal examination. He was also questioned urologically; he had never consulted a urologist before and had not undergone any urological procedure. Since an asymptomatic urinary tract infection was the most likely cause among other causes, this diagnosis was first considered. No urinalysis was performed in the initial evaluation. On suspicion, a complete urine analysis was performed. Pyuria was detected on microscopic examination. Subsequently, 100.000 CFU/mL Escherichia coli growth was detected in midstream urine culture. We diagnosed an asymptomatic urinary tract infection, and the PSA elevation was attributed to the current clinical condition. The necessary treatment was arranged, and nitrofurantoin 100 mg oral tablet 2x1 treatment was started in accordance with the antibiogram, and conservative recommendations were explained. Approximately 4 weeks after the treatment, the pathologies in the patient's laboratory examination were resolved in the outpatient clinic control, and the PSA level was measured as 2 ng/mL. The patient was referred to the urology clinic as a precaution, and no additional recommendations were applied in the urological evaluation. He was also taken under regular follow-up.

DISCUSSION

PSA is found at physiological levels in every man. Normal male serum PSA levels are usually lower than 4 ng/mL (7). PSA levels are frequently used as a screening tool for prostate cancer, but their elevation can indicate many clinical conditions. It has a vast etiological scale, such as ejaculation, urinary tract infection, prostatitis, prostate abscess, BPH, acute urinary retention, and prostate cancer. In addition, lower PSA levels have been detected in men with a high body mass index. This has been attributed to the estrogenic effect on adipose tissue. For example, medications that affect testosterone levels in hypogonadism patients or the use of 5-α reductase inhibitors in patients diagnosed with BPH cause changes in PSA levels (8). PSA is found at physiological levels in every man. Normal male serum PSA levels are usually lower than 4 ng/mL (7). PSA levels are frequently used as a screening tool for prostate cancer, but their elevation can indicate many clinical conditions. It has a vast etiological scale, such as ejaculation, urinary tract infection, prostatitis, prostate abscess, BPH, acute urinary retention, and prostate cancer. In addition, lower PSA levels have been detected in men with a high body mass index.

This has been attributed to the estrogenic effect on adipose tissue. For example, medications that affect testosterone levels in hypogonadism patients or the use of 5-α reductase inhibitors in patients diagnosed with BPH cause changes in PSA levels (8).

Table 1: Causes of PSA Level Elevation

- Prostate Cancer
- Urinary Tract Infection
- Acute Urinary Retention
- Benign Prostatic Hyperplasia
- Digital Rectal Examination
- Ejaculation
- Prostate Biopsy
- Prostate Surgery
- Prostatitis

There are case reports of noncancerous causes of elevated PSA. They are usually seen at a PSA level of less than 50 ng/mL (9).

Prostatitis is an important and common cause of PSA elevation. Nadler et al. found that prostatitis caused an increase in PSA levels based on biopsy results from 148 patients with PSA levels above 4 ng/mL. Therefore, many physicians prescribe antibiotic treatment to their patients before repeating the PSA test (10). Another study on 72 patients with prostatitis revealed that PSA increased above 4 ng/mL due to prostatitis (11). In urinary tract infections seen in men, the prostate and seminal vesicles are frequently affected; therefore, current guidelines do not recommend PSA measurement in patients with acute prostatitis.

In our study, the cause of PSA elevation was an asymptomatic urinary tract infection, which is consistent with the literature. At this point, the most important part for us was the patient's request for the PSA test and the fact that he stated that he had relatives in his circle who had previously had high results and were subjected to further examination due to prostate cancer. Based on the biopsychosocial approach principle of the Family Medicine Specialization, the patient was given the necessary information before the examination, but we still performed the examination. Due to developing technological opportunities, especially internet access, and due to sources open to disinformation regarding prostate cancer screening with PSA, on the one hand, we managed our patient's concern about the possibility of prostate cancer. On the other hand, we followed up on a test result that was higher than usual.

A urine culture is usually one of the first steps in diagnosing a urinary tract infection. E. coli remains the most common organism responsible for this (12). Urine culture is usually one of the first steps in diagnosing a urinary tract infection. E. coli remains the most common organism responsible for this. In our patient, we performed a complete urinalysis and urine culture examination to exclude urinary tract infection at the first encounter. The urine culture revealed significant E. coli growth. Here, we deepened our differential diagnosis

with more cost-effective tests to clarify the differential diagnosis before considering the possibility of cancer due to elevated PSA. The findings we detected on microscopy, until the culture results indicated that we should not rush to diagnose cancer. In patients with active bacterial prostatitis and elevated PSA, the test is usually repeated to see if PSA levels have returned to baseline levels after the resolution of the acute infection. If PSA levels remain high, further diagnostic procedures for prostate cancer are performed (7). In our patient, when the PSA test was repeated 4 weeks later, the test results had returned to normal levels, so there was no need for further examination.

As can be seen, PSA is affected by many factors, from drug use to cancer. An evaluation should be made specific to the patient and clinical condition. For all these reasons, the reasons for the increase in PSA should be taken into consideration. Although our patient did not have any symptoms that would suggest urinary system infection, the fact that there was no palpable mass on rectal examination during our physical examination, no history of prostate cancer in the family, no drug use, and no other additional complaints eliminated us from other reasons that increase PSA. In accordance with the clinical result, an asymptomatic urinary system infection was considered in the foreground, and a complete urinalysis and urine culture examination were performed to exclude this diagnosis. With all these examinations, the patient was diagnosed with an asymptomatic urinary system infection; the PSA elevation was attributed to this condition, and a follow-up examination was planned. In the follow-up examinations, it was determined that the PSA level had returned to normal, and the urinary system infection had disappeared.

CONCLUSION

Cases in the literature about the relationship between elevated PSA levels and prostate cancer, and this case shows that although PSA testing is requested as a marker in exceptional cases, not every PSA screening will be due to prostate cancer. Benign causes should always be kept in mind, and decisions should be evaluated together with the clinical evaluation. A complete urine test should also be performed on every patient whose PSA level is to be measured. Antibiotic therapy and control evaluation should be performed according to this evaluation. In such a case, the screening indication and the patient's history should be reviewed again.

Ethics Committee Approval: The presented study is qualitative and consent wasobtained by giving information about the study by one-toone interviews with the subjects who agreed to participate. The study was carried out by paying attention to the Declaration of Helsinki.

Peer-review: Externally peer- reviewed

Author Contributions: Concept: MK, AAA, Design: MK, AAA, Data Collection: MK, AAA, Analysis and Interpretation: MK, MKO, BCA, OE, AAA, Writing: MK, MKO, BCA, OE, AAA.

Conflict of Interest: The authors declared no conflict of interest.

Financial Disclosure: The authors declared that this study has not received no financial support.

REFERENCES

1. Whitaker H, Tam JO, Connor MJ, Grey A. Prostate cancer biology & genomics. Transl Androl Urol. 2020;9(3):1481–91.
2. Baltacı S, Gökçe İ Prostate Cancer. In: Anafarta K, Arıkan N, Bedük Y, editors. Basic Urology. Ankara: Detail Press; 2011. s. 802-3
3. Özsöyler M, Güzelöz Z, Keser M Knowledge and Attitudes about Cancer Screening Tests of Patients aged 35 years and Over Applying to Family Medicine Outpatient Clinic. Forbes Medicine Journal (Online). 2023; 4(1): 76 - 83.
4. Çifçili SS. Screenings to be done in Periodic Health Examination in Individuals Over 65 Years of Age. Clinical Family Medicine. 2017;9(2):37-42.
5. Mottet N, van den Bergh RC, Briers E, Van den Broeck T, Cumberbatch MG, De Santis M, et al. EAU-EANM-ESTRO-ESUR-SIOG Guidelines on Prostate Cancer—2020 Update. Part 1: Screening, Diagnosis, and Local Treatment with Curative Intent. European Urology. 2021;79(2):243-62.
6. Chen Y, Yan H, Xu Y, Chen K, Yang R, Yang J, et al. Analysis of the predictive value of the prostate-specific antigen-to-neutrophil ratio for the diagnosis of prostate cancer. Discov Onc. 2025;16(1).
7. Nepal A, Sharma P, Bhattarai S, Mahajan Z, Sharma A, Sapkota A, et al. Extremely Elevated Prostate-Specific Antigen in Acute Prostatitis: A Case Report. Cureus. 2023; 15(8), e43730.
8. Kutlu O, Koksal IT. Efforts for Improving the Efficiency of PSA: PSA Density, PSA Velocity, Age-specific PSA, and Free and Complexed PSA. Turkish Urology Seminars. 2013;3(3):55-60.
9. Kan HC, Hou CP, Lin YH, Tsui KH, Chang PL, Chen CL. Prognosis of prostate cancer with initial prostate-specific antigen >1,000 ng/mL at diagnosis. Onco Targets Ther. 2017;10:2943-9.
10. Pylväläinen J, Talala K, Raitanen J, Rannikko A, Auvinen A. Association of prostate-specific antigen density with prostate cancer mortality after a benign systematic prostate biopsy result. BJU Int. 2025;135(5):841–50.
11. Azab S, Osama A, Rafaat M. Does normalizing PSA after successful treatment

of chronic prostatitis with high PSA value exclude prostatic biopsy? Transl Androl Urol. 2012;1(3):148–52.

12. Yebes A, Toribio-Vazquez C, Martinez-Perez S, Quesada-Olarte JM, Rodriguez-Serrano A, Álvarez-Maestro M, et al. Prostatitis: A Review. Curr Urol Rep. 2023;24(5):241-51.

13. Flocks RH, Urich VC, Patel CA, Opitz JM. Studies on the antigenic properties of prostatic tissue. I. J Urol. 1960;84(2):134–143.

Middle Black Sea Journal of Health Science / Mid Blac Sea J Health Sci
August 2025; 11(3): 250-256

CASE REPORT
DOI: 10.19127/mbsjohs.1665455

Marchiafava–Bignami Disease in a Chronic Alcohol User: A Case Report Emphasizing Early Diagnosis and Multidisciplinary Management

Şükran Kaygısız[1](ID)

[1]Ordu University, Faculty of Medicine, Department of Neurology, Ordu, Türkiye

Received: 15 March 2025, Accepted: 26 March 2025, Published online: 30 August 2025

Abstract

Diagnosing acute neurological deficits in chronic alcohol users is challenging due to atypical presentations and incomplete histories. Marchiafava–Bignami disease (MBD) is a rare disorder characterized by demyelination and necrosis of the corpus callosum, often extending to adjacent white matter. A 36-year-old male presented to the emergency department with sudden-onset speech disturbance and word-finding difficulty that began one day prior. Later that evening, he developed nausea, vomiting, imbalance, and hand tremors. The patient had a 10-year history of chronic alcohol use and recent illicit alcohol consumption. Brain magnetic resonance imaging (MRI) revealed diffusion restriction in the corpus callosum and posterior parietal white matter, while contrast-enhanced images showed no pathological enhancement. Laboratory studies indicated elevated homocysteine, normal vitamin B12 levels, and thrombocytopenia. Although an infectious process was initially considered, the absence of fever and normal leukocyte counts led to a preliminary diagnosis of MBD. The patient was admitted to neurology and treated with intravenous thiamine (100 mg daily) and aggressive hydration for 10 days. Following treatment, significant improvement was observed in speech, balance, nausea, and vomiting, although hand tremors persisted. Suspected alcohol withdrawal prompted psychiatric consultation and subsequent treatment. Follow-up imaging and Electroencephalography (EEG) revealed resolution of abnormalities, and the patient was discharged with only mild tremor and minimal dysarthria. This case emphasizes that rare conditions such as MBD should be considered in the differential diagnosis of acute neurological deficits in chronic alcohol users. Early recognition and prompt treatment, with diffusion-weighted MRI serving as a key diagnostic tool, are essential for minimizing permanent neurological damage.

Keyword: Marchiafava–Bignami disease (MBD), alcohol dependence, encephalopathy, corpus callosum, thiamine

Suggested Citation: Kaygisiz S. Marchiafava–Bignami Disease in a Chronic Alcohol User: A Case Report Emphasizing Early Diagnosis and Multidisciplinary Management. Mid Blac Sea Journal of Health Sci, 2025;11(3):250-256.

Address for correspondence/reprints:

Şükran Kaygısız

Telephone number: +90 (452) 226 52 00

E-mail: eminepirim09@hotmail.com

INTRODUCTION

MBD is a rare demyelinating disorder predominantly seen in chronic alcohol users, characterized by degeneration of the corpus callosum and diffuse white matter abnormalities (1). Acute neurological manifestations, including dysarthria, ataxia, and tremor, may mimic other encephalopathic or demyelinating conditions (2). Early recognition and treatment are crucial in minimizing permanent neurological sequelae (3). This report describes a case of MBD in a 36-year-old male who presented with acute neurological deficits in the context of chronic and illicit (methanol) alcohol use.

CASE

A 36-year-old male presented to the emergency department with a complaint of speech disturbance that began suddenly one day prior. The patient, who had no known chronic illnesses or history of regular medication use, experienced an abrupt onset of word-finding difficulty and stuttering. Believing that his symptoms would resolve spontaneously, he did not initially seek medical care. Later that evening, his symptoms were accompanied by nausea, vomiting, and imbalance. On the day of presentation, he developed observable tremors in his hands and a generalized sensation of tremor, along with impaired balance during ambulation. Notably, he did not report headache, any new visual disturbances, or shivering.

The patient's history revealed approximately 10 years of continuous alcohol use and, more recently, illicit alcohol (the chemical compound methanol) consumption for one week. During the initial history-taking in the emergency department, no information regarding alcohol use was provided. His brain computed tomography (CT) was normal. Owing to lesions observed on MRI studies, an initial consultation with the infectious diseases department was requested with a preliminary suspicion of encephalitis. However, the absence of fever and normal leukocyte counts led the infectious diseases specialist to recommend a neurology consultation, deeming an infectious process unlikely. Taking this into consideration, lumbar puncture and cerebrospinal fluid analysis were not prioritized or deemed necessary at this stage.

Neurological examination in the emergency department revealed that the patient was alert, cooperative, and oriented. Cranial nerve evaluation showed bilateral horizontal nystagmus and decreased visual acuity at a distance of approximately three meters, consistent with sequelae secondary to macular

pathology. The patient's speech was dysarthric with cerebellar characteristics, and bilateral postural and kinetic tremors were noted. There was no motor deficit, and deep tendon reflexes were normal. Cerebellar testing was bilaterally impaired, and during tandem gait, the patient was unable to maintain a straight line after the second step. No fever, neck stiffness, or pathological reflexes were detected.

Diffusion-weighted MRI demonstrated areas of restricted diffusion in the posterior corpus callosum, bilateral posterior parietal deep white matter, and anterior corpus callosum. Contrast-enhanced MRI revealed linear FLAIR hyperintensities in the bilateral periventricular white matter, without evidence of pathological contrast enhancement on postcontrast sequences (Figure 1).

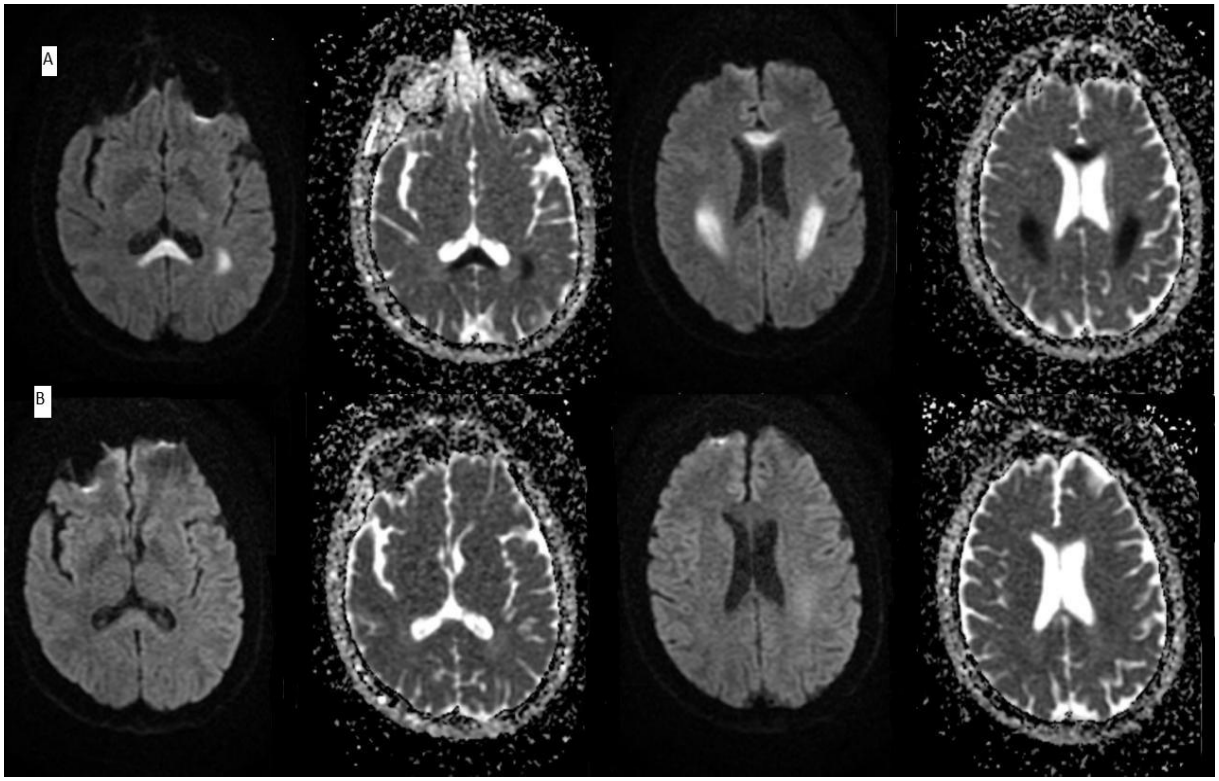

Figure 1. Diffusion-weighted MRI, A: Lesions before treatment, B: Recovery after treatment

A comprehensive ocular assessment including visual acuity, visual field testing, and retinal imaging were integrated into the clinical management of patients.

Laboratory findings were significant for a vitamin B12 level: 229 pg/mL (normal: 200–900 pg/mL), Vitamin D: 12.1 ng/mL (normal: 30–100 ng/mL), Sodium: 141 mmol/L (normal: 135–145 mmol/L), Potassium: 4.33 mmol/L (normal: 3.5–5.1 mmol/L), Calcium: 8.80 mg/dL (normal: 8.6–10.2 mg/dL), TSH: 1.17 µIU/mL (normal: 0.4–4.0 µIU/mL), T3: 3.97 pg/mL (normal: 2.0–4.4 pg/mL), T4: 1.77 ng/dL (normal: 0.9–2.3 ng/dL), an elevated homocysteine level of 38 µmol/L (normal: 5–15

µmol/L),, and thrombocytopenia with a platelet count of 83,000/µL (normal: 150,000–450,000/µL),. Based on the clinical and radiological findings, a preliminary diagnosis of MBD was made, and the patient was admitted to the neurology service for further evaluation and management. EEG revealed diffuse background slowing, although no focal epileptic activity was identified.

The patient was diagnosed with MBD and commenced on intravenous thiamine therapy (100 mg daily for 10 days), followed by a plan for intramuscular maintenance treatment. Aggressive hydration (5000cc/ per day) was administered during hospitalization. While there was marked improvement in speech disturbance, imbalance, nausea, and vomiting as observed on follow-up diffusion MRI 10 days later, the tremors in his hands persisted. Additionally, the patient developed episodes of agitation and intermittent sweating, prompting a psychiatric consultation. Alcohol withdrawal was considered, and the patient was treated with three days of intravenous benzodiazepine (10 mg/day) therapy, followed by oral propranolol, benzodiazepine, alprazolam, and sertraline, with recommendations for outpatient psychiatric follow-up. During hospitalization, serial laboratory evaluations demonstrated a gradual increase in platelet counts. Ten days of post-admission, the neurological examination revealed only mild tremors, slight tandem gait disturbance, and minimal dysarthric speech.

One month later, follow-up diffusion MRI was normal, and FLAIR sequences showed near-complete resolution of the previously observed hyperintensities. Control EEG and laboratory studies were also reported as normal

DISCUSSION

The diagnostic process for acute neurological deficits in chronic alcohol users remains complex, largely due to atypical presentations and incomplete patient histories. In cases such as this, where the patient presented with sudden-onset speech disturbances, motor incoordination, and tremor, the differential diagnosis initially included encephalitis. However, the absence of fever, normal leukocyte counts, and the specific pattern of restricted diffusion observed on MRI redirected the workup toward a metabolic or toxic etiology, ultimately supporting a diagnosis of MBD (1,4,).

MBD is characterized by demyelination and necrosis of the corpus callosum, often extending to adjacent white matter structures. The pathogenesis of this disorder is multifactorial, with chronic alcohol toxicity, nutritional deficiencies (notably thiamine), and metabolic disturbances, such as elevated homocysteine, playing significant roles (5,6). Recent studies indicate that even when serum vitamin B12 levels appear normal, elevated homocysteine levels may reveal underlying metabolic dysfunction that predisposes patients to white matter injury (7,8).

Advanced neuroimaging techniques, particularly diffusion-weighted MRI and FLAIR sequences have enhanced diagnostic accuracy by revealing subtle white matter changes characteristic of MBD. Serial imaging

is essential not only for confirming the diagnosis but also for monitoring the treatment response. Improvements in diffusion abnormalities following early thiamine administration have been consistently associated with better clinical outcomes, emphasizing the critical role of prompt intervention (2,3).

In addition to neuroimaging, comprehensive laboratory evaluation is imperative. Recent literature emphasizes that routine assessments should extend beyond vitamin B12 to include homocysteine measurements, given the latter's association with neurotoxicity in alcohol-related conditions (5). Moreover, studies have revealed a significant correlation between chronic alcohol consumption and thrombocytopenia, suggesting that hematologic parameters can serve as indirect markers of alcohol-induced neurotoxicity (8).

The complexity of MBD necessitates a multidisciplinary approach to patient care. Coordination among neurology, radiology, infectious diseases and psychiatry is crucial, particularly because alcohol withdrawal can further complicate the clinical picture and impede neurological recovery. Current guidelines advocate for early initiation of benzodiazepines and beta-blockers to manage withdrawal symptoms, alongside aggressive nutritional support and thiamine replacement therapy (3,4). Additionally, emerging evidence suggests that adjunctive neuroprotective agents, including antioxidants and agents targeting neuroinflammation, may further enhance recovery and minimize long-term deficits, although more robust clinical trials are needed to validate these approaches (9-11).

Ultimately, early recognition and comprehensive management of MBD can mitigate the risk of permanent neurological sequelae. Future research should focus on establishing standardized diagnostic protocols that integrate advanced neuroimaging, detailed metabolic profiling, and novel therapeutic strategies to optimize outcomes in patients with MBD (10,11).

Considering that methanol consumption may lead to vision loss at the cellular level, it is crucial to emphasize the importance of detailed ophthalmological profiling during both the treatment and follow-up processes. Methanol-induced neurotoxicity, particularly its impact on the optic nerve and retinal cells, may result in subclinical or progressive visual impairment that could go unnoticed without thorough evaluation.

CONCLUSION

In conclusion, early recognition and comprehensive management of MBD are critical in mitigating the risk of permanent neurological sequelae in chronic alcohol users. Integration of advanced neuroimaging with detailed metabolic profiling facilitates accurate diagnosis, while prompt thiamine replacement and supportive care can significantly improve

clinical outcomes. Early detection of alcohol-related visual disturbances may contribute significantly to timely intervention and improved prognostic outcomes. Future research should focus on standardizing diagnostic protocols and exploring novel therapeutic strategies to optimize patient recovery and prevent long-term disability.

Ethics Committee Approval: The presented study is qualitative and consent wasobtained by giving information about the study by one-toone interviews with the subjects who agreed to participate. The study was carried out by paying attention to the Declaration of Helsinki.

Peer-review: Externally peer- reviewed

Author Contributions: Concept: ŞK, Design: ŞK, Data Collection and Processing: ŞK, Analysis and Interpretation: ŞK, Writing: ŞK.

Conflict of Interest: The author declared no conflict of interest.

Financial Disclosure: The authors declared that this study has not received no financial support.

REFERENCES

1. Hillbom M, Saloheimo P, Fujioka S, Wszolek ZK, Juvela S, Leone MA. Diagnosis and management of Marchiafava-Bignami disease: a review of CT/MRI confirmed cases. J Neurol Neurosurg Psychiatry. 2014;85(2):168-173. doi:10.1136/jnnp-2013-305979
2. Liu C, Wang H, Xie B, Tian S, Ding Y. Clinical analysis of Marchiafava-Bignami disease. BMC Neurol. 2024;24(1):389. Published 2024 Oct 14. doi:10.1186/s12883-024-03901-y
3. Lee SH, Kim J, Han C. Low Psychological Resilience Predict the Risk for Alcohol Use Disorder in General Population: National Mental Health Survey of Korea 2021. Clin Psychopharmacol Neurosci. 2025;23(1):53-64. doi:10.9758/cpn.24.1171
4. Xie JY, Li RH, Yuan W, et al. Advances in neuroimaging studies of alcohol use disorder (AUD). Psychoradiology. 2022;2(4):146-155. Published 2022 Nov 24. doi:10.1093/psyrad/kkac018
5. Moretti R, Caruso P. The Controversial Role of Homocysteine in Neurology: From Labs to Clinical Practice. Int J Mol Sci. 2019;20(1):231. Published 2019 Jan 8. doi:10.3390/ijms20010231
6. Jesse S, Bråthen G, Ferrara M, , Keindl, M., Ben-Menachem, E., Tanasescu, R et al. Alcohol withdrawal syndrome: mechanisms, manifestations, and management. Acta Neurol Scand. 2017;135(1):4-16. doi:10.1111/ane.12671
7. Tanner-Smith EE, Cronce JM, Patrick ME, Shirley MC. Brief alcohol interventions for young adults: Strengthening effects,

disentangling mechanisms, and scaling up for impact. Psychol Addict Behav. 2022;36(6):573-580.

8. Martin PR, Singleton CK, Hiller-Sturmhöfel S. The role of thiamine deficiency in alcoholic brain disease. Alcohol Res Health. 2003;27(2):134-142.
9. Pervin Z, Stephen JM. Effect of alcohol on the central nervous system to develop neurological disorder: pathophysiological and lifestyle modulation can be potential therapeutic options for alcohol-induced neurotoxication. AIMS Neurosci. 2021;8(3):390-413. Published 2021 Apr 9. doi:10.3934/Neuroscience.2021021
10. Tian TY, Pescador Ruschel MA, Park S, et al. Marchiafava-Bignami Disease. [Updated 2023 Jul 24]. In: StatPearls [Internet]. Treasure Island (FL): StatPearls Publishing; 2025 Jan-. Available from: https://www.ncbi.nlm.nih.gov/books/NBK526007/
11. Singh S, Wagh V. Marchiafava Bignami Disease: A Rare Neurological Complication of Long-Term Alcohol Abuse. Cureus. 2022;14(10):e30863. Published 2022 Oct 30. doi:10.7759/cureus.30863

Middle Black Sea Journal of Health Science / Mid Blac Sea J Health Sci
August 2025; 11(3): 257-261

CASE REPORT
DOI: 10.19127/mbsjohs.1665455

High-Dose Propafenone Overdoses: A Case with Mortality and Treatment Approaches

Eser Uyanık[1](ID), Ömer Yusuf Erdurmuş[1](ID)

[1]Ordu State Hospital, Ordu, Türkiye,

Received: 15 March 2025, Accepted: 01 May 2025, Published online: 30 August 2025

Abstract

Propafenone is an antiarrhythmic drug used in the treatment of supraventricular and ventricular arrhythmias. Fatal poisoning is rarely described and the number of cases in the literature is quite small. When taken in high doses, it may cause serious rhythm disturbances and death, especially on the cardiovascular system. In this case report, the effect of IV lipid therapy and other treatment modalities in a patient who took high dose propafenone for suicidal purposes is discussed.

We report a case of propafenone overdose in which the patient presented with loss of consciousness, tonic-clonic seizure, and widened QRS complex after ingestion of a high dose of propafenone.

This case highlights the potential for serious cardiotoxicity with propafenone poisoning. Intoxication with sodium channel blockers should be considered in patients with coma, seizures, hypotension, pulseless electrical activity and acidosis.

Early diagnosis and primary detoxification can provide life-saving interventions. However, in cases of late hospital admission and overdose, or suicidal ingestion, the effectiveness of the for mentioned treatments may decrease. Therefore, it is important to recognize the case and keep propafenone poisoning in mind.

Keyword: Cardiotoxicity, poisoning, propafenone.

Suggested Citation: Uyanik E, Erdurmus OY. High-Dose Propafenone Overdoses: A Case with Mortality and Treatment Approaches. Mid Blac Sea Journal of Health Sci, 2025;11(3):257-261.

Address for correspondence/reprints:

Eser Uyanık

Telephone number: +90 (544) 596 56 16

E-mail: dr.eser.uyanik@gmail.com

INTRODUCTION

Propafenone is a 1C antiarrhythmic agent according to the Vaughan Williams classification. It regulates heart rhythm by blocking sodium channels. It is effective in the treatment of paroxysmal atrial fibrillation attacks and life-threatening ventricular

tachycardias (1). When taken in high doses, it may cause serious rhythm disturbances and death, especially on the cardiovascular system(2). Propafenone is highly bound to plasma proteins and IV lipid emulsion, which can be used in treatment, can reduce the unwanted side effects of the drug in the body by creating a lipid compartment. In our country, most of the poisoning cases occur due to suicidal drug overdose(3). In this case report, the effect of IV lipid therapy and other treatment modalities in a patient who took high dose propafenone for suicidal purposes is discussed.

CASE

A nineteen-year-old male patient took 30 tablets of propafenone (Rytmonorm®) 150 mg orally (4500 mg in total) with the intention of committing suicide and was brought to the emergency room by ambulance after his relatives called 112. The exact time of drug intake was not known and the amount taken was estimated by looking at the empty drug boxes. The patient had vomiting and confusion. The vital signs at the time of admission were as follows: body temperature 36.5°C, arterial blood pressure 80/50 mmHg, heart rate 79 beats/minute, respiratory rate 22/minute, peripheral oxygen saturation 97% and Glasgow Coma Score (GCS) 12. Electrocardiography revealed 1st degree AV block and right bundle branch block.

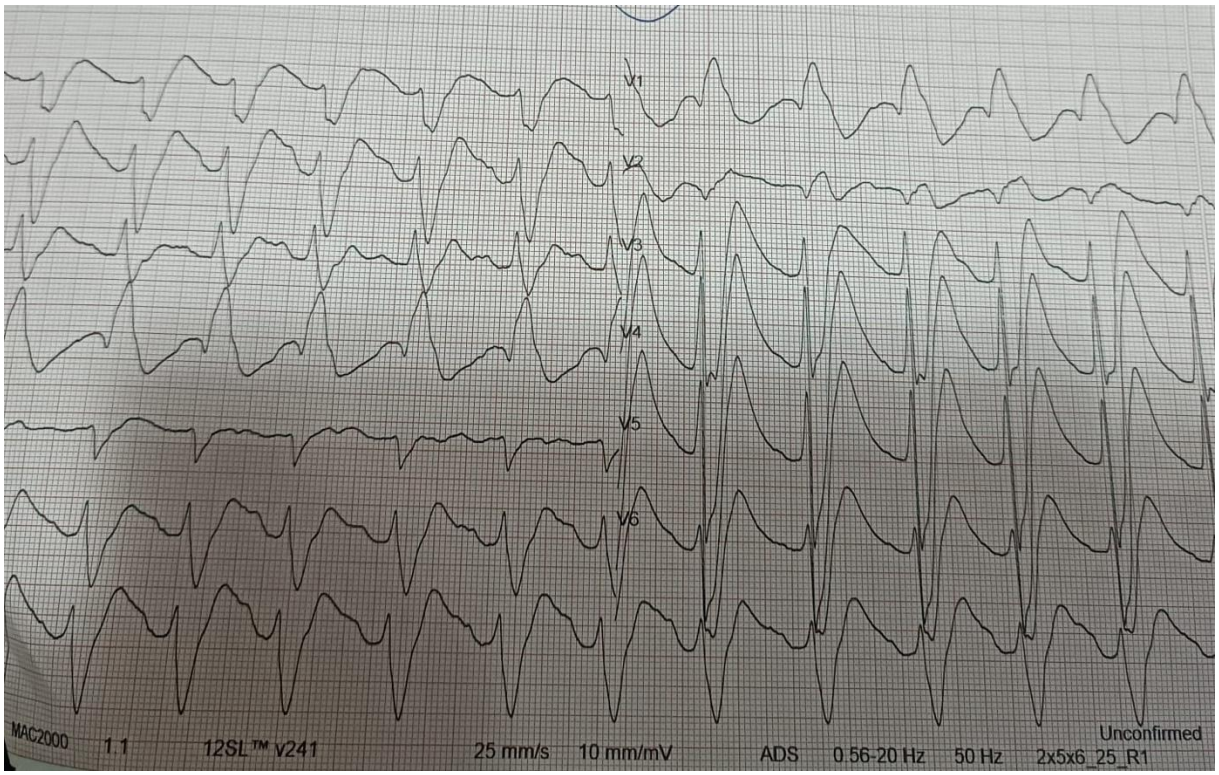

Figure 1. Right bundle branch block and First-degree atrioventricular (AV) block in the ECG of our patient with propafenone intoxication

Spontaneous but irregular and superficial respiration developed 15 minutes after admission, followed by generalized tonic-clonic seizures, which were evaluated as status epilepticus. Therefore, the patient was intubated. Arterial blood gas analysis revealed pH 6.9, PCO_2 65 mmHg, PO_2 40.5 mmHg, HCO_3 12.1 mEq/L, lactate 12.2 mmol/L. Hemogram and biochemistry values were within normal limits. The patient administered IV bicarbonate, neutralized fluid therapy (insulin + dextrose) and calcium gluconate and then transferred to the intensive care unit.

In the intensive care unit, bolus IV 20% lipid emulsion was started at a dose of 1.5 mL/kg on the recommendation of the poison counseling. Despite the addition of high dose inotropic therapy, hypotension and bradycardia persisted, followed by cardiac arrest, and despite advanced cardiac life support, the patient was admitted as an exitus.

DISCUSSION

Propafenone is an antiarrhythmic drug with local anesthetic properties and minor B-adrenergic inhibitory activity. It is commonly used in the treatment of ventricular arrhythmias, supraventricular extrasystole and Wolf-Parkinson-White syndrome (4). The pharmacokinetic profile of the drug varies between individuals. Propafenone is absorbed from the gastrointestinal tract after oral ingestion and metabolized in the liver by cytochrome P450 2D6 isoenzyme. Individual differences in the activity of this isoenzyme due to genetic polymorphisms can markedly affect the bioavailability and elimination of half-life of propafenone (5).

There is no specific antidote for propafenone toxicity. Therefore, patients should be monitored rapidly, and supportive treatment should be provided. In hypotensive patients, fluid support, inotropic treatment, if necessary, should be initiated and airway safety should be ensured. Gastric lavage and activated charcoal administration may prevent excessive drug absorption if performed in the early period. However, in our patient, the exact time of drug intake was not known and activated charcoal treatment and gastric lavage were not administered considering the risk of aspiration because the level of consciousness gradually deteriorated.

Bicarbonate, glucagon, insulin + dextrose, calcium and IV lipid emulsion are used in the treatment of cardiac side effects caused by propafenone. IV lipid emulsion reduces the adverse effects of the drug by creating a separate lipid compartment in the plasma (6). It can also reduce the toxic effects of intracellular drugs at the cellular level. In the literature, it is stated that IV lipid emulsion can be used as rescue therapy in severe poisoning due to lipophilic drugs.

Although the recommended protocols are still controversial, it is generally continued as 1.5

mL/kg bolus followed by 0.25-0.5 mL/kg/min infusion (7). The American College of Medical Toxicology emphasizes that IV lipid emulsion therapy can be used in serious conditions such as cardiac arrest (8). In our case, it was observed that the amount of propafenone taken was one of the highest doses reported in the literature, and it was thought that the effect of IV lipid emulsion treatment was not at the desired level due to late presentation.

Alkaline agents such as bicarbonate are widely used in the treatment of cardiac toxicity associated with sodium channel blockers. These agents inhibit the binding of sodium channel blockers to sodium channels by raising intracellular pH, thereby reducing cardiac depression. Bicarbonate therapy has an important role in reducing cardiac side effects due to propafenone toxicity. In our case, volume loading, inotropic support and sodium bicarbonate therapy were applied.

Severe cardiovascular and neurological complications such as coma, hypotension, metabolic acidosis, generalized tonic-clonic seizures, cardiac arrest and pulseless electrical activity (PEA) may develop at toxic doses of propafenone (9). These findings reveal that the clinical picture of our patient shows a typical similarity with the cases described in the literature.

CONCLUSION

Intoxication with sodium channel blockers should be considered in patients with coma, seizures, hypotension, pulseless electrical activity and acidosis. Bicarbonate treatment is of vital importance in this type of poisoning. Although there is no specific treatment for propafenone intoxication, IV lipid emulsion therapy can be used as a life-saving option and is known to increase the survival rate. However, early diagnosis and primary detoxification are of great importance for the efficacy of treatment. In cases of late hospital admissions and overdose, the efficacy of current treatments may decrease. In our case, the amount of propafenone ingested was one of the highest doses reported in the literature. This situation reveals once again the vital importance of early intervention.

Acknowledgements: We would also like to thank all emergency medicine and intensive care workers who helped in the preparation phase of the case to add it to the literature, and the patient's parents who gave permission for its publication.

Ethics Committee Approval: The presented study is qualitative and consent wasobtained by giving information about the study by one-toone interviews with the subjects who agreed to participate. The study was carried out by paying attention to the Declaration of Helsinki.

Peer-review: Externally peer- reviewed

Author Contributions: Concept: EU, OYE, Design: EU, OYE, Data Collection and Processing: EU, OYE, Analysis and Interpretation: EU, OYE, Writing: EU, OYE,

Conflict of Interest: The author declared no conflict of interest.

Financial Disclosure: The authors declared that this study has not received no financial support.

REFERENCES

1. Polat N. Cardiac arrest secondary to propafenone overdose. Dicle Med J Dicle Tip Derg. 2014;41(3):611–3.
2. Bayram B, Köse I, Avcı S, Arslan A, Acara Ç. Successful Treatment of Propafenone Intoxication with Intravenous Lipid Emulsion. Pharmacother J Hum Pharmacol Drug Ther. 2015;35(10):e149–52.
3. Sönmez E. Evaluation of intoxication cases admitted to Emergency Department of a University Hospital. Dicle Med J Dicle Tip Derg. 2012;39(1):21–6.
4. Oates JA, Wood AJJ, Funck-Brentano C, Kroemer HK, Lee JT, Roden DM. Propafenone. N Engl J Med. 1990 Feb 22;322(8):518–25.
5. Üstündağ M, Orak M, Güloğlu C, Özhasenekler A, Durgun HM. Lethal toxicity of propafenone in a case of suicidal attempt. Turk J Emerg Med 2007;7(3):132-135.
6. Jacob J, Heard K. Second case of the use of intravenous fat emulsion therapy for propafenone toxicity. Clin Toxicol. 2011;49(10):946–7.
7. Temiz S, Akelma H, Kaçar CK, Uzundere O, Kaya S, Yektaş A. Intravenous Lipid Emulsion Treatment After High Dose Propafenone Intake for suicide: Case report. J Cardio-Vasc-Thorac Anaesth Intensive Care Soc. 2019;25(3):202–5.
8. American College of Medical Toxicology. ACMT Position Statement: Interim Guidance for the Use of Lipid Resuscitation Therapy. J Med Toxicol. 2011;7(1):81–2.
9. Stancak B, Markovic P, Rajnic A, Petrikova V. Acute toxicity of propafenone in a case of suicidal attempt. Bratisl Lek Listy. 2004;105(1):14–7.

Middle Black Sea Journal of Health Science / Mid Blac Sea J Health Sci
August 2025; 11(3): 262-267

CASE REPORT
DOI: 10.19127/mbsjohs.1665455

From Clinical Suspicion to Diagnosis: A Case Report of Three Siblings Diagnosed with Scarlet Fever at a Family Health Centre

Dilara Canbay Özdemir[1](ID), İzzet Fidancı[1](ID)

[1]Ankara Pursaklar District Health Directorate, Ankara, Türkiye
[2]Hacettepe University Faculty of Medicine, Department of Family Medicine, Ankara, Türkiye

Received: 16 April 2025, Accepted: 29 May 2025, Published online: 30 August 2025

Abstract

Scarlet fever is an eruptive disease caused by *Streptococcus pyogenes* and is particularly common in children. It highlights the importance of the role of general practitioners in the rapid diagnosis and treatment of scarlet fever. The diagnosis was made based on clinical findings, characteristic rashes, and strawberry tongue, and appropriate antibiotic treatment was started. The course of the cases and the initial assessment at the family health center demonstrate the need for recognition of scarlet fever in primary care to prevent complications and community transmission through early intervention. In this case, the holistic perspective of family doctors in primary care, diagnosis, treatment, and follow-up processes with multidisciplinary thinking are discussed through the cases of scarlet fever developing simultaneously in siblings living in the same house.

Keyword: Scarlet fever, *Streptococcus pyogenes*, rash, family practice

Suggested Citation: Canbay Ozdemir D, Fidancı I. From Clinical Suspicion to Diagnosis: A Case Report of Three Siblings Diagnosed with Scarlet Fever at a Family Health Centre. Mid Blac Sea Journal of Health Sci, 2025;11(3):262-267.

Address for correspondence/reprints:

Dilara Canbay Ozdemir

Telephone number: +90 (538) 814 79 57

E-mail: dilara.canbay7@gmail.com

INTRODUCTION

Scarlet fever (scarlatina) is a contagious, acute illness brought about by group A beta-hemolytic streptococcus (*Streptococcus pyogenes*) that appears mostly in children between 5 and 15 years of age. Scarlet fever is spread by droplets of respiratory secretions and is quickly transmitted where human contact is close, e.g., schools and daycare centers (1, 2). Clinically, the illness begins with the acute onset of fever, pharyngitis, diffuse erythematous rash with a sandpaper feel, and classic "strawberry tongue." The rash usually initiates in the axillary, cervical, and thoracic areas and generalizes later (3).

Pathogenesis is largely mediated through erythrogenic exotoxins elaborated by the bacteria, causing the rash and systemic symptoms. Diagnosis is usually clinical but may be augmented by rapid antigen detection testing (RADT) or throat culture. Treatment with antibiotics and diagnosis early enough are significant to avoid complications like acute rheumatic fever and post-streptococcal glomerulonephritis (4, 5).

In the past several years, there has been a recent resurgence in the number of scarlet fever cases in countries like the United Kingdom and China, once again highlighting the epidemiological significance of this infection in children (6, 7). Family medicine practitioners and other primary care doctors must consider scarlet fever when making a differential diagnosis of febrile rash illness in a child. Moreover, collective screening of family members can also help in the identification and control at an early stage.

This article reports two concurrent pediatric cases of scarlet fever in siblings living in the same home. With these cases, we would like to highlight diagnostic, therapeutic, and follow-up strategies relevant to family practice.

CASE

Two girls, aged five and seven, presented themselves at a family health center, having experienced symptoms including sore throats and fevers. The two developed the symptoms two days before coming to the clinic, the child aged five years, and five days before the one aged seven. Both had fevers ranging from 38°C, based on parents' reports at home. Both children's medical histories were uneventful, without any chronic illnesses or ongoing medications known. They both had complete and up-to-date vaccination schedules. It was noted that the seven-year-old had attended a dermatology outpatient department before for the rash and had received valacyclovir and a topical preparation. Not having improved, she re-presented to dermatology three days ago and was prescribed another topical preparation. On further questioning, it was found that the children's 12-year-old brother was also complaining of a sore throat. Tonsillitis was found on examination, but this patient did not have strawberry tongue or a rash.

Physical examination revealed bilateral tonsillar enlargement with exudates, blanching papular rashes on the trunk and back, and classic "strawberry tongue" in both patients (Figure 1A-B). Systemic examination findings were within normal limits.

Both children were prescribed a ten-day course of oral amoxicillin, and home isolation was recommended. Clinical improvement and symptom resolution were confirmed in all cases by phone follow-up.

Figure 1. Strawberry tongue appearance in two pediatric patients with scarlet fever. (Figure 1A is the tongue of a 7-year-old patient, and Figure 1B is that of a 5-year-old sibling.). Both tongues have diffused erythema and hypertrophic, enlarged papillae—changes that are pathognomonic for scarlet fever and are manifestations of streptococcal toxin-mediated inflammation

DISCUSSION

Scarlet fever, which is induced by Group A Streptococcus (GAS), is an extremely infectious, toxin-mediated disease that mostly affects children aged 5 to 15 years. In spite of efficacious antibiotics, the disease still generates outbreaks and is a public health issue because it has a high potential for transmission and also due to its complications, such as acute rheumatic fever and post-streptococcal glomerulonephritis (1, 2).

Its classic clinical presentation—fever, pharyngitis, "strawberry tongue," and disseminated, blanching erythematous rash—is still a useful clinical diagnosis criterion, especially in regions where laboratory facilities are lacking (4).

In the present case series, two siblings presented together with classical symptoms and characteristic exanthema. The common household and simultaneous onset of symptoms heavily suggest intrafamilial transmission, highlighting the infectious character of the disease and the risk of outbreaks in closed populations such as families, schools, and kindergartens. This argues in favor of early recognition and reporting, particularly in primary care, where such clusters usually first become evident. What is most educative in this series of cases is the fact that one of the children was first misdiagnosed in a dermatology clinic, the rash being given a viral or allergic etiology. This is actually typical of a common clinical pitfall: under-recognition of scarlet fever as part of the differential diagnosis of childhood exanthems, particularly in a setting where streptococcal infections are not deemed as frequent or in the instance of incomplete presentation. These delays in diagnosis not only lengthen the illness course but also allow continued transmission both within households and in the community.

Such examples highlight the invaluable function of the primary care clinicians, who are best placed to discern patterns among family members and relate individual presentations to more generalized epidemiological hints.

The contextual and holistic evaluation that family medicine promotes is particularly useful in identifying diseases that may present insidiously or variably in different people. In this instance, having the ability to observe a

number of siblings within the same clinical umbrella provided us with a composite view that allowed for earlier diagnosis and intervention. In addition, in resource-limited settings in which laboratory testing (i.e., throat culture or rapid antigen detection) is not available or is delayed, the importance of careful physical examination and clinical judgment becomes even more essential. Knowledge of classic findings like Pastia's lines, convalescent desquamation, or the sandpaper rash can significantly enhance clinical judgment.

From a public health perspective, the cases also point to the value of heightened surveillance and education in communicable childhood diseases. Though scarlet fever's incidence has fallen spectacularly since pre-antibiotic days, recent years have seen episodic recrudescence in a number of regions, implicating either shifting bacterial virulence or lapses in herd immunity (5). Primary care systems must therefore remain vigilant and responsive. Prompt notification to the public health authorities and proper education of the family can restrict the spread and reduce complications.

Finally, this series of cases shows the value of integrative and multidisciplinary thinking in the setting of primary care. Integrating environmental, family, and clinical variables at the same time and having a high level of suspicion allowed for intervention early on. Not only is such a treatment better for individuals, but it also serves to safeguard the larger community. In summary, scarlet fever remains a diagnostic and public health challenge. General practitioners are well placed to identify outbreaks, initiate early treatment, and institute preventive measures. In the event of potential re-emergence of the disease, rededication to conventional clinical competence, situational awareness, and early intervention is essential to the successful control of the disease.

CONCLUSION

Scarlet fever carries a good prognosis if diagnosed and treated early and adequately; otherwise, it may lead to severe complications if not treated. As is evident from the case, primary care clinicians play a central role in diagnosing and treating these everyday childhood infective illnesses early.

Family medicine is practiced using a holistic approach that extends beyond personal symptoms, including family, environmental, and societal factors. In this instance, the concurrent examination of two siblings and consideration of the family background permitted the prompt diagnosis and instituting of therapy in a timely fashion.

In addition, careful and methodical physical examination was found to have characteristic rash findings not previously noted in other practice settings. This confirms the importance of physical examination and clinical skills in family medicine.

Finally, this case series illustrates the essential role of the family doctor in the prevention, diagnosis, and management of infectious illness via a holistic and patient-centered approach. A practice of diligent physical examination and contextual assessment improves diagnostic precision in pediatric exanthems and also minimizes unnecessary referral and complication risk.

Ethics Committee Approval: This case report was conducted in accordance with the principles of the Declaration of Helsinki. Written informed consent was obtained from the patient for the publication of this case report and any accompanying images. Ethical approval was not required for this single-patient case report in accordance with institutional policies.

Author Contributions: Concept: DCO, Design: DCO, Data Collection and Processing: DCO, Analysis and Interpretation: DCO, IF, Writing: DCO, IF.

Conflict of Interest: The authors declared no conflict of interest.

Financial Disclosure: The authors declared that this study has not received no financial support.

REFERENCES

1. Pardo S, Perera TB. Scarlet fever [Internet]. In: StatPearls. Treasure Island (FL): StatPearls Publishing; 2025 Jan– [updated 2025 Feb 6; cited 2025 May 25]. Available from: https://www.ncbi.nlm.nih.gov/books/NBK507889/
2. Centers for Disease Control and Prevention (CDC). Scarlet Fever [Internet]. [cited 2025 Apr 15]. Available from: https://www.cdc.gov/group-a-strep/about/scarlet-fever.html
3. Managing scarlet fever. Drug Ther Bull. 2017;55(9):102. https://doi.org/10.1136/dtb.2017.8.0529
4. Guy R, Williams C, Irvine N, Reynolds A, Coelho J, Bennett E, et al. Increase in scarlet fever notifications in the United Kingdom, 2013/2014. Euro Surveill. 2014;19(12):20749. doi:10.2807/1560-7917.ES2014.19.12.20749
5. Public Health England. Guidelines for the public health management of scarlet fever outbreaks in schools, nurseries and other childcare settings [Internet]. 2017 [cited 2025 Apr 15]. Available from: https://www.gov.uk/government/publications/scarlet-fever-managing-outbreaks-in-schools-and-nurseries
6. Lamagni T, Guy R, Chand M, Henderson KL, Chalker V, Lewis J, et al. Resurgence of scarlet fever in England, 2014–16: a

population-based surveillance study. Lancet Infect Dis. 2018;18(2):180–7. https://doi.org/10.1016/S1473-3099(17)30693-X

7. Wu R, Xiong Y, Wang J, Li Y, Zhang X, Liu H, et al. Epidemiological changes of scarlet fever before, during and after the COVID-19 pandemic in Chongqing, China: a 19-year surveillance and prediction study. BMC Public Health. 2024;24:2674. https://doi.org/10.1186/s12889-024-20116-5

Middle Black Sea Journal of Health Science / Mid Blac Sea J Health Sci
August 2025; 11(3): 268-283

REVIEW
DOI: 10.19127/mbsjohs.1527654

Basic chromosome definitions and staining techniques

Nihan Küçük Yılmaz[1(ID)], Ceren Börçek Kasurka[1(ID)], Yasemin Esin Aydın[1(ID)], Aleyna Kaya[1(ID)]

[1]Yalova University, Faculty of Medicine, Department of Medical Pharmacology, Yalova, Türkiye
[2]Ordu University, Faculty of Arts and Sciences, Molecular Biology and Genetics, Ordu, Türkiye

Received: 18 December 2024, Accepted: 12 January 2025, Published online: 30 August 2025

Abstract

The essential molecules that preserve genetic information, control expression, and guarantee accurate and complete transfer are chromosomes. Any disruption in any of these stages will also be reflected in the organism. Therefore, understanding the "normal" of chromosomes—such as normal packing or normal separation—is crucial for identifying the root causes of disorders.

From a health sciences perspective, identifying the relationship between chromosomes and disorders is the first step toward diagnoses, advanced research for numerous diseases, and even treatment recommendations. While more complicated, quick, and accurate methods have emerged due to methodological developments, traditional chromosomal approaches continue to be the most important and innovative in many labs.

In the context of all mentioned above, this review gives a general overview of the packaging and classification of eukaryotic chromosomes as well as the grouping of human chromosomes. It also presents the basic concepts underlying the G, C, Q, R, and T banding and NOR staining techniques and discusses their consequences for human chromosomes.

Keyword: banding techniques, chromosome structure, chromosome classification

Suggested Citation: Kucuk N, Borcek Kasurga C, Esin Aydin Y, Kaya A. Basic chromosome definitions and staining techniques. Mid Blac Sea Journal of Health Sci, 2025;11(3):268-283.

Address for correspondence/reprints:

Nihan Küçük

Telephone number: +90 (530) 322 22 52

E-mail: nihankucuk55@gmail.com

INTRODUCTION

Basic Definitions

Chromosomes are the genetic units that provide heredity in living organisms so that they can continue their vital activities and pass on their genetic material to future generations. Chromosomes can be observed most clearly and stably during metaphase. Karyotyping is performed with chromosomes obtained from the metaphase stage using chemicals such as colchemid, which inhibit spindle threads to stop cells in the metaphase of mitosis and to collect mitotic cells. Molecular techniques have been developed to compare the karyotypes of different species. Although there are many techniques for chromosomal identification and karyotype preparation for clinical research, the length of the chromosomes and their degree of fixation, spreading, and staining determine their analysis potential. Depending on the state of all these parameters, abnormalities and polymorphisms on the chromosomes can be identified.

The word "chromosome" is a combination of the Greek words kroma (colour) and soma (body). Chromosomes were first observed by the German botanist Wilhelm Friedrich Benedikt Hofmeister in the dividing pollen mother cells of the plant Tradescantia and named by the German anatomist Heinrich Wilhelm Gottfried von Waldeyer (1-4). Genes, which carry the information that customizes all the proteins that make up an organism, are the most significant function of DNA. This genetic information includes which cells make which proteins, when and in what quantities. In the cell nucleus, eukaryotic DNA is separated into several chromosomes. An extremely long linear DNA molecule and proteins that encase it in a denser structure make up each chromosome. The term "chromatin" refers to this complex. Chromosomes are linked to numerous proteins involved in gene expression, DNA replication, and DNA repair in addition to the proteins involved in DNA packing (Fig. 1). During the interphase of cell division, DNA condenses and replicates (5).

Each of the two copies of DNA synthesized during cell division, packaged with a protein complex and anchored together by a centromere, is called a "chromatid". Each chromosome has two chromatids. "Sister chromatids" is the term for these. Sister chromatids are split apart and dispersed into two new nuclei during the later phases of cell division (6).

From the prophase stage of cell division, the long chromatin thread folds back on itself, shortening its length and increasing its diameter to become metaphase chromosomes. These chromosomes differ in number and shape from organism to organism. In most living organisms, the number of chromosomes varies between 12 and 50. There is no connection between the high number of chromosomes and the development of the organism. In the

reproductive cells of developed plants and animals, there is only one copy of each chromosome. This number of chromosomes is called "haploid chromosome number" and is represented by the letter "n" (5).

Somatic cells, which are body cells other than reproductive cells and a few specialized cell types, have two of each chromosome. These chromosomes are referred to as "homologous chromosomes" since one comes from the mother and the other from the father. The even number of chromosomes is called "diploid chromosome number" and is shown as "2n".

The chromosomes in the somatic cells of diploid organisms, which are similar in shape, are autosomes. These chromosomes carry genes that determine the hair colour, blood type, etc. of the organism. Gonosomes are chromosomes whose shapes can be the same or different depending on the sex of the organism. Gonosomes carry the genetic information that determines the sex of the organism and regulates its developmental process. When specifying the number of chromosomes of a living organism, autosomes are specified by number. Gonosomes are represented by letters such as "X" and "Y". Although the number of chromosomes that make up the genomes of eukaryotes varies widely, the way they are packaged is similar (7).

The DNA macromolecule is surrounded by basic proteins called histones. In this way, structures called "nucleosomes" are formed, which are subunits of chromatin. There are two types of histones: core and linker histones. Core histones are well-conserved proteins with a molecular weight of 11,000-16,000 Da. Linker histones are more variable proteins with a molecular weight of just over 20,000 Da. The core histones are H2A, H2B, H3 and H4, two of each; the linker histone is H1. 142 hydrogen bonds are formed at the junction of the histone core and DNA in each nucleosome. Between the phosphodiester backbone of DNA and the amino acid backbone of histones, around half of these linkages occur. In the nucleosome, a variety of salt bridges and hydrophobic interactions maintain DNA and protein together. Furthermore, the amino acids arginine and lysine are abundant in all histones. The positive charge of these amino acids converts the negative charge of the DNA backbone into neutral (4, 8-10).

Karyology is the branch of science that deals with studies on cell genetics. The term karyotype encompasses the number, size and morphology of chromosomes of an organism and even other distinguishing features (11, 12). In other words, karyotype is the ordering of metaphase chromosomes of a species according to their shape, size and appearance. Karyotype researches are performed in tissues and cells in which mitosis is observed, that is, tissues and cells that can actively reproduce. Karyotype analysis can be used to determine the number of chromosomes of a species, the sex

chromosomes of some species, the similarities and differences between the same species and different species, and the diagnosis of chromosomal diseases (13). Some researchers state that the formation of new species in animals as a result of karyotype changes occurs as a result of morphological rearrangement of chromosomes or quantitative changes in heterochromatin (14). Accordingly, the two measurable and identifiable characteristics of a chromosome are chromosome length and centromere index. Within the length of the chromosome, the characteristics evaluated are the centromere index, the arm length and the relative length of the chromosome. While centromere index (CI) and arm ratio provide information about the size of the chromosome itself, relative length describes the size relationship of the chromosome with other chromosomes (15, 16).

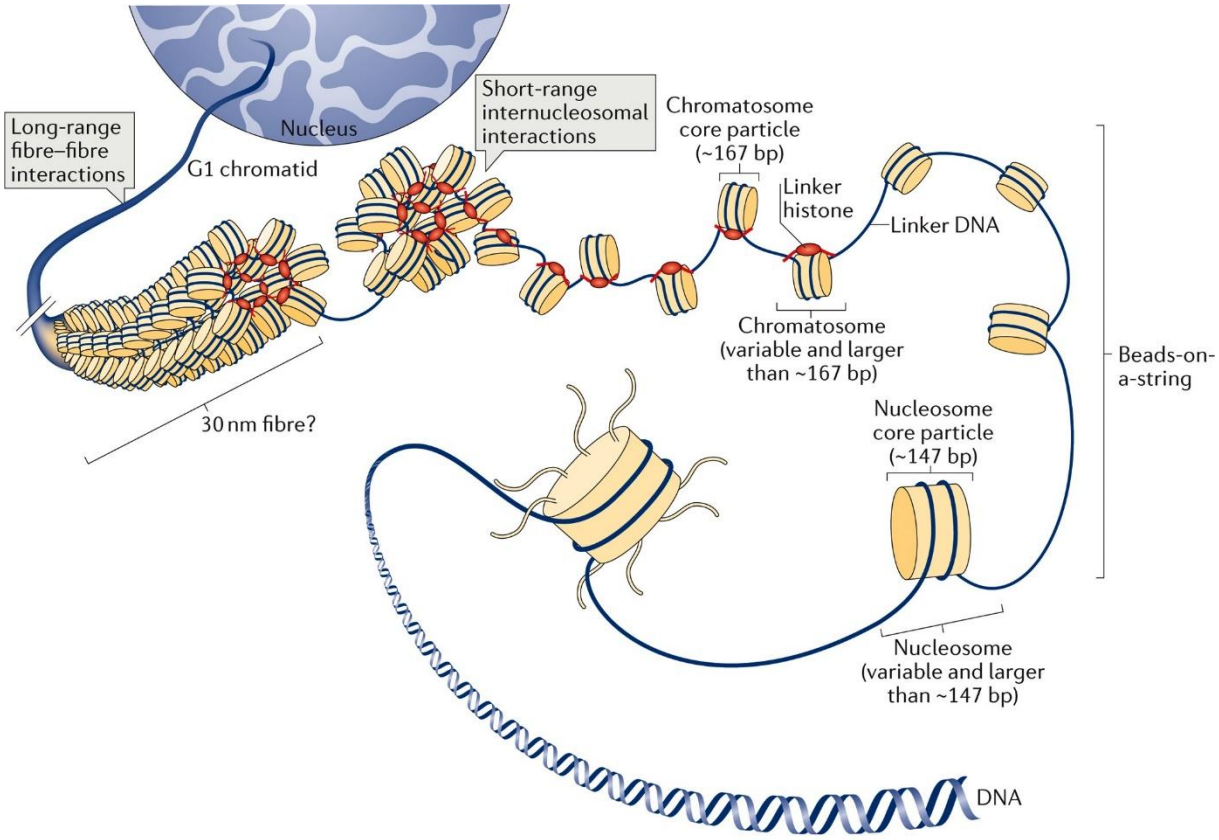

Figure 1. Chromatin packing stages (10).

Ultrastructure Of Chromosomes

An individual's chromosome morphology includes the number of chromosomes in the set, their relative lengths, arm ratios, secondary constriction, the position of NOR and satellite regions, and differences in euchromatin and heterochromatin bands. Chromosome morphology can vary according to the stages of cell division. The outer parts of chromosomes consist of chromosome arms, centromere, telomere, secondary constriction, satellitic DNA and kinetochore. The inner parts consist

of chromonema, chromomeres, matrix and pellicle. Chromonemata are chromatin strands embedded in the matrix, folded into two coiled spirals, which can be seen in early prophase and sometimes in interphase. Each chromatin strand contains about eight microfibrils of double-stranded DNA. These fibrils are tightly wound together. These coils are of two types, "paranemic" and "plectonemic". Paranemic coils are formed if the chromonemal fibrils are easily separable; plectonemic coils are formed if they are tight and intertwined and cannot be easily separated (17, 18). The loop, granular or bead-like structures arranged vertically in a single row along the chromoneme are called "chromomeres". Chromomeres carry genes on them during inheritance and can synthesize or accumulate their nucleic acids or nucleoproteins (19, 20). The gel-like, colourless structure of achromatic material covering the chromonema is called the "matrix". The matrix acts as a sheath that isolates genes during cell division. On the matrix is a thin membrane called a "pellicle" (21).

The chromosome region in the primary constriction that binds sister chromatids together and also helps the kinetochore, a disk-shaped protein complex that allows the spindle threads to attach to the chromosomes during cell division and thus separate the sister chromatids from each other, to come together is called the centromere. A complete kinetochore can consist of 80 or more proteins. Subcomplexes of these proteins in the kinetochore are involved in microtubule attachment, microtubule polymerization and motor-directed movements. Other kinetochore proteins are part of the microtubule checkpoint that allows cells with correctly assembled spindle threads to pass into anaphase (22, 23). The specialized DNA sequences at the ends of eukaryotic chromosomes are called "telomeres". Telomeres are composed of simple, short repeated nucleotide sequences. These sequences prevent the end-to-end splicing of chromosomes and ensure that the chromosome ends replicate correctly without shortening during cell division (24, 25). The region of the chromosome where the nucleus is formed and where random repeats of the gene sequence responsible for rRNA synthesis are found is called "NOR"; the nucleolar organising region. The constriction, usually located in the NOR and sometimes associated with satellitic DNA, is called the "secondary constriction (26, 27). The heterochromatic chromosome end region, located beyond the secondary constriction, with very short, round or elongated, satellite-like spheres attached to one arm of the chromosome, is called "satellite DNA". This structure is attached to the chromosome's main body by a thin chromatin thread. Chromosomes carrying this structure are called "SAT chromosomes". In addition, a chromosome contains highly dense

heterochromatin dark-coloured chromatin regions that prevent transcription, which is gene translation, and less dense, light-coloured euchromatin regions that enable gene expression (28) (Figure 2).

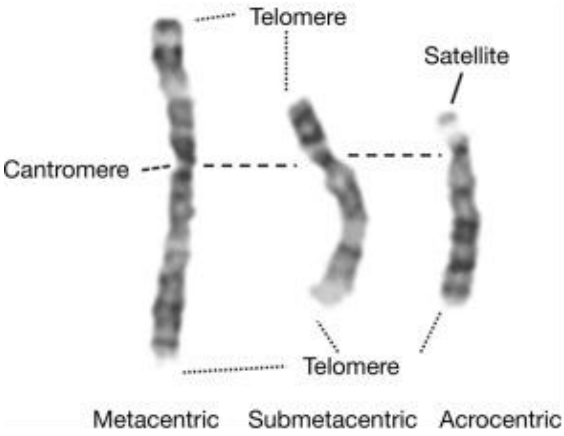

Figure 2. A human chromosome (29)

Classification of Chromosomes:

Chromosomes can be classified as monocentric, dicentric and polycentric according to the number of centromeres (5). Monocentric chromosomes are also analyzed in four classes according to the position of their centromeres. Metacentric chromosomes with the centromere in the middle, acrocentric chromosomes with the centromere near one end, telocentric chromosomes with the centromere at one end, and submetacentric chromosomes with the centromere between the middle and the end of the chromosome but closer to the middle. The chromatids on either side of the centromere are chromosome arms (27, 30) (Figure 3).

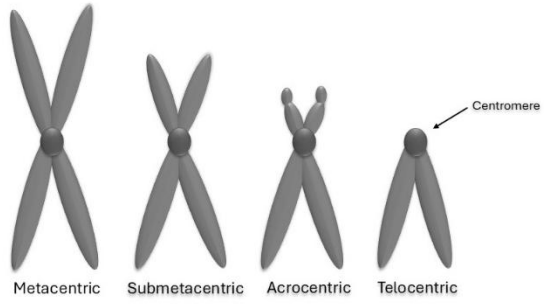

Figure 3. Chromosome classes

Staining and Banding of Chromosomes

After the chromosome preparations obtained from various tissues of the animals are stained with standard Giemsa staining, C-banding and other staining techniques such as NOR banding, the best quality metaphase plates are photographed under a microscope and transferred to the computer. For chromosome measurements (shape, length, arm length, NF value, etc.) and karyotype analysis, the metaphase photographs transferred to the computer are organized using various special software. In a diagram called an ideogram, the numbers of the chromosomes of the karyotype and their statistical values, such as length, and short and long arm values, are generated. Visually, the karyotype presentation can be done in different ways. Simply and manually, metaphase chromosomes are photographed where the chromosomes are clearly visible. The chromosomes in this photograph are cut and matched on paper. Karyotype arrangement can be done in various ways. First, chromosomes can be grouped according to centromere location (metacentric, submetacentric, etc.) and then they can be arranged in order of size. If desired, the chromosomes can be arranged on a line from largest to smallest with the same centromere alignment. In general, the karyotype of organisms with sex chromosomes is made so that the sex chromosomes are placed last (31-33). The most widely used methods for chromosome identification (karyotyping) are

G-and R-banding, which can be used to detect deletions, inversions, or amplifications of chromosome segments, as well as irregularities in the number of chromosomes and material translocations across chromosomes. This has significantly influenced human genetics and medicine (34). Depending on the staining technique used, the bands may have a light colour in one method and a dark colour in another method.

Banding techniques are divided into two basic groups:

i. Staining techniques in which the entire chromosome appears as light and dark bands. G, Q & R banding techniques listed among this group

ii. Techniques that stain specific bands or structures on the chromosome C, T and Nor banding techniques listed among this group.

Standard Giemsa Staining and G-Banding:

The G banding technique was introduced in 1971 and is now widely used in clinical cytogenetic laboratories. The Giemsa staining technique was first used by the chemist Gustav Giemsa for the pathologic identification of the malaria parasite and later modified for the staining of Treponema pallidum (35, 36). Giemsa is a dye that binds DNA by intercalation when exposed to visible light. Compared to fluorochromes, visible light dyes are more stable and can create more distinct bands. Anionic eosin dyes like eosin Y and cationic thiazine dyes combine to form Giemsa stain. Two molecules of the same chemical swiftly intercalate into the negative DNA molecule and stain it blue because the positive thiazine dye molecules are smaller. After binding the two thiazine molecules, the anionic eosin molecule gives the DNA a purple stain. Giemsa more effectively stains hydrophobic areas (37, 38).

Some researchers have used different properties of giemsa staining in their studies on mouse chromosomes. In the method, histone and nonhistone proteins are denatured with trypsin and Giemsa is introduced into the regions of DNA rich in Adenine-Thymine bases and containing several active genes that replicate late in the S phase. These darkly stained regions are called heterochromatin. The lightly stained regions are euchromatin regions rich in Guanine-Cytosine bases containing a large number of active structural genes. In this technique, 400-550 light and dark bands specific to each chromosome pair can be seen and any structural irregularity (5-10 mb) can be identified by deviations in the band characteristics specific to that chromosome (39, 40).

Constitutive chromatin banding; C-Banding

Constitutive chromatin or C-banding was discovered by Heitz in 1928 and is characterized by dark regions in the interphase nucleus. The DNA of heterochromatin regions on the chromosome or nucleus is tightly

packed. The darker regions are called heterochromatin and the lighter regions are called euchromatin. Euchromatin is low in density, accessible and usually more easily transcribed, whereas heterochromatin is typically highly condensed, inaccessible and ordered by nucleosomal sequences. Constitutive chromatin or C-banding was discovered by Heitz in 1928 and is characterized by dark regions in the interphase nucleus. The DNA of heterochromatin regions on the chromosome or nucleus is tightly packed. The darker regions are called heterochromatin, and the lighter regions are called euchromatin. Euchromatin is low in density, accessible and usually more easily transcribed, whereas heterochromatin is typically highly condensed, inaccessible and ordered by nucleosomal sequences. Heterochromatin blocks (C-bands) contain repetitive DNA sequences and are inactive. Therefore, these blocks are unlikely to be degraded and can be preserved for generations. Although C-bands are present across the chromosome, they are most frequently seen in the centromere region. Chromatin is treated with acidic and basic solutions, followed by Giemsa staining, to create C-banding. The main applications of C-banding are in the research of chromosomal polymorphisms in the population and in assessing the gene coding capacity of different genome segments, particularly in the presence of small marker chromosomes of unknown origin. This technique has little value in clinical laboratories. In healthy people, the majority of the long arm of the Y chromosome, pericentric heterochromatin, and the short arms and satellites of acrocentric chromosomes are C-band positive, devoid of active genes, and vary in size. The C-banding method is also an important technique for taxonomic studies, the detailed study of species chromosomes, chromosomal species identification, and the identification of the sex chromosomes of a species

(41-44).

Silver Staining; NOR Staining

In the 1930s, Heitz and then McClintock observed that the less dense regions of mitotic chromosomes have a numerical relationship in terms of the number and length of secondary constrictions, and today the size and constrictions of these regions are referred to as the nucleus organizing region or NOR. Until the 1960s, the precise function of the NOR was not clear until it was realized that it contains genes encoding 18S, 5.8S and 28S ribosomal RNAs. It was later recognized that the nucleolus is the most prominent structure in the nucleus of a cell, and is involved in different functions such as ribosomal RNA (rRNA) transcription, rRNA preprocessing and regulation of ribosome subunits. Contrary to the general acceptance that the nucleolus was considered only as the anatomy of the nucleus, the naming of the nucleolus as the cytological expression of gene

action in the early 1960s was considered a major breakthrough in cytogenetics. NOR regions are heterochromatin regions and due to their light refractive properties, chromosome preparations can be prepared and NORs can be visualized rapidly and clearly by ammonia or formic acid silver nitrate staining. Silver staining (Ag-NOR) is the reaction in which silver is reduced as a result of the binding of non-histone proteins to ionic silver. In humans, NORs are found on the short arms of chromosomes; chromosomes 13, 14, 15, 21 and 22. However, the long arm can also be found close to the centromere or in the centromere region. The NOR technique is used in taxonomic studies, determination of intraspecific and interspecific relatedness and various chromosome variations. In the determination of interspecific heteromorphism, the absolute number of NORs in the genome and the position and localization of NORs in the chromosome are evaluated, while in the evaluation of intraspecific heteromorphism, NOR size and the distribution of active NORs in the cell are taken into account (45-47).

Quinacrine bandin; Q-Banding

It is the first technique to determine Adenine-Thymine rich regions in the chromosomes, in the late 1960s. Metaphases stained with Fluorochrome dyes such as quinacrine mustard (quinacrine) and dihydrochloride quinacrine (atebrin) and examined under fluorescence microscopes show regions consistent with the bands in the G banding technique. G banding Chromosomes and the Y chromosome and the centromeric regions of chromosomes 1, 9 and 16 and centromere and satellite regions of acrocentric chromosomes and Y chromosome variations because it allows for the evaluation of chromosome variations. Used to identify heteromorphisms (48-50).

Reverse Banding ;R-Banding

Since the method stains the Guanine-Cytosine-rich regions of DNA, the reverse staining of the G and Q banding technique occurs. In other words, dark-stained regions in G and Q banding are observed as light in R banding and light-stained regions are observed as dark. In fluorescent R banding, R bands are observed in yellow-green colour. R-banding is used to detect terminal region anomalies (irregularities larger than 2-3 Mb in the telomere regions) of chromosomes that are difficult to detect with G-banding techniques. Theoretically, R-bands can highlight gene-rich chromatin, which makes it easier to identify subtle structural changes in the regions of the genome that are most likely resulting in phenotypic abnormalities (51).

Telomere banding; T-Banding:

A method based on the staining of telomeres, the structures at both ends of chromosomes that keep the chromosome ends closed and thus stable, preventing chromosomes from joining end-to-end to form dicentric or ring

chromosomes. After chromosomes are incubated at 87°C in a phosphate or PBS buffer, they are stained with either acridine orange (OA) or Giemsa solution. Heat-stable zones with a high concentration of C-G pairs are called T-bands. Although they comprise around 65% of all identified genes, they only make up 15% of all bands. Only chromosomal abnormalities such as deletions or translocations larger than 2-3 Mb can be detected by T-banding (52).

Identifying of Human Chromosomes

A group of 17 pioneering researchers who had previously published human karyotypes came together in Denver, Colorado, in 1960 to establish the groundwork for the renowned communication tool now known as An International System for Human Cytogenetic Nomenclature, or ISCN, to efficiently and methodically describe chromosomal changes (53).

According to the ISCN (43) chromosomes coloured by non-banding techniques are divided into seven groups (A-G) according to their length and centromere position (Fig 4):

Group A (1-3 chromosome pairs): The chromosomes in this group are noticeably longer and metacentric than the other chromosomes. Chromosome pair 1 is the longest chromosome pair. Chromosome 2 is more submedian than chromosome pairs 1 and 3 because its centromere is not exactly in the middle.

Group B (chromosome pairs 4-5): Chromosome 5 is slightly smaller than chromosome 4 in these chromosome pairs, which are distinctly submetacentric because the short arm is about 1/4 the length of the long arm. However, it is very difficult to distinguish between these two chromosome pairs as they look very similar to each other.

Group C (chromosome pairs 6-12 and the X chromosome): The chromosome pairs in this group are medium-sized and submetacentric. It is very difficult to distinguish these chromosomes from each other based on size and centromere characteristics alone.

Group D (13-15 chromosome pairs): These chromosomes are medium-sized, acrocentric and satellite chromosomes with an appearance that can be easily distinguished from other chromosomes.

Group E (16-18 chromosome pairs): Among these chromosome pairs, chromosome pair 16 is metacentric and chromosome pairs 17-18 are submetacentric. Chromosome pair 16 has a secondary stenosis on its long arm.

Group F (chromosome pairs 19-20): These chromosomes, which resemble a butterfly in appearance, are short and metacentric.

Group G (chromosome pairs 21-22 and the Y chromosome): Chromosomes 21-22 are short and acrocentric and have satellites. The Y

chromosome is similar in length to the other two chromosomes but can be distinguished from chromosome pairs 21-22 because it lacks a satellite. (taken from 1998 article)

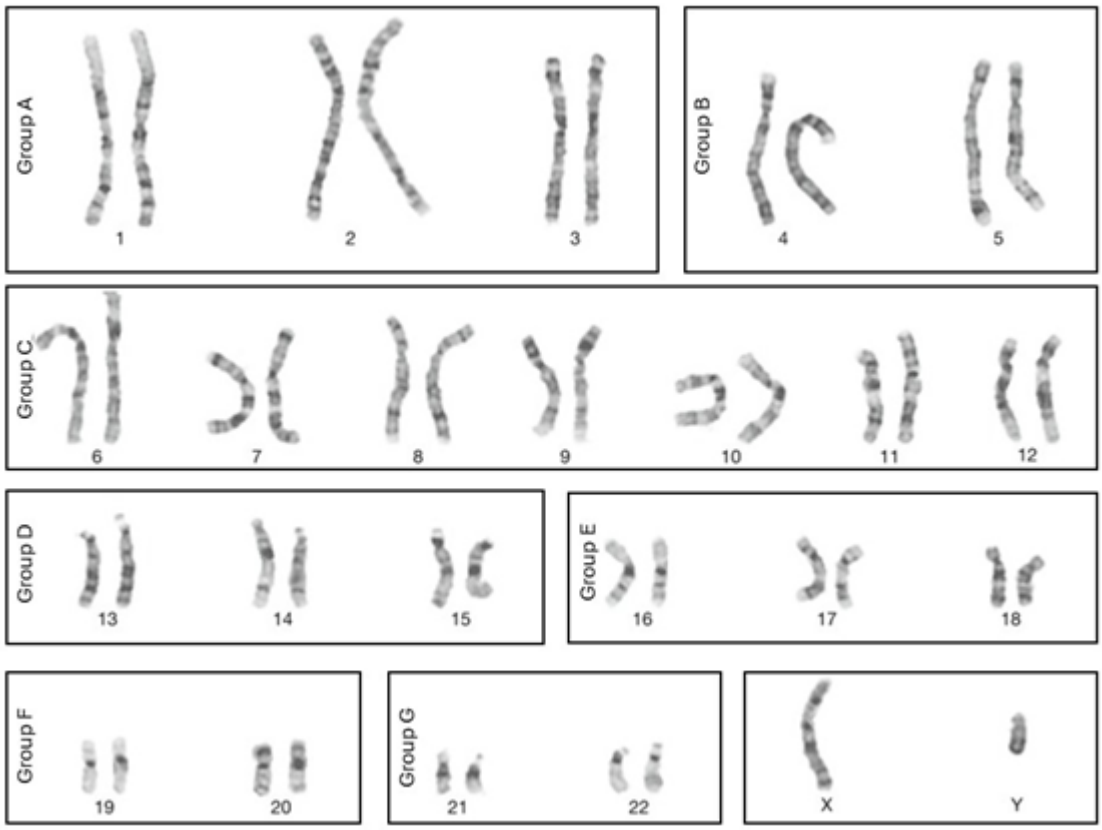

Figure 4. G-banded human chromosome and chromosome groups. (modified from (54)).

CONCLUSION

Cells have chromosomes, which can be analysed and well visualized, using deconstructing chemicals and can be stained for various purposes. Chromosomal abnormalities like deletions or translocations, linked to disorders can be detected via karyotyping. In addition to revealing karyotype variations that would have been significant in speciation, comparisons of chromosomal banding patterns can validate evolutionary links across species.

The study and identification of chromosomes and their component structures have attracted much attention in recent years. Reliable new techniques are now available to induce the division of large numbers of cells using mitogens to stimulate specific cell types. To identify all 24 human chromosomes at once and assess complicated chromosomal disorders, new methods are being developed for clinical and research facilities.

An essential method for analyzing the chromosomes of plants and animals is chromosomal banding. Using traditional dyes like Giemsa to consistently stain chromatin allowed for the first observation of chromosomes. Q-, G-, or R-banding can now be

used to precisely identify each chromosome in the karyotype, resulting in distinctive banding patterns. Specialized staining methods like C-banding and silver staining can be used to identify specific areas like centromeres and NORs. A first step toward a better understanding of chromosome structure is the chromosome banding technique. Modern chromosome analysis techniques like Fluorescence in situ Hybridisation (FISH) , can be combined with basic chromosome banding procedures to produce more accurate results on chromosomal abnormalities.

Table 1. Summary of basic chromosome techniques (modified from (33))

Type of banding	Used stain	Targeted area of staining	Application/comparison
Q-banding	Quinacrine	*Repetitive AT-rich DNA; *The chromosome's long arm (the Y chromosome, the centromere polymorphism areas on chromosomes 1 and 16);	The Q band was the first chromosomal staining technique used to identify the chromosomes. The G strip and the distance between each band produced by this method are comparable. Fluorescence microscopy shows the brilliant Q bands, which nearly match the dark G bands. The method's use is restricted by its affordability, the quick darkening of the bands it produces, and the toxicity of the fluorescent components.
G-banding	Giemsa	* Repetitive AT-rich DNA * For the detection of heterochromatin polymorphisms, specifically the pre-centromere sections of all chromosomes, the heterochromatin areas of chromosomes 1, 2, 5, and the end of the Yq, as well as the satellites of the chromosomes;	This technique is frequently used to identify the chromosomes of mammals. It is also recognized as a phylogenetic research approach, particularly in clinical cytogenetic studies. Plant chromosomes cannot be stained with G staining. The chromosomes' structural and functional components are reflected in the G-band layout. DNA sections rich in T and A are represented by dark bands, which often replicate late in the synthesis process. Same as the Q-banding pattern except for a single additional bond near the centromere of chromosomes 1 and 16
R-banding	Variety of techniques	The repetitive GC-rich DNA is found in the chromosome's terminal regions.	This method makes the dark regions of the G strip in the R strip and the light regions of the G strip dark. The primary method for detecting human telomere region deletion is the use of R-strips. Any genes that are expressed permanently (housekeeping genes) and around half of the GC-rich tissue-specific genes are stained in the R-stripe. The R tape method is less popular than the G tape approach due to its poor precision.
C-banding	Variety of techniques	* All chromosomes' centromere regions (rich in A and T made of structural heterochromatin), * Chromosomes 1, 3, 9, and 16's heterochromatin regions, * The telomere sections in the Y chromosome's long arm	This technique is applied to identify permanent heterochromatin regions of the genome. The pattern and extension of the strips can vary considerably from one type to the other. C-strips are applied to study the polymorphism resulting from DNA recombination in centromere regions. In plants, because of the inefficiency of the G-band, the C-band is used to identify chromosomes.
T-banding (telomere)	Giemsa	The telomeres, or terminal sections of chromosomes	The T strip is one variety of the R strip. Chromosomes treated more strictly show less staining, except the heat-resistant telomere sections. Both fluorescent and non-fluorescent T-tape methods are available.
NOR_banding	Silver nitrate	* The investigation of acrocentric chromosomal polymorphism * Staining of nucleotide organizing areas	This method is used to investigate chromosomal polymorphisms. Using this method, Nucleus Organizer Regions (NORs) of the acrocentric chromosomes' satellite stem are specifically stained.

Peer-review: Externally peer-reviewed

Author Contributions: Concept: EU, Design: EU, Data Collection and Processing: EU, Analysis and Interpretation: EU, Writing: EU

Conflict of Interest: The author declared no conflict of interest.

Financial Disclosure: The author declared that this study has not received no financial support.

REFERENCES

1. Heng J, Heng HH. Karyotype coding: The creation and maintenance of system information for complexity and biodiversity. Biosystems. 2021;208:104476.
2. Witty MJH. Pollen Development, Membranes and Features of the Nucleus in Tradescantia and related genera: A Translation of Wilhelm Hofmeister's 1848 Paper 'Ueber die Entwicklung des Pollens.'.15:75-86.
3. Liehr T. Molecular Cytogenetics in the Era of Chromosomics and Cytogenomic Approaches. 2021;12.
4. Alberts B, Johnson A, Lewis J, Raff M, Roberts K, Walter P. Chromosomal DNA and its packaging in the chromatin fiber. Molecular Biology of the Cell 4th edition: Garland Science; 2002.
5. Allison LA. Fundumental molecular biology. Ankara: Palme; 2014.
6. Doğan A, Kumbıçak Z. Cytogenetic studies on some spider species belonging to the family Lycosidae (araneae) distributed in Göreme National Park [Master thesis]. Nevşehir Nevşehir Hacı Bektaş Veli University; 2014.
7. Therman E, Susman M. Human chromosomes: structure, behavior, and effects: Springer Science & Business Media; 2012.
8. Miller OJ, Therman E, Miller OJ, Therman EJHC. The chemistry and packaging of chromosomes. 2001:61-77.
9. Li Y, Agrawal V, Virk RKA, Roth E, Li WS, Eshein A, et al. Analysis of three-dimensional chromatin packing domains by chromatin scanning transmission electron microscopy (ChromSTEM). Scientific Reports. 2022;12(1):12198.
10. Fyodorov DV, Zhou B-R, Skoultchi AI, Bai Y. Emerging roles of linker histones in regulating chromatin structure and function. Nature Reviews Molecular Cell Biology. 2018;19(3):192-206.
11. Saygun S. Comparison of chromosome structures of various flatfish (Pisces, Pleuronectiformes) living in the Black Sea [Master thesis]. Samsun: Ondokuz Mayıs University; 2005.
12. Karyology definition 2024 [Available from: https://www.genome.gov/genetics-glossary/Karyotype.

13. Nadler CF, editor Chromosomal evolution in rodents. Comparative Mammalian Cytogenetics: An International Conference at Dartmouth Medical School Hanover, New Hampshire, July 29—August 2, 1968; 1969: Springer.
14. Madian N, Jayanthi K, Somasundaram D, Suresh SJM. Identifying centromere position of human chromosome images using contour and shape based analysis. 2019;144:243-59.
15. Schweizer D, Ehrendorfer FJPS, Evolution. Giemsa banded karyotypes, systematics, and evolution in Anacyclus (Asteraceae-Anthemideae). 1976;126:107-48.
16. Asadi-Corom F, Mirzaie-Nodoushan H, Calagari MJPGR. Comparative karyological features of several populations of Populus euphratica Oliv., grown under different environmental conditions in Iran. 2024:1-7.
17. Syafriani E, Somala MUA, Triani NJNS, Proceedings T. Biotechnology for Beginner Student. 2021:10-6.
18. Krietenstein N, Abraham S, Venev SV, Abdennur N, Gibcus J, Hsieh T-HS, et al. Ultrastructural details of mammalian chromosome architecture. 2020;78(3):554-65. e7.
19. Nicodemi M, Pombo AJCoicb. Models of chromosome structure. 2014;28:90-5.
20. Macgregor HCJCr. Chromomeres revisited. 2012;20:911-24.
21. Das D. Essential practical handbook of cell biology & genetics, biometry & microbiology: A laboratory manual: Academic Publishers; 2017.
22. Paulson JR, Hudson DF, Cisneros-Soberanis F, Earnshaw WC, editors. Mitotic chromosomes. Seminars in cell & developmental biology; 2021: Elsevier.
23. Navarro AP, Cheeseman IM, editors. Kinetochore assembly throughout the cell cycle. Seminars in cell & developmental biology; 2021: Elsevier.
24. Schleif R. Genetics and molecular biology: The Johns Hopkins University Press; 2023.
25. Chakravarti D, LaBella KA, DePinho RAJC. Telomeres: history, health, and hallmarks of aging. 2021;184(2):306-22.
26. Berns MW, Cheng WKJECR. Are chromosome secondary constrictions nucleolar organizers?: A re-examination using a laser microbeam. 1971;69(1):185-92.
27. Hasterok R, Borowska-Zuchowska N, Robaszkiewicz EJIJoMS. Cytomolecular Organisation of the Nuclear Genome. MDPI; 2022. p. 13028.
28. Thakur J, Packiaraj J, Henikoff S. Sequence, chromatin and evolution of satellite DNA. International journal of molecular sciences. 2021;22(9):4309.
29. O. J. Miller, Therman E. Human Chromosomes: Springer Science & Business Media.; 2011.

30. Emiroğlu Ü. Chromosomes: Basic concepts and mechanisms. Izmir: Ege University Publications 2017.
31. Kumar S, Kiso A, Kithan NAJC-c, molecular strategies for analysing heredity material. IntechOpen L. Chromosome banding and mechanism of chromosome aberrations. 2021:45-60.
32. Sharma A. Chromosome techniques: CRC Press; 2020.
33. Montazerinezhad S, Emamjomeh A, Hajieghrari BJMBR. Chromosomal abnormality, laboratory techniques, tools and databases in molecular Cytogenetics. 2020;47(11):9055-73.
34. Bickmore WA, editor Karyotype Analysis and Chromosome Banding2001.
35. Milani DAQ, Tadi P. Genetics, Chromosome Abnormalities. StatPearls [Internet]: StatPearls Publishing; 2023.
36. Deepthi B, Prayaga AK, Rukmangadha NJJoC. Comparison of modified ultrafast giemsa stain with the standard may grunwald giemsa stain in FNAC of various organs. 2022;39(4):174-9.
37. Dutta U. Essentials of Cytogenetic and Molecular Cytogenetic Laboratory Testing: Cambridge Scholars Publishing; 2022.
38. Huisinga K, Brower-Toland B, Elgin S. The contradictory definitions of heterochromatin: Transcription and silencing. Chromosoma. 2006;115:110-22.
39. Moore CM, Best RG. Chromosome Preparation and Banding. eLS.
40. Stockert JC, Blázquez-Castro A, Horobin RWJFAoD, Chromatin. Identifying different types of chromatin using Giemsa staining. 2014:25-38.
41. Pederson TJCSHpib. The nucleolus. 2011;3(3):a000638.
42. McKay RJC. The mechanism of G and C banding in mammalian metaphase chromosomes. 1973;44(1):1-14.
43. Shaffer LG, McGowan-Jordan J, Schmid M. ISCN 2013: an international system for human cytogenetic nomenclature (2013): Karger Medical and Scientific Publishers; 2013.
44. Arsham MS, Barch MJ, Lawce HJ. The AGT cytogenetics laboratory manual: John Wiley & Sons; 2017.
45. Zhu JJ, Qi H, Cai LR, Wen XH, Zeng W, Tang GD, et al. C-banding and AgNOR-staining were still effective complementary methods to indentify chromosomal heteromorphisms and some structural abnormalities in prenatal diagnosis. 2019;12:1-11.
46. Trere DJM. AgNOR staining and quantification. 2000;31(2):127-31.
47. Rahman N, Rahman M, Zaman SU. Diagnostic Utility of Modified Method of AgNOR Staining in the Evaluation of Benign and Malignant Effusions. European

Journal of Medical and Health Sciences. 2024;6(5):160-9.

48. Nabil A, Sarra F. Q-Banding 2017 [1-3]. Available from: https://faculty.ksu.edu.sa/sites/default/files/q-banding_amor_2017.pdf.
49. Comings DE, Kovacs BW, Avelino E, Harris DCJC. Mechanisms of chromosome banding: V. Quinacrine banding. 1975;50:111-45.
50. Van der Ploeg MJEjohE. Cytochemical nucleic acid research during the twentieth century. 2000;44(1):7.
51. Wyandt HE, Wilson GN, Tonk VS. Human chromosome variation: heteromorphism, polymorphism and pathogenesis: Springer; 2017.
52. Chai H, Li P. Banding cytogenetics. Cytogenetics and molecular cytogenetics: CRC Press; 2022. p. 7-26.
53. Chauhan A. Principle and Techniques of Chromosome Banding: A Primitive Method for Chromosome Analysis. Essentials of Basic and Applied Sciences: Crdeep journals; 2022.
54. Miller OJ, Therman E. Human chromosomes. 4 ed. New York, USA: Springer 2011.